A simulation study of nanoparticle-based SERS biosensing platforms with application towards glioma detection

by

Soumyadeep Saha

A thesis
presented to the University of Waterloo
in fulfillment of the
thesis requirement for the degree of
Master of Applied Science
in
Electrical and Computer Engineering – Nanotechnology

Waterloo, Ontario, Canada, 2023

Author’s Declaration

I hereby declare that I am the sole author of this thesis. This is a true copy of the thesis, including any required final revisions, as accepted by my examiners.

I understand that my thesis may be made electronically available to the public.

Abstract

Gliomas are the most commonly occurring primary brain tumour with poor prognosis and high mortality rate. Currently, the diagnostic and monitoring options for glioma mainly revolve around imaging techniques, which often provide limited information and require supervisory expertise. Liquid biopsy is a great alternative or complementary monitoring protocol that can be implemented along with other standard diagnosis protocols. However, standard detection schemes for sampling and monitoring biomarkers in different biological fluids lack the necessary sensitivity and ability for real-time analysis. Lately, biosensor-based diagnostic and monitoring technology has attracted significant attention due to several advantageous features, including high sensitivity and specificity, high-throughput analysis, minimally invasive, and multiplexing ability. In this thesis, we have focused our attention on glioma and presented a literature survey summarizing the diagnostic, prognostic, and predictive biomarkers associated with glioma. Further, we discussed different biosensory approaches reported to date for the detection of specific glioma biomarkers. Current biosensors demonstrate high sensitivity and specificity, which can be used for point-of-care devices or liquid biopsies. However, for real clinical applications, these biosensors lack high-throughput and multiplexed analysis, which can be achieved via integration with microfluidic systems.

Design of surface-enhanced Raman scattering (SERS) based biosensing platforms for cancer detection require careful optimization of nanostructure size and interparticle gap to facilitate resonance of localised plasmons and thus maximize enhancement factor. In this thesis, we discussed a simple modeling strategy of nanoparticle-based SERS biosensing platform, which can even be extended to other complex nanostructures as per design requirement. A comprehensive simulation study has been conducted to understand the effects of polarization dependence on the enhancement factor of the system. A new phenomenon of local hotspot switching is observed in multiple nanosphere systems which hasn’t been reported in literatures yet. Finally, validation experiments were performed on a simple self-assembled gold nanoparticle substrate with methylene blue as Raman probe molecule.

Acknowledgements

I would like to thank my supervisors Prof. Sushanta Mitra and Prof. Manoj Sachdev for their continuous mentoring and support towards my master’s research.

I would like to thank every member of Micro and Nano-Scale Transport Lab for helping me and guiding me towards my experimental research.

I would like to thank Prof. Juewen Liu and Prof. Mahla Poudineh to be a part of my thesis reading committee, whose suggestions and comments helped me to significantly improve the quality of this thesis.

Dedication

I would like to dedicate this research work to the ones I love, my parents, Anon and lastly everyone from my “GYPSY” group.

Table of Contents

List of Figures

List of Tables

Chapter 1
Introduction[a]

1.1. Glioma and importance of biosensors in cancer management

Gliomas are tumours found in the central nervous system of human. They owe their genesis to abnormal tissue growth in the glial cells of the brain and spine. This type of malignancy shows significantly high death rate and poor prognosis, due to multiple factors including higher chances of metastasis and recurrence[1]. Around 28.2% of all deceased in Canada in 2021[2] were directly or indirectly linked with cancer, making it the most common cause of death in this country. Glioblastoma multiforme (GBM), a subtype of glioma, is the most predominant and aggressive form of brain cancer, killing 225,000 people annually[3]. It accounts for over 60% of all brain tumours in adults[3], with a merely 12-14 months of survival time (median) in Canada[4] which gets even lower to less than 4% for age-group 45 – 64 and 14% for younger adults (20 – 44 years old)[4]. Such devastating numbers makes early detection of gliomas through current biosensing technology a crucial task for glioma cancer management.

Currently, the primary diagnosis of glioma is accomplished by taking brain scans or magnetic resonance imaging (MRI), followed by tissue biopsy for decisive grading and characterization of the tumour[5]. Although tissue biopsies are the go-to technique for diagnosis of any form of brain tumour, resection from it during the biopsy procedure requires very invasive surgical interventions which may cause brain swelling or degrade neural functioning[6]. Moreover, some tumours might be present in a surgically inaccessible location[7]. Liquid biopsy is an alternative technique to probe into the tumour in a minimally invasive manner by detecting

---

[a] Adapted from S. Saha, M. Sachdev, and S. K. Mitra, 'Recent advances in label-free optical, electrochemical, and electronic biosensors for glioma biomarkers', Biomicrofluidics, vol. 17, no. 1, p. 011502, Jan. 2023, doi: 10.1063/5.0135525. [221]

and quantifying tumour diagnostic biomarkers in bodily fluids. Liquid biopsy can also allow to monitor a tumour prognosis via prognostic biomarker. Currently, prognosis of brain tumours is monitored by imaging methods such as MRI[5], however there are significant chances of pseudoprognosis[8] with imaging methods. This makes liquid biopsy a great technique to complement with current standards.

At present, the mainly approved glioma detection methods are imaging techniques like magnetic resonance imaging (MRI) and computerized tomography (CT) scans, which are backed up by tissue biopsy. All these techniques are costly and required to be done under the supervision of an expert. Also, most of these treatment protocol starts after the onset of symptoms, which sometimes is too late for the patient to get effective treatment. Advancement in biosensor technologies for sensitive and specific detection of biomarkers associated with glioma holds great promise in terms of point-of-care treatment and liquid biopsies. Biosensors can provide information about biomarkers that arise at the initial stages of cancer, providing a window for early diagnosis and thus better survival rates for glioma. Depending on the transduction principle, different biosensing technologies like optical, electrochemical or electrical biosensors have shown great potential for cancer diagnosis. The real-time evaluation of cancer biomarkers drug resistant mutations will allow a physician to implement precision medicine, which could be beneficial for the overall survival of the patient.

1.2. Thesis Organisation and Motivation

This thesis begins with a comprehensive review of glioma biomarkers and various biosensors developed for their detection and monitoring in Chapter 2. Numerous reviews have been published in recent years inspecting biosensor development for different forms of cancers like lung cancer[9–13], breast cancer[14–17], prostate cancer[18–21] and so on. However, we didn't notice any such study related to brain cancer biomarkers. A possible reason for such lack of reviews could be the rarity of brain cancer occurrence when compared to the other major cancers. Nonetheless, the poor prognosis and extremely low survival rate for brain cancer has inspired numerous research groups to invest their time in developing biosensors capable of detecting associated biomarkers for glioma. In this review, we discussed the recent advances made in the development of such biosensors. We focused our review to label-free detection schemes. While labelled detection schemes are more established and can detect cancer with very high sensitivity and accuracy, it is very difficult to implement real-time analysis with labelled approach. Label-free detection schemes are much more suitable for real-time analysis and provides an important drive towards precision medicine. This review presents the current advances in label-free detection schemes and indicate research gaps that need to be worked in order to establish label-free biosensing on par with labelled schemes. The review begins with a brief literature survey of the plethora of biomarkers reported to be associated with glioma and continues to review different biosensing technologies divided according to their transduction principle. Tables have been prepared at the end of each section enlisting all the key literatures related to biosensor for the detection of glioma. At last, a brief perspective of future research in this field has been discussed with respect to different application types like POC devices, liquid biopsies and even implantable biosensors.

It can be deduced from the literature review that design of an optical biosensing platform enhanced with nanostructures is crucial to ensure maximum sensitivity of the device. For a nanoparticle-based SERS biosensing platform, sensitivity is corelated to the enhancement factor of the device, which depends on several design parameters such as nanostructure size and shape, interstructure nanogaps and incident wavelength[22–25]. Therefore, it is necessary to determine proper values of all parameters to ensure maximized enhancement factor and thus minimize the limit of detection. Finite difference models of metal nanoparticle systems have been described in literature as an effective approach to capture the intrinsic phenomenon of the localised surface plasmon resonance and surface plasmon coupling [26, 27], which constitutes the underlying cause of high enhancement factor in SERS biosensing platforms. Such models have been implemented to optimize the dimensions of different nanostructures[28–32] as well understanding the characteristics of local plasmon resonance such as dependence of incident polarization[33]. In Chapter 3, we discuss the implementation of a similar model of nanoparticle-based SERS biosensing platform using COMSOL Multiphysics[34] and performed a comprehensive simulation study with both gold and silver nanoparticles, taking into consideration different systems of single nanosphere, multiple nanospheres and periodic array of nanospheres. The multiple nanospheres model provides a comprehensive understanding of the resonating localised surface plasmons. From our simulations, we described the phenomenon of polarization dependence of enhancement factor and also observed a novel phenomenon of multiple hotspots switching, which hasn't been reported in literature yet. On the other hand, the periodic nanosphere model provides a realistic optimization platform for design of a SERS biochip. Taking one such simulation case as reference we validated the design methodology with experiments in Chapter 4 over self-assembled gold nanoparticles on a SiO_2 substrate and methylene blue as Raman probe molecule, corelating the experimentally achieved enhancement factor with the simulation results. A final conclusion along with the future scope of this work has been presented in Chapter 5.

Chapter 2
Background and Literature Review[b]

2.1. Biomarkers for Glioma

Biomarkers can be defined as a set of quantitative chemical molecules or physiological characteristics which acts as an indicator of certain processes under normal condition, or under external intervention[35]. Biomarkers can range from very simple measurements, such as pH, blood pressure or temperature, to complex biomolecules like DNA, proteins or enzymes. Along a treatment process, biomarkers play a vital role related to the treatment direction and outcome. Depending on the clinical continuum, biomarkers can be classified into several types such as diagnostic, prognostic, predictive biomarkers and so on. A clinical continuum generally begins with screening of *diagnostic biomarker* in order to detect the presence or absence of certain diseases. Then *prognostic biomarkers* are screened to determine how likely a particular clinical event is in a patient such as disease recurrence or progression. *Predictive biomarkers* or therapeutic biomarkers are used to determine if an individual is more or less likely to develop a favourable or unfavourable symptom when exposed to an external factor such as a medical product or environmental agent[36].

Glioma shed different types of its tumoral contents into circulation, which can be extracted from bodily fluids as potential biomarkers[37]. The sampling and probing of these biomolecules from a bio-fluid is called liquid biopsy[38]. Liquid biopsies have certain advantages over tissue biopsies during cancer management[39, 40]. It gives a minimally invasive route to capture real time cancer activities, which is particularly useful for deep lying glioma tissues where surgical

---

[b] Adapted from S. Saha, M. Sachdev, and S. K. Mitra, ‘Recent advances in label-free optical, electrochemical, and electronic biosensors for glioma biomarkers’, Biomicrofluidics, vol. 17, no. 1, p. 011502, Jan. 2023, doi: 10.1063/5.0135525. [221]

access is limited. It can also be a viable option for patients with recurrence and ineligible for surgical intervention. For glioma, liquid biopsy can be carried out either by sampling blood through venepuncture, or by sampling cerebrospinal fluid (CSF) through lumbar puncture[41].

Blood-brain barrier (BBB) complicates the liquid biopsy for gliomas. For a tumour-specific material to enter the blood stream and become a potential biomarker, it needs to cross the tight junction of BBB regulated by several transmembrane proteins like claudin-3 and claudin-5[42]. Recent studies have shown that GBM can induce an inflamed microenvironment, which can decrease the 'tightness' of a BBB junction[43] or even disrupting its function[44], making it more permeable. This allows several biomarkers to cross the BBB junction circulate into the bloodstream. Different types of such circulating biomarkers associated with glioma are described in the upcoming sections and some important biomarkers are summarized in Table 2.1. Please note that most of the biomarkers mentioned in this review are "potential biomarkers" for glioma. Unlike other form of cancer like lung cancer, breast cancer or prostate cancer, glioma does not have specific FDA approved biomarkers yet. It is noted from the literature review that this is still research in progress. A panel of such biomarkers, however, can be utilised to increase the accuracy of glioma detection. Figure 2.1 summarises the transport of different biomarkers from a GBM.

2.1.1. microRNA

MicroRNAs (miR) are small non-coding RNA with around 22 nucleotides. They do not participate in protein transcription phase directly, but interacts with the messenger RNAs (mRNA) and dictate gene expression[45, 46]. MicroRNAs play a crucial role in the carcinogenesis of cancer cells[47], thus making them a potential biomarker for malignancy. Up to date, over 300 different miRNAs has been reported to be correlated with glioma and therefore, meta-analysis of these studies over larger sample[48] is required to select a panel of microRNAs for diagnostic, prognostic or predictive applications. Nonetheless a handful of significant microRNAs has been summarised in Table 2.1, depending on the frequency of them reported over different literatures.

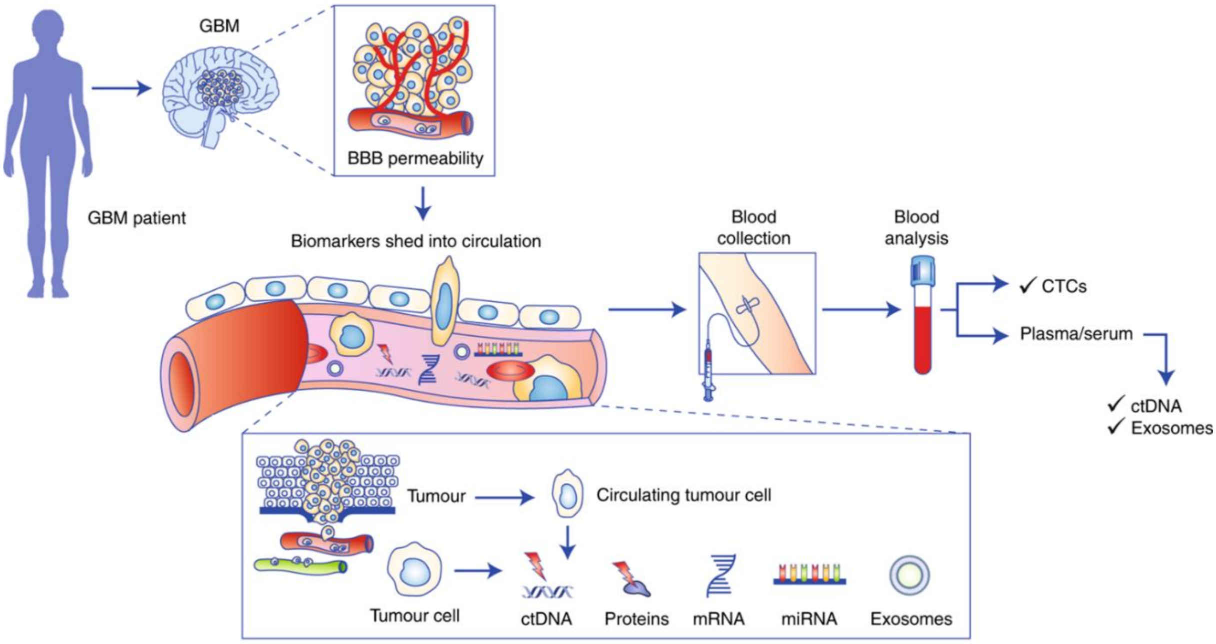

Figure 2.1: *A schematic representation of the pathway of biomarker flow from a brain tumour through the blood brain barrier into the blood circulation. Reproduced from Muller Bark et. al., Br J Cancer 122, 295–305 (2020)[5]. Copyright 2020 Springer Nature.*

miR-21 has shown great promise as a possible diagnostic marker for glioma detection[48]. Significant upregulation of miR-21 has been observed in the pre-operative serum samples of GBM patients[49]. Upregulation of miR-21 is also associated with poorer progression of glioma[50, 51] with negative correlation to overall survival and progression-free survival[47, 52, 53]. Upregulated miR-21 correlates to poorer response to temozolomide (TMZ)[54], a therapeutic drug for glioma, and radio-resistance[55]. miR-10b and miR-221 has also shown great promise as prognostic biomarkers[50, 51, 56]. On the other hand, as a predictive biomarker, miR-181d can be deemed very useful. Elevated levels of miR-181d are observed to be associated with decreased level of O^6-methylguanine-DNA methyltransferase (MGMT) expression (a genomic marker for glioma, to be discussed in Section 2.1.4)[57] and overall better response to TMZ therapy[54].

The short life-span of microRNA[58] in body fluids (< 3hrs) along with their trace amount makes them a challenging biomarker for cancer management. Despite that, numerous optical and electronic biosensors have been developed with remarkable limit of detection for analysis of microRNAs sampled from serum and blood.

2.1.2. Extracellular Vesicles

Extracellular Vesicles (EVs) are cell released lipid bounded vesicles which plays a significant role in cell-to-cell communication. Usual contents of an EV include mRNA, miRNA, DNA, cellular proteins and so on[59]. These vesicles carry cellular materials from one cell to another, even distance apart, and plays an influential role in controlling the cellular phenotype of recipient[60]. Therefore, EVs can help in glioma progression by promoting processes such as angiogenesis, invasion, migration, etc.[61]. EVs can be broadly categorised into two types based on their sizes and origin. These are exosomes and microvesicles (MVs). Exosomes are smaller EVs with diameter ranging from 30-150 nm and originates from endosomal membrane. MVs are relatively larger in size, around 50-1300 nm, and originates via budding of cell membrane[60].

Exosomes can be characterised by their surface proteins and inner contents, making them a viable analyte for current biosensors. Presence of membrane-associated proteins like cluster of differentiation 63 (CD63), CD9 and CD81 are signature markers for exosomes released by any cell[60]. Higher concentration of exosomes has been correlated to presence and recurrence of glioma[62]. Internal environment of exosomes has also showed elevated levels of certain microRNAs associated with glioma such as miR-21[63]. Other studies observed presence of glioma-associated mutation in exosomes such as EGFRvIII mutation[64–66] and IDH1 mutation[66, 67].

Detecting surface proteins with current biosensing strategies (optical or electrochemical) are advantageous over probing the inner environment, as fewer pre-processing steps are required for sample preparation. This makes certain membrane-associated proteins of great interest.

For instance, mutation in epidermal growth factor receptor variant-III (EGFRvIII) can express itself as EGFRvIII mutant protein on the glioma cell and glioma-associated exosome surfaces[68]. Another extracellular matrix protein called transforming growth factor-beta-induced protein (TGFB1) is observed to be upregulated and produced by glioma cells under hypoxic condition[69]. The protein is also associated with malignant progression and promotion of angiogenesis in glioma[69, 70]. Cluster of differentiation protein 44 and 133 are also found to be associated with glioma progression and thus can be useful to track tumour malignancy[71–73]. Such surface proteins can be simply captured on a biosensing surface using antibody or aptamer probes for sensitive and specific detection, given they are effectively isolated from the heterogenous medium.

2.1.3. Proteins

Certain proteins and peptides play a pivotal role in cancer-related processes like angiogenesis, proliferation and vascularization. Elevated levels of such proteins can act as a great diagnostic biomarker. For example, glial fibrillary acidic protein (GFAP) is important to aid for astrocytic structures and stability, and thus act as a marker for brain strokes[74] and trauma[75]. However, GFAP levels are found elevated in glioma patients[76–79]. One of the reasons of elevated GFAP in glioma patients is the destruction of glial cells and opening of BBB[43, 44]. This makes GFAP a potential diagnostic marker for glioma. YKL-40 (Chitinase 3-like 1) is another protein which is known to stimulate angiogenesis, cell proliferation and prevent apoptosis[80]. YKL-40 is present in higher concentration in GBM patients and associated with a significantly worse overall survival[81]. Patients with partial and total resection of glioma have shown significant difference in YKL-40 levels, with the later showing lower levels[82]. Another example of protein biomarker for glioma is vascular endothelial growth factor or VEGF. VEGF is a growth factor that aids in formation of new blood vessels in the periphery of glioma tissue (also known as neovascularization) and has been observed at elevated levels in malignant glioma patients[83–85].

2.1.4. Circulatory Tumour DNA

Alterations, even a single base-pair (single nucleotide polymorphism), of specific genes like tumour- suppressor genes, protooncogenes, cell cycle regulator genes, etc. are proven to be an essential step for cancer development[86]. These genetic mutations can be monitored by capturing trace amount of circulatory tumour DNA (ctDNA) or cell-free DNA (cfDNA) ejected into the blood stream or CSF by apoptotic or necrotic cells[87]. The amount of ctDNA also correlates to the prognosis of the cancer, with higher amount of ctDNA often present in later stage patients[88]. Several genetic mutations have been reported to be linked with glioma such as MGMT promoter methylation[89–93], isocitrate dehydrogenase 1 (IDH1) mutation[41, 94–96], 1p/19q codeletion[41, 89], EGFR amplification[41, 64, 65, 94], Phosphatase and tensin homolog (PTEN) methylation[41, 89, 94] and so on. Most of the reported studies have extracted ctDNA from the blood-stream or CSF of glioma patients, and quantified the sequence using PCR based techniques. Trace amounts of ctDNA (~0.01% of total blood cfDNA pool) combined with its short life-span[97] (half-life <1.5 hour) makes their detection a challenging task. Few devices reported recently, focusing on ctDNA detection, will be discussed in Section 2.3.2.

2.1.5. Metabolites

Metabolites are the ultimate product yields through different genomic or transcriptomic processes. Alteration in the relative concentration of these low molecular weight molecules in various biofluids can be a potential indicator of the state of the malignancy. In relation to glioma, few studies have been performed to pin down potential metabolic biomarkers. For instance, cysteine can be considered as a diagnostic glioma biomarker. Cysteine is the precursor of glutathione synthesis and plays a key role in survival of glioma cells[98] and poor progression-free survival in GBM[99]. Upregulation of cysteine is observed in serum of GBM patients[100]. Another potential biomarker is Glutamate. It is produced as a by-product of glutathione synthesis in glioma cells and plays a central part in glioma malignant phenotype[101]. Release of large amount of glutamate leads to excitotoxic death in neighbouring neurons, thereby generating more space for cell motility[102]. Glutamate levels in bodily fluids can be a potential biomarker for glioma.

Table 2.1: *A brief summary of important glioma biomarkers.*
↑: upregulation; =: presence for detection; ↓: downregulation; −: poor progression or therapeutic outcome on upregulation; +: better progression or therapeutic outcome on upregulation.

Biomarker Type	Biomarker		Classification		References
		Diagnostic	Prognostic	Predictive	
microRNA	miR-21	↑	−	−	[48, 49, 52, 54, 103–112]
	miR-10b	↑	−	−	[56, 104, 111, 113, 114]
	miR-155	↑	−		[106, 115]
	miR-15b	↑	+		[112, 116, 117]
	miR-222	↑	−		[48, 51, 118, 119]
	miR-221	↑	−		[52, 107, 118–122]
	miR-124	↓		+	[52, 105, 123]
	miR-125b	↓	−	+	[118, 124]
	miR-7-5p	↓			[125]
	miR-181d	↓		+	[54, 57]
Extracellular Vesicles	EGFRvIII protein	=/↑	−		[64–66, 68, 126]
	CD44	↑	−		[70–73, 127–130]
	CD133	↑	−		[128, 131]
	TGFB1	↑	−		[69, 70, 132, 133]
	MCT1	↑	−		[134–137]
	MCT4	↑	−		[138, 139]
Proteins	GFAP	↑			[76–79]
	VEGF	↑	−		[83–85]
	YKL-40	↑	−		[76, 80–82, 140]
Circulatory Tumour DNA	EGFR amplification	=/↑	−		[41, 64, 65, 94]
	MGMT promoter methylation	=/↑	−		[89–93]
	IDH1 mutation	=/↑	−		[41, 94–96]
	1p/19q codeletion	=/↑	−		[41, 89]
Metabolites	Glutamate	↑		+	[101, 102, 141–143]
	Cysteine	↑			[98, 100]

2.2. Biosensors for Glioma

2.2.1. Optical Biosensors

Optical biosensors are analytical devices in which the biorecognition element of the sensor is integrated with an optical transduction system[144]. Wide range of optical properties of the sensor surface can be probed for optical biosensing such as refractive index, wavelength, intensity and so on. An effective quantitative method for liquid biopsy analysis requires low limit of detection (LOD) with high-throughput multiplexed screening in real-time under small sample volume[145, 146]. Considering these requirements, optical biosensors have displayed promising performance. Depending on the principle of detection, optical biosensors are classified into several categories like surface plasmon resonance (SPR), surface-enhanced Raman scattering (SERS), fluorescence, colorimetric, etc. Section 2.3.1.1 and section 2.3.1.2 will discuss these major techniques with example of research works related to glioma detection, summarized in Table 2.2.

2.2.1.1. Surface Plasmon Resonance

Surface plasmon resonance or SPR is the sensitive optical detection of analytes utilizing evanescent wave near the surface. When an electromagnetic wave is irradiated on the interface of a dielectric material and metal, the conduction electrons start to oscillate in resonance with the electromagnetic wave. This resonance oscillation can propagate through the interface in form of a non-radiative transverse-magnetic (TM) wave known as surface plasmon polariton (SPP) wave. The evanescent field penetrates into both the media up to a certain decay length, with depth of penetration larger on the dielectric side. This makes the SPP wave extremely sensitive to small changes in refractive index (RI) of the dielectric medium. When analytes combine with the surface receptor probes, the RI of the medium increases, thereby increasing the propagation constant of the excited SPP wave. This property makes up the underlying principle of SPR biosensing.

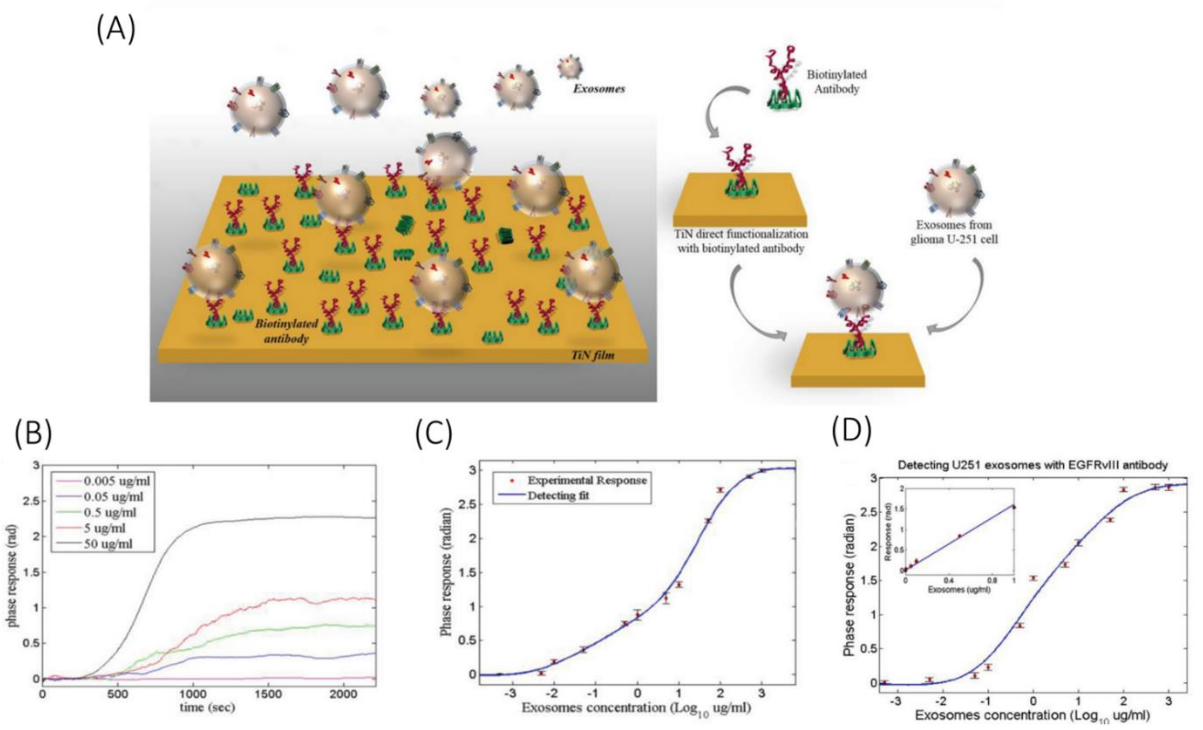

Figure 2.2: *Schematic illustration of (a) functionalization of TiN surface with anti-CD63 ABs for detection of U251 glioma-derived exosomes, (b) SPR response of the TiN-anti-CD63 biosensor and (c) its sensor calibration curve for detection of exosomal protein CD63. (d) Sensor calibration curve for detection of exosomal protein EGFRvIII. Reprinted with permission from Qiu et. al., Adv. Funct. Mater. 29, 1806761 (2019)*[147] *. Copyright 2019 John Wiley and Sons, Inc.*

One of the first papers reported in terms of glioma detection was based on SPR. Qiu *et. al*.[147] developed a TiN SPR chip to detect U251 glioma cells derived exosomes. The exosomes were initially isolated from the U251 cultured cell line using a standard isolation protocol combining centrifuge and filtration[148]. The TiN surface was functionalised with exosomal protein CD63 and EGFRvIII specific antibodies (ABs). The device reported a very low LOD of 4.29 ng/mL for CD63 exosome marker and 2.75 ng/mL for EGFRvIII exosome marker, and was able to sensitively detect exosomes derived from mouse serum. The slope of the calibration curve was about 0.36 for CD63 and 1.601 for EGFRvIII, with dynamic range extending up to 500 µg/mL, as shown in Figure 2.2. The paper also reported that the TiN sensor have almost twice the sensitivity when compared to a traditional Au sensor, and a 15% improvement in LOD. The increase in sensitivity, however, can be reasoned by taking in consideration the direct and indirect functionalization standards used for TiN and Au surface respectively.

Nanostructures of size equivalent to the wavelength of light can facilitate far more sensitive detection of biomarkers via confinement of surface plasmon, also known as localised surface plasmon resonance (LSPR). Thakur *et. al.*[149] reported a modified version of their previous TiN SPR chip[147] by introducing nanoholes on the surface of TiN nanofilm [Figure 2.3]. This allowed for localization and amplification of the surface electromagnetic wave. The sensor was functionalized with specific ABs for EGFRvIII, CD44 and CD163 respectively and showed high sensitivity towards exosomal surface protein CD44 with a very low LOD of 3.46 ng/mL and the calibration curve slope of 1.447. Each biomarker was required to be isolated with individual pre-processing steps from the cultured cell line. Moreover, the paper demonstrated that the biosensor was able to quantify major glioma biomarkers isolated from the CSF and blood serum (with the help of a Total Exosome Isolation kit[148]) of an GBM mouse model, which is a potential development towards liquid biopsy.

Nanoparticles enabled LSPR biosensors have also been explored in recent times. Thakur *et. al.*[148] reported a biosensor surface by self-assembled gold nano-islands (AuNIs) over SiO_2 surface. This sensor surface was utilized in one of their later publications[137] for label-free quantification of exosomal surface protein CD147 and MCT1. The exosomes were derived from the blood serum of a glioma mouse model following standard protocols[148]. A later publication from the same group modified the AuNIs surface of the biosensor by integrating TiO_2 columnar thin films (TiO_2-CTFE-AuNI)[150] . This device couples TiO_2 with gold nano-islands for improved sensitive detection of exosomal surface protein CD63 and glioma biomarker BIGH3 (also known as TGFB1) [Figure 2.4(a)]. The device functionalized with respective ABs reported a LOD of 4.24 ng/mL for CD63 and 3.84 ng/mL for BIGH3. With respect to only AuNIs, the integration of TiO_2 improved the LOD by 13% and increased the sensitivity (calibration curve slope) by almost 2.5 times.

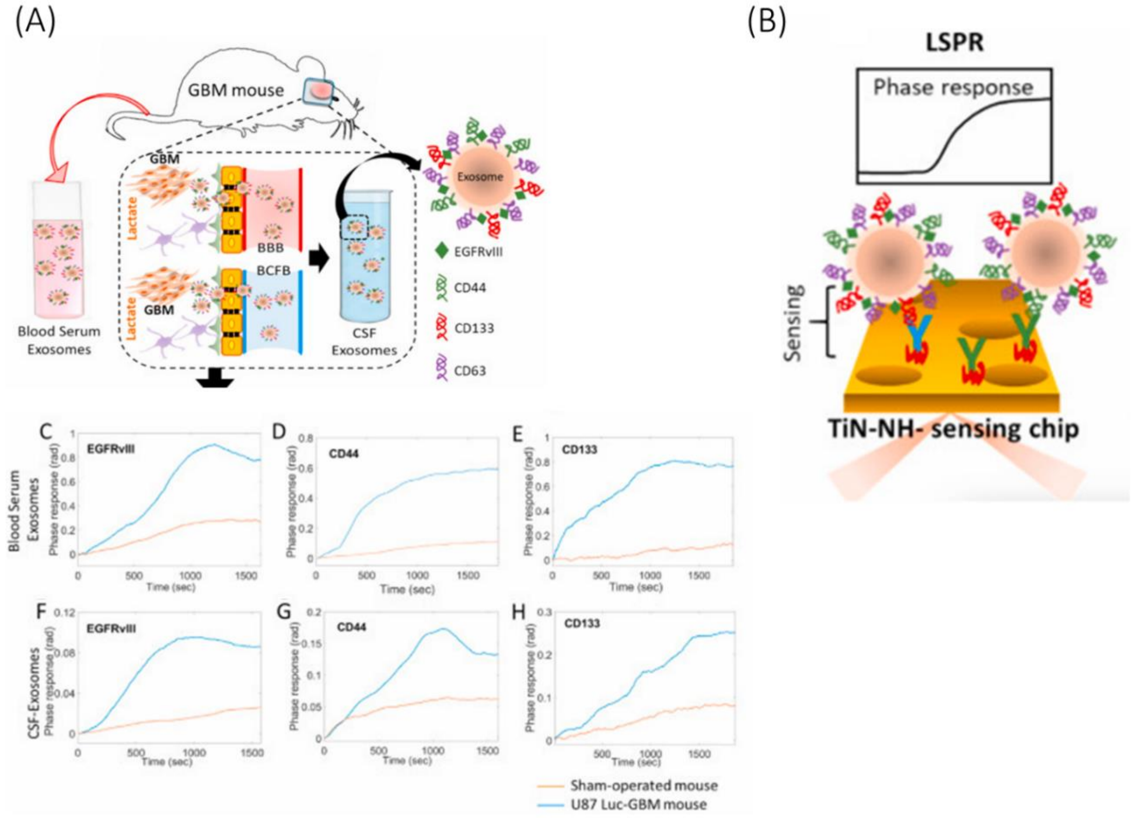

Figure 2.3: *Schematic illustration of (a) exosomes derived from the blood serum and CSF of a GBM mouse model, and (b) its ultrasensitive detection using TiN nanohole LSPR biosensor. SPR phase response of the biosensor for exosomes derived from (c-e) blood serum and (f-h) CSF, (c,f) for EGFRvIII, (d,g) for CD44 and (e,h) for CD163. Reprinted with permission from Thakur et. al., Biosens Bioelectron* ***191****, 113476 (2021)[149]. Copyright 2021 Elsevier.*

In the report by Liu *et. al.*[151], an LSPR chip is demonstrated by integrating Ag nanostructures over self-assembled Au nano-islands [Figure 2.4(d)]. The Ag@AuNI chip functionalized with anti-CD63 and anti-MCT4 antibodies reported a very low LOD of 0.38 ng/mL and 1.4 ng/mL respectively, which is almost 75% improvement over only AuNI LSPR chip. The sensitivity of the device (slope of the calibration curve) also improved by over 1.5 times. The device detected elevated levels of GBM biomarker exosomal protein MCT4 derived from the blood samples of a GBM mouse model with a remarkable LOD of 0.4 ng/mL. Such devices have proven to attain remarkable sensitivity for pre-processed samples with isolated exosomes, but may not be specific enough to work under complex real biofluids such as blood or CSF.

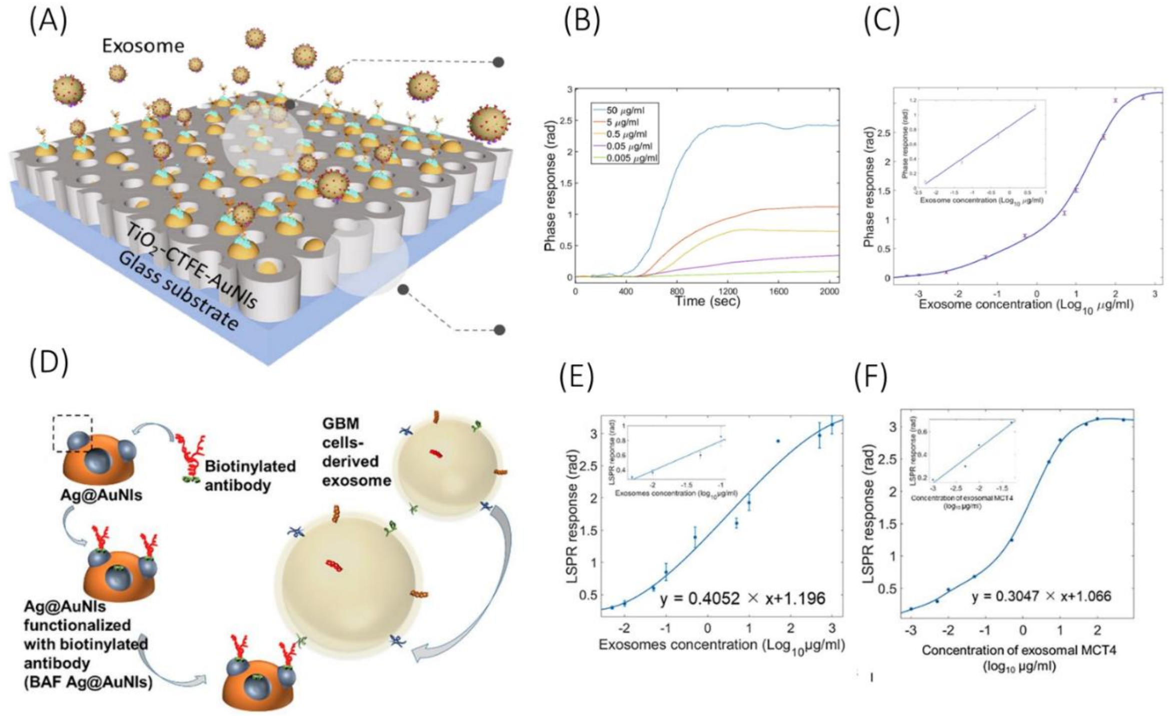

Figure 2.4: *Schematic representation of (a) TiO_2-CTFE-AuNI sensing chip and its (b) LSPR phase responses against BIGH3 protein from glioma-derived exosomes, (c) sensor calibration curve. (d) Schematic illustration of The Ag@AuNI chip functionalized with anti-MCT4 antibodies along with their calibration curves for detection of MCT4 protein from (e) U87 derived exosomes and (f) blood serum derived exosomes. Scheme (a-c) are reprinted with permission from Xu et.al., Chemical Engineering Journal* ***415****, 128948 (2021)[150]. Copyright 2021 Elsevier. Scheme (d-f) are reprinted with permission from Liu et. al., Chemical Engineering Journal* ***446****, 137383 (2022)[151]. Copyright 2022 Elsevier.*

LSPR based biosensing has been implemented for microRNA detection as well. Hao *et.al.*[152] reported a highly sensitive LSPR chip based on gold nanorods. The complementary target sequence used in the sensogram experiments matches with miR-16-5p (sequence data found in miRbase[153]) which has been reported to be a tumour suppressor and found downregulated in glioma[154, 155]. The device demonstrated a LOD of 0.045 pM with the Au nanorods, which increases to 0.054 nM without the Au nanorods. The streptavidin functionalised Au nanorods can interact with the 3' biotin of the molecular beacon receptor probe only after the microRNA hybridizes with the probe and removes the steric hindrance. The report does not present any test with real biofluids or biomarkers isolated from them.

SPR and LSPR biosensors shows great promise towards clinical application with certain limitations like long pre-processing steps, lack of multiplex analysis and low-throughput are still required to be worked on.

2.2.1.2. Surface Enhanced Raman Spectroscopy

Raman scattering is a type of optical scattering phenomenon where the scattered light from a sample molecule changes it wavelength upon interaction with it. When a sample molecule absorbs the incoming light, it gets promoted from its ground vibrational state, to a higher vibrational energy state. The higher energy state corresponds to the wavelength of the incoming light. Upon re-emission, the sample molecule may return to an energy state lower than its previous ground vibrational state, emitting a light with larger wavelength than the incoming light. This demonstrates anti-Stokes scattering. Similarly, when the sample molecule returns to an energy state higher than its previous ground vibrational state, emitting a light of smaller wavelength, it produces Stokes scattering[156]. Usually for a typical biomolecule, the most dominant scattering phenomenon is observed as Rayleigh scattering, where the molecule returns to its original ground state, producing zero wavelength shift. This produces a large peak at the center of a Raman spectrum. This followed by Stokes scattering, or positive wavelength shift, which are usually taken into consideration for biomolecular analysis. Anti-Stokes peaks are rare and difficult to observe in most biomolecules. The phenomenon of Raman scattering is very intrinsic to individual vibrational states of a molecule, and thus Raman spectroscopy has been applied in various fields, including biological sensing.

Many biomolecules demonstrate characteristic peaks or fingerprint peaks in Raman spectrum, peaks with a practical level of intensity at a fixed wavelength shift, which can be used for detection of that biomolecule. These characteristic peaks are often missed in spontaneous Raman scattering, since it is a weak phenomenon[157]. Therefore, certain enhancement techniques are applied to amplify the intensity of these Raman signals, therefore identifying accurate fingerprint peaks and increasing the sensitivity of the biosensing system. Noble metals like gold or silver are often used as substrates for such enhancement. Such noble metals with abundant free electrons demonstrate desirable optical properties including resonating excitation of surface plasmons, which helps in enhancement of Raman signals. This phenomenon of enhancement of Raman scattering intensity via surface modification is known as surface-enhanced Raman scattering or SERS. Depending on the application, a SERS substrate can have a uniform metallic surface coating, demonstrating a uniform enhancement and better reproducibility, or it can have arrays of metallic nanostructures, which produces irregular enhancement over the surface, but often produces enhancement in the range of 10^{10} and 10^{11}, enabling detection of single molecules[158].

Metallic nanostructures tap into localised surface plasmon resonance for high amplification of SERS signal. When two nanostructures come at close proximity to one another, with a gap of single digit nanometers, the two localised plasmons forms a dipolar coupling in the nanogap, resulting in an electric field enhancement of very high magnitude. Such gaps on a SERS substrate are known as “SERS hotspots”. Hotspots are desirable for a SERS biosensing systems, as they enable the detection of analytes at very low concentration (~pM). The enhancement factor for a particular hotspot depends on both the sizes of the nanostructures and the gap between them. The total enhancement factor from a SERS system comes from electromagnetic (EM) enhancement due to coupling of the incident and Raman electromagnetic fields with the SERS substrate[157], and chemical enhancement due to charge transfer mechanism of the adsorbed molecule with the SERS substrate[159]. Modeling and simulation of EM enhancement factor can be done within a linear system, whereas, simulation of chemical enhancement require modeling under non-linear systems, which are relatively complex. In any case, the EM enhancement factor is the main contributor of the total enhancement factor of a SERS system, far exceeding the contributions from chemical enhancement.

Jalali *et. al.*[160] reported a biosensing platform based on Raman spectroscopy for detection of extracellular vesicles extracted from two different GBM cell lines – U373 and U87. Extraction was performed with a standard pre-processing protocol[161]. The nanostructure implemented in the device was an optimised gold nanobowtie, which showed an enhancement factor of 9×10^5 in average electric field. A microfluidic device is integrated with the SERS chip for effecting loading of EVs and multiplexed detection of two EV types. The device demonstrated a LOD of 1.32×10^5 particles/mL over a linear range of 10^5 to 10^8 particles/mL. Another study by Kim *et. al.*[162] demonstrated a sandwich assay for sensitive and multiplexed detection of microRNAs – 21, 10b and 373. The microRNAs were isolated from a cancer cell line using a RNeasy Mini Kit. The SERS chips used head-flocked gold nanopillars for LSPR enhancement. The sandwich assay consists of two single stranded DNA probes – capture and detection probes, combined forms the complementary sequence of the target miRNA. The detection probe plays a significant role in identifying the fingerprint peak of the target microRNA[163]. The biosensor reported a LOD of 3.53 fM for miR-10b, 2.17 fM for miR-21 and 2.13 fM for miR-373. The study however used PBS as a substrate indicating that the biosensor may fall short when concerned with real biofluids.

SERS biosensing technique is often limited by its low-throughput analysis due to time consuming spectral acquisition. Other than that benchtop Raman detectors are bulky and required to be maintained at very low temperatures, making them costly and unsuitable for point-of-care applications. In recent times, Raman spectrometers have been efficiently miniaturized to handheld devices with detectors working under room temperature. Such devices are suitable for point-of-care applications and gained attention in the sensor research community[164]. SERS integrated with microfluidic devices can be implemented for clinical liquid biopsies, where microfluidic platforms may allow high-throughput, multiplexed and automated analysis, while SERS biosensing platform allows ultra-high sensitive detection of clinical biomarkers. Integration of nanoparticle-based SERS biosensing platform with microfluidics can be done by immobilizing nanoparticle/ nanostructures on the microfluidic channels/chambers. Such devices can be operated in both static and continuous flow manner, however care need to be taken for control of injection flow, mixing of target molecules and reaction time[165, 166]. Another strategy is segmented flow with microdroplet based strategies, where each microdroplet consists of target biomolecules and colloid nanoparticles. This strategy is useful each droplet acts as individual reaction sites and prevents the memory effect or adsorption of nanoparticles[167, 168].

Table 2.2: *Summary of optical biosensors for detection of glioma biomarkers.*

Optical Biosensor Type	Biomarkers	Specimen	Linear/Dynamic range	LOD	Reference
Biotinylated anti CD63 and anti-EGFRvIII AB on TiN chip	Exosomal protein CD63 and EGFRvIII	Exosomes derived from U251 cell line and mouse serum	*0.005 – 1000 µg/mL* (dynamic)	CD-63: *4.29 ng/mL* EGFRvIII: *2.75 ng/mL*	Qiu *et. al.* (2019)[147]
TiN nanohole (NH) LSPR chip with biotinylated antibodies	Exosomal protein CD63, CD44 and CD133 (and EGFRvIII)	Exosomes derived from U87 GBM cell line, blood serum, and CSF	*0.005 – 50 µg/mL* (dynamic)	CD44: *3.46 ng/mL*	Thakur *et. al.* (2021)[149]
Self-assembly (SAM)-AuNI LSPR biosensor chip	Exosomal protein MCT1 and CD147	Exosomes derived from U251, U87, U118 and A172 GMs and blood serum	-	-	Thakur *et. al.* (2020)[137]
TiO2-columnar thin films (CTF)-Au Nanoislands (AuNI) LSPR chip	Exosomal protein CD63 and BIGH3	Exosomes derived from U251 cell line	*0.001 – 500 µg/mL* (dynamic)	CD63: *4.24 ng/mL* BIGH3: *3.84 ng/mL*	Xu *et.al.* (2021)[150]
Ag@AuNI LSPR chip with biotinylated anti CD63 and anti-MCT4 AB	Exosomal protein CD63 and MCT4	Exosomes derived from U87 cell line and mouse blood-serum	*0.0005 – 50 µg/mL* (dynamic)	CD-63: *0.38 ng/mL* MCT4: *1.4 ng/mL*	Liu *et. al.* (2022)[151]

				MCT4 from blood-serum: *0.4 ng/mL*	
SPR based biosensor with streptavidin functionalised Au nanorods for signal amplification	MicroRNA-16-5p	-	Without Ste-AuNR: *0.1-100 nM* (linear) With Ste-AuNR: *0.1-100 pM* (linear)	Without Ste-AuNR: *0.054 nM* With Ste-AuNR: *0.045 pM*	Hao *et. al.* (2017)[152]
SERS based biosensor with head flocked Au nanopillar	MicroRNA 10b, 21, 373	-	-	10b: *3.53 fM* 21: *2.17 fM* 373: *2.16 fM*	Kim *et. al.* (2019)[162]
SERS based biosensor embedded with nanobowtie shaped antennas	EVs	Extracellular vesicles derived from U87 and U373 GM cell line	10^5 *to* 10^8 *particles/mL* (linear)	1.32×10^5 *particles/mL*	Jalali *et. al.* (2021)[160]

2.2.2. Electrochemical Biosensors

Electrochemical biosensors are commonly referred to electroactive surfaces, typically a biorecognition layer over an electrode which transduces the biochemical activity over the surface in form of electric signals. An electrochemical biosensor usually consists of three electrodes. A working electrode (WE) is where all the biorecognition reaction and chemical to electrical transduction takes place. A reference electrode (RE) which sits in the solution, but at a distance from the reaction surface and provides a constant potential (measurement normal) proportional to the solution. And lastly auxiliary electrode (AE) which is the source of current to the working electrode[169]. RE and AE are required to be conductive and stable.

Electrochemical biosensors are very attractive for point-of-care applications owing to simple design parameters, compatibility with electronics and potential for miniaturization. These biosensors also provide detection of ultra-low analyte concentration within a very low settling time. Depending on measurement techniques, there are few categories of electrochemical biosensing such as voltammetry, amperometry and impedimetry.

In voltametric measurements, the potential on the WE are varied within a certain range with respect to RE and the current between the WE and AE is monitored. Types of voltametric techniques are: *Cyclic voltammetry (CV)* – where the potential is varied in a ramp fashion between two potential values back and forth to find the current-voltage hysteresis curve during a redox reaction. CV measurements usually gets effected by non-Faradaic currents, which lowers the overall sensitive detection[170]. *Differential pulse voltammetry (DPV)* – where a pulsed potential of constant amplitude but varying dc base value after each pulse is applied at the WE and the current measurements are taken at two periods in time, just prior to the application of pulse and at the end of the pulse. These sampling periods are selected to allow the non-Faradaic currents to decay. The difference in the two current values with respect to the voltage forms the DPV curve with the peak height proportional to the concentration of the analyte. *Square wave voltammetry (SWV)* – where the potential pulses applied at the WE are similar to DPV, but the current is sampled at two time periods, one at the forward pulse and one at the reverse pulse. The SWV plot also depicts the difference of two sampled current with respect to voltage. SWV offers certain advantages over CV as the difference of two sampled current reduces the measurement of background (charging) current. SWV is often preferred over DPV as well due to its lower sweeping time, resulting in a faster scan and thus higher sensitivity.

Amperometry measurements are simpler than voltammetry, where the WE is applied with a constant potential and the generated current is observed, which is a function of the redox reaction. *Impedimetric* measurements are useful when analyte-ligand reaction process changes certain resistive or capacitive properties of electrochemical system. Electrochemical impedimetric spectroscopy (EIS) is a measurement of current response to an applied electric voltage, where the frequency of the voltage is varied, to probe the variation of complex impedance of the system.

Several literatures have reported sensitive detection of glioma biomarkers using one or more of the different electrochemical biosensing techniques. For instance, Ganganboina *et. al.*[171] recently reported an electrochemical biosensor for sensitive quantification of glioma cells derived from human serum, where isolation of glioma cells required certain pre-processing steps. Herein they prepared a complex nanocomposite consisting of sulphur doped graphene quantum dots deposited over gold nanoparticles decorated carbon nanosphere, which served the dual role of enhancement of electrochemical activity and conjugation of angiopep-2, a receptor for lipoprotein receptor protein 1 (LRP1) expressed abundantly on glioma cell surface. Using EIS over glioma cells derived from human serum, the biosensor reported a very low LOD of 40 cells/mL over a linear range of 100 – 100000 cells/mL. The device while showing great sensitivity towards glioma cell, still requires isolation of glioma cells from human serum. Another interesting study by Hu *et. al.*[172] implemented a bimetallic (Co and Ni) metal organic framework (MOF) over a gold electrode for miRNA-126 detection expressed in rat C6 glioma cells. The MOF probes were optimised at Co: Ni = 1:1 for an enhanced electrochemical response in comparison to monometallic MOF. The complementary DNA (cDNA) strands as miRNA receptors were immobilised over the MOF through metal binding with cDNA strands, as illustrated in Figure 2.5(a). Using EIS, the sensor demonstrated a LOD of 0.14 fM with a linear range of 1fM – 10 nM [Figure 2.5(c)] and a signal-to-noise ratio (SNR) of 3. The study however used synthetic miRNAs for testing and thus miRNAs extracted from cultured cell line or real biofluids may show a reduced sensor performance. A similar method using bimetallic MOF was also reported by Guo et. al., 2020[173]. Herein the MOF was made up of Cu and Ni and have a graphene like 2D structure. The metal centres exhibited mixed valences (Cu^0 /Cu^+ /Cu^{2+} and Ni^{2+}/Ni^{3+}) which endowed for electrochemical signal amplification. Using aptamer as probe, the biosensor detected the presence of C6 glioma cells and EGFR in human serum samples. Different concentrations of C6 glioma cells and EGFR were added to real human serum samples via standard addition. Analysis using EIS and CV techniques demonstrated a LOD of 0.72 fg/mL for EGFR 21 cells/mL for C6 glioma cells. The applicability of such devices under complex real fluids like serum is very promising.

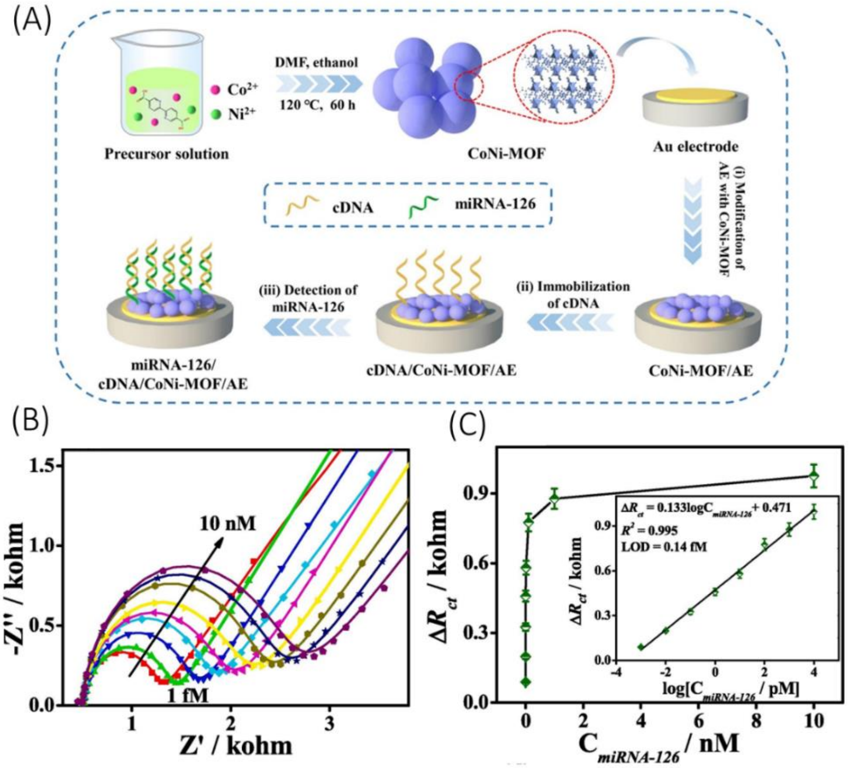

Figure 2.5: *(a) Illustration of the fabrication process of CoNi-MOF based biosensor for miR-126 detection. (b) EIS Nyquist plots for detection of miRNA-126 at different concentrations (1 fM - 10 nM) and (c) calibration curve of the CoNi-MOF based biosensor with the inset as the linear fit with respect to logarithm of miR-126 concentration. Reprinted with permission from Hu et. al., Appl Surf Sci* ***542****, 148586 (2021)[172]. Copyright 2021 Elsevier.*

Sun *et. al.*[174] demonstrated an electrochemical biosensor with peptide as receptor. A designed peptide (H−C-acp-acp-FALGEA-NH_2), is assembled for recognition of exosomal protein EGFR and EGFRvIII derived from GBM. Isolation of exosomes were done using differential centrifuge method. The biosensor used methylene blue (MB) attached with Zr-MOF for electrochemical signal amplification. EIS and SWV analysis revealed a LOD of 7.83×10^3 particles/µL with a linear range of $9.5\times10^3 - 1.9\times10^7$ particles/µL. The biosensor demonstrated high accuracy of GBM detection when tested with clinical samples. In details, lower SWV currents were observed for samples taken post-surgery than its pre surgical values. Another study by Wang *et. al.*[175] also used MB for sensitive detection of miR-21 extracted from CSF of medulloblastoma patients using target-induced redox signal amplification. The CSF samples were centrifuged initially before diluting with 40-fold PBS solution for biosensing analysis. Herein, partial cDNAs were immobilized over AuNPs loaded over a glassy carbon electrode. When the target attaches with the partial cDNA, the unhybridized part of the target miR hybridizes with a guanine-rich auxiliary strand. This auxiliary strand act as a binder for methylene blue near the sensor surface. With DPV technique, the sensor demonstrates a LOD of 56 fM and a SNR value of 3. Such biosensors can be applicable for human CSF samples as well.

Amperometry technique has been implemented by Scoggin *et. al.*[176] and Poorahong *et. al.*[177] for sensitive detection of metabolic biomarkers Glutamate (Glu) and α-Ketoglutarate (αKG) respectively. Scoggin *et. al.*[176] observed the real time glutamate uptake of CRL-2303 glioma cells with respect to normal astrocytes cell as control. The biosensor consists of platinum microelectrode array immobilized with glutamate oxidase (GlOx). GlOx catalyses Glu into αKG, ammonia and H_2O_2, which again oxidizes over the Pt electrode to release two electrons. Thus, the current value is directly correlated to the Glu concentration. The biosensor showed a LOD of 6.3 ± 0.95 µM in the basal media and 0.16 ± 0.02 µM in PBS buffer. While such devices show good sensitivity under pathological conditioned cell cultures, isolation of metabolites for liquid biopsy usually require long pre-processing steps. Poorahing *et. al.*[177] reported a similar device for αKG detection. The device consists of carbon fibre electrode with immobilized glutamate dehydrogenase (GluD). The device surface was further modified with ruthenium rhodium nanoparticles. GluD catalyses αKG into L-glutamate in presence of β-nicotinamide adenine dinucleotide (NADH) and ammonia. The quantification of αKG is done by detection of depleted NADH (NAD^+). Amperometric measurements revealed a LOD of 20 µM with a linear range of 100 µM – 600 µM and a sensitivity of 42 µA/M. The study only showed sensor performance under PBS solution and may not hold up against complex matrices like serum and plasma.

A summary of different electrochemical biosensors implemented for detection of glioma biomarkers are enlisted in Table 2.3.

Table 2.3: Summary of electrochemical biosensors for detection of glioma biomarkers.

Analysis technique	Characteristics	Biomarkers	Specimen	LOD	Linear/Dynamic Range	SNR	Reference
EIS on glassy carbon electrode	Complex nanocomposite	Glioma cells	Glioma cells diluted in PBS solution and 10% human serum solution.	*40 cell/mL*	*100 – 100000 cells/mL* (linear)	-	Ganganboina et. al. (2021)[171]
EIS on Au electrode	CoNi bimetallic MOF	microRNA 126	miR-126 extracted from rat glioma C6 cells.	*0.14 fM*	*1 fM – 10 nM* (linear)	SNR =*3*	Hu et. al. (2021)[172]
EIS and CV on Au electrode	Graphene-like 2D CuNi MOF. Aptamer as receptor.	C6 glioma cells and EGFR.	C6 glioma cell extracted from human serum samples.	EGFR: *0.72 fg/mL* C6 glioma cells: *21 cells/mL*	EGFR: *1 fg/mL – 1ng/mL* (dynamic) C6 glioma cells : *50 cells/mL –* 10^{5} *cells/mL* (dynamic)	-	Guo et. al. (2020)[173]
EIS and SWV on Au electrode	Peptide as receptor. Zr-MOF with MB.	EGFR and EGFRvIII on GBM derived exosomes	GBM-derived exosomes in Tris-HCL solution.	7.83×10^{3} *particles/µL*	9.5×10^{3}-1.9×10^{7}*particles/µL* (linear)	-	Sun et. al. (2020)[174]
DPV on glassy carbon electrode	Target-induced electrochemical redox amplification (e-TIRSA)	microRNA -21	miR-21 extracted from CSF of medulloblastoma patients.	*56 fM*	*0.5 - 80 pM* (dynamic)	SNR =*3*	Wang et. al. (2022)[175]
Amperometry on Ceramic-based Platinum	-	Glutamate	Glutamate uptake observed in cultured astrocytes (control) and	*6.3 ± 0.95 µM* in basal media	*10 – 570 µM* (linear)	-	Scoggin et. al. (2019)[176]

microelectrode array			CRL-2303 glioma cells (pathological condition)	*0.16 ± 0.02 µM* in PBS buffer			
Amperometry on Carbon fibre electrode	Electrode doped with Ruthenium-Rhodium nanoparticles.	Alpha-ketoglutarate	-	*20 µM*	*100 µM – 600 µM* (linear)	-	Poorahong et. al. (2011)[177]

2.2.3. Electronic Biosensors

Electronic biosensors can be considered as a sub-category of electrochemical biosensors; however, the underlying transduction principle are very different. Electronic biosensors are often based on the principle of field effect transistors (FETs), fabricated in a microelectronic technology. In a typical FET, the potential applied at the gate electrode modulates the conductivity, or more accurately carrier mobility, of the underlying channel. The modulation occurs primarily due to tuning of electric field by the gate electrode, resulting in subsequent attractive or repulsive coulombic interactions. FET based biosensors implements the same principle for detection of target analyte. An electronic biosensor will replace the gate electrode of an FET with a biorecognition layer (ligands). Analytes binding with the receptor layer can modulate the channel conductance and therefore results in an amplified change in current[178, 179]. The underlying amplification of FET makes them highly sensitive to analyte concentration, even at single molecule level[180]. Along with their low settling time, low power consumption and compatibility with MOS fabrication technology, electronic biosensors seem very promising for future clinical application.

The most common type of FET based transducers reported for glioma detection is silicon nanowire (SiNW). It has been theoretically established that cylindrical nanowire structures have inherent, substantial advantage over planar biosensors regarding detection of ultra-low analyte concentration under reasonable settling time[181]. The primary reason behind these orders of magnitude difference in LOD (pM vs nM) is due to the geometry of the biosensor itself. In a planar sensor, the analyte charges can influence the channel conductance from only one side, while in a cylindrical nanowire biosensor, the analyte can envelope the entire channel surface, thereby having a much higher influence over the channel conductivity.

Malsagova *et. al.*[182] reported a high-k dielectric silicon-on-insulator (SOI) nanowire biosensor for detection of a synthetic analogue of microRNA-21. Herein, complementary oligonucleotide probes were used as receptor, which were covalently immobilized over the nanowire surface through silanization process. High-k dielectric coating of Al_2O_3 (2 nm) and HfO_2 (8 nm) were applied over the SOI nanowire for improved stability. The biosensor reported a very low LOD of 0.1 fM with only 10% alteration in current value over 8 hours of testing under K phosphate buffer. However, the paper didn't report any tests with actual biofluids. Li *et. al.*[183] reported an array of 120 silicon nanowires for sensitive detection of tumour biomarker ctDNA. The specific gene target was PIK3CA E542K ctDNA whose mutation plays a pivotal role in promoting GBM pathogenesis[184]. The oligonucleotides of the ctDNA sequences were prepared synthetically. The paper reported a remarkable LOD of 10 aM over a linear range of 0.1 fM to 100 pM when tested with ctDNA spiked in healthy human serum [Figure 2.6(f-g)]. When tested with one or two base mismatched target sequences, the device reported a significant level of signal decrement, implementing the specificity of the device at single nucleotide level. Such devices are very promising for high accuracy clinical applications as they can withhold real biological fluids. Similar silicon nanowire biosensor was reported by Wu *et. al.*[185] demonstrating the sensitive detection of $BRAF^{V599E}$ gene mutation (now designated as $BRAF^{V600E}$)[186], which is present in higher percentage in epithelioid GBMs[187]. The 60 nm wide SiNW biosensor reported a LOD of 0.88 fM with a relative standard deviation (RSD) of only 12%. The target synthetic oligonucleotides in this study were tested only with PBS solution and not with any serum or plasma samples.

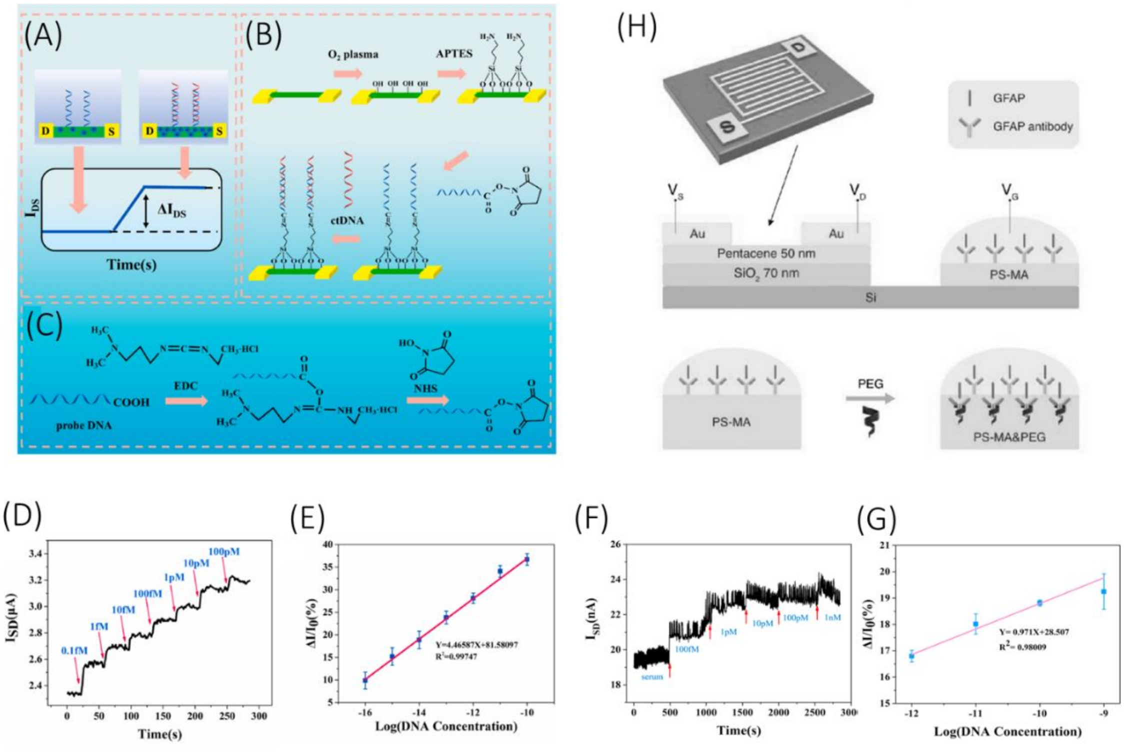

Figure 2.6: *(a) Working principle of the SiNW-array FET biosensor. (b) Stepwise process of fabrication of SiNW-array FET biosensor. (c) Carboxyl groups activation by EDC/NHS. (d) The real-time response and (e) calibration curve of the SiNW-array FET biosensor for different concentrations of ctDNA. (f) The real-time response and (g) calibration curve of the SiNW-array FET biosensor for different concentrations of ctDNA in human serum. (g) Device architecture of the extended gate OFET biosensor for sensitive detection of GFAP. Scheme (a-g) are reprinted with permission from Li et. al., Biosens Bioelectron* ***181****, 113147 (2021)[183].Copyright 2021 Elsevier. Scheme (h) is reprinted with permission from Song et. al., Adv Funct Mater* ***27****, 1606506 (2017)[188]. Copyright 2017 John Wiley and Sons, Inc.*

Graphene FETs (gFET) have also been explored for biosensing applications owing to their high charge carrier mobility and high electronic sensitivity conveyed by surface charge[189, 190]. A typical gFET current-voltage characteristic consist of a current minimum at Dirac voltage point. Introduction of any charged species for partial coverage of the graphene surface shift the Dirac voltage point proportional to the concentration of the species. Xu *et. al.*[191] demonstrated an on-chip monolayer graphene FET device for accurate quantification of metabolic biomarker GFAP derived from human plasma samples. The plasma samples were centrifuged and frozen prior to testing, but no isolation step is mentioned by the study. The on-chip gFET biosensor array contains two sensing areas, each with six gFET devices and one reference gold electrode integrated on chip for low power liquid-based gating. The sensing areas were immobilized with anti-GFAP antibodies. The LOD of the device is reported to be 400 aM when tested in buffer and 4 fM when tested with plasma. The sample-to-response time of the device was less than 15 mins. On comparing the biosensor performance factors like sensitivity and response time against other standard quantification methods like single-molecule array (Simoa) and ELISA, it outperformed both of them. Another gFET device has been developed and reported by Ban *et. al.*[192] for direct DNA methylation profiling. The device incorporates a DNA tweezer probe, consisting of a normal strand and a weak strand, for sensitive detection of targeted gene. When the target gene comes near the vicinity of the probe, it hybridizes with the normal strand by displacing the weak strand due its high binding affinity. At picomolar level concentration, the sensor was able to differentiate a non-methylated DNA from a methylated one with eight methyl cytosines (MDT8). The device also reported to differentiate between MDT2 and MDT2a and MDT2b, where the two cytosine groups are present at different locations, further demonstrating the high sensitivity of the biosensor to determine the position of methylation as well. Such biosensors can be applied for methylation screening of ctDNA derived from bodily fluids, however biofluidic matrices may lower the screening efficiency.

Organic FETs (OFET) are also an interesting option for biosensing applications owing to their low-cost simple fabrication and biocompatibility with biofluids. Song *et. al.*[188] reported an extended gate OFET biosensor for sensitive detection of GFAP. The extended gate structure (gate far away from the transistor body) is often used in organic transistors to protect the organic layer from prolonged exposure and damage to moisture. A thin layer of pentacene has been used in this case as a p-type semiconductor as shown in Figure 2.6(h). The extended gate structure is constructed with a PS-MA layer decorated with anti-GFAP antibodies and polyethylene glycol membrane (PEG). The significance of PEG in the biolayer is to address a key issue in electronic biosensing associated with Debye screening length. The formation of a small electrical double layer (characteristic length λ_D) on the surface of the biosensor shields the influence of charged biomolecules above the characteristic length, thereby reducing the sensitivity of the device and prohibiting its application under high salt concentration. Presence of negatively charged PEG at the biolayer extends the effective characteristic length of the double layer, thereby allowing detection of GFAP at higher PBS concentration. The device reported sensitive detection of GFAP at 0.1X PBS solution (~15 mM) higher than typical 0.01X PBS solution used for such applications. These devices can be applied directly to biological fluids which usually consist of high salt concentration with minimal dilution. The sensor also reported a LOD of 1 ng/mL over a dynamic range of 0.5 ng/mL to 100 ng/mL, however the reported sensor performance was done at a lower gate voltage, which makes it susceptible to noise interference and lower SNR value. When tested against other proteins of similar size and charge, the device shows great specificity towards GFAP. Another study by Selvaraj *et. al.*[193] reported an electrolyte gated OFET with sensitivity towards miRNA-21-5p. The required oligonucleotide sequence is synthesized as per the miRNA-21-5p sequence. The device consists of two gold electrolyte gate electrode, one immobilized with thiolated complementary probes (G2) and another with 2-Mercaptoethanol (ME) monolayer (G1). Before the OFET detection, G2 is first incubated in a buffer containing target analyte miR-21-5p. Upon testing the OFET driven by both the gate electrode separately, G2 showed a variation of OFET threshold voltage with different concentration of target, while G1 acted as a control. This allows the differential response measurement between the sensing and reference electrodes. Upon testing, the device reported an excellent LOD of 35 pM over a dynamic range up to 300 pM. Test with real biofluid may increase the LOD value obtained in this study.

A simple device consisting of aluminium interdigitated electrodes over a silicon wafer is recently reported by Li *et. al.*[194] for detection of microRNA-363. The oligonucleotide is synthesized as per miR-363 sequence. The interdigitated structure was fabricated using standard photolithography process and complementary probes of miR-363 was immobilized over the electrodes using gold nanoparticles as the linker. The sensor working principle is based on the dipole moment between the two electrodes, where the ionic movements near the surface changes the dipole moment upon molecular interaction. The device reported a LOD of 10 fM and showed good linearity over the range 1 fM to 100 pM, when tested with miR-363 spiked in human serum.

Electronic nanobiosensors can attain remarkable LOD at attomolar level. However fundamental problems like Debye screening length limitations and instability of silicon devices under different biofluids limits the application of such sensors, requiring further research targeting reliability of these devices. Table 2.4 summarizes different electronic biosensors implemented for detection of glioma biomarkers.

Table 2.4: *Summary of electronic biosensors for detection of glioma biomarkers.*

Type of electronics	Biomarkers	Specimen	LOD	Linear/Dynamic Range	RSD	Reference
SOI Nanowire coated with high k dielectric material	microRNA-21	oDNA: synthetic analogue of miR in K phosphate buffer;	10^{-16} *M*	10^{-17} *M* - 10^{-14} *M*	-	Malsagova et. al. (2018)[182]
Si Nanowire	PIK3CA E542K ctDNA	Oligonucleotides in PBS solution. ctDNA spiked in human serum.	In PBS:*10 aM* In serum sample*: 10 fM.*	In PBS: *0.1 fM – 100 pM* (linear) In serum sample: *1 pM – 1 nM* (linear)	-	Li et. al. (2021)[183]
Si Nanowire	$BRAF^{V599E}$ ($BRAF^{V600E}$)	Target DNA with respective mutation in PBS solution.	*0.88 fM*	*10 fM – 100 pM* (dynamic)	RSD: *12%*	Wu et. al. (2009)[185]
Graphene FET	Glial Fibrillary Acidic Protein (GFAP)	GFAP extracted from human blood samples and diluted in PBS.	In buffer: *20 fg/mL (400 aM)* In human plasma: *231*	In buffer: *20 fg/mL – 200 fg/mL* (linear) In human plasma: *230 fg/ml – 230 pg/mL.* (linear)	-	Xu et. al. (2022)[191]

			fg/mL (4 fM)			
Graphene FET	Methylation profiling	Methylated DNA in buffer solution.	-	-	-	Ban et. al. (2020)[192]
Extended Gate Organic FET	Glial Fibrillary Acidic Protein (GFAP)	GFAP in 0.1X PBS solution	*1 ng/mL*	*0.5 ng/mL – 100 ng/mL.* (dynamic)	-	Song et. al. (2017)[188]
Dual Gate OFET	microRNA-21	miR-21 in buffer solution	*35 pM*	*Up to 300 pM (dynamic)*	-	Selvaraj et. al. (2021)[193]
Interdigitated electrode	microRNA-363	miR-363 spiked in human serum samples	*10 fM*	*1 fM – 100 pM (linear)*	-	Li et. al. (2022)[194]

2.3. Future Research Perspective

The detection and quantification of various biological markers related to cancer have undeniable significance in personalised medicine. Current biosensor-based detection technologies can provide high sensitivity towards a particular biomarker at an ultra-low analyte concentration, which is a promising step forward. They can outperform numerous standard biomarker detection technologies, like polymerase chain reaction (PCR), RTPCR, ELISA and so on. Depending on the type of application, these biosensors are required to pass certain criterion like high sensitivity, specificity, high throughput, multiplexed analysis, etc. before they can be applied to actual clinical platforms. Different biosensing applications include point-of-care (POC), liquid biopsies and implantable devices. Current standing and future perspective of these biosensors based on particular application has been described in Sections 2.4.1 – 2.4.3.

2.3.1. Point-Of-Care (POC) Devices

POC devices are usually handheld devices which can quickly detect the occurrence of certain pathological condition by testing a biofluid directly or with minimum pre-processing. One of the most successful and widely available POC devices is the pregnancy test kit, which are lateral flow assay based colorimetric sensors for quantified detection of hCG in urine samples. A POC device in general requires to be highly sensitive, reliable, rapid, portable, have the ability to detect analyte in a complex medium with the medium is required to be sampled in a minimally invasive manner. In terms of glioma, biomarkers were found from readily available biofluids like urine or saliva[5] and can be used for POC applications. The required sensitivity and rapid detection can be achieved by optical biosensing, however low signal intensity could increase the false positive rates. Electrochemical and electronic biosensors can also achieve very low LOD (at fM- aM level), rapid detection and their compatibility with CMOS fabrication systems also allows cost reduction and swift miniaturization, making them a promising candidate for POC applications. However, certain fundamental problems in electronic biosensors such as Nernst limit, Debye screening length and degradation of silicon in continuous presence of salt currently limits their reliability and thus practical applications. Nonetheless, their ability for ultra-low aM level detection still makes them an attractive option.

2.3.2. Liquid Biopsy

Liquid biopsy is a very helpful tool in cancer management by allowing a dynamic view of the tumour prognosis, specifically for glioma where tissue biopsies are often positionally complicated. Biosensor technologies can allow liquid biopsies to be a point-of-care treatment option. Simultaneous analysis of multiple biomarkers in real time is an urgent requirement in glioma management process and can be achieved using multiplexed biosensing. Most current biosensors are designed for detection of only a couple of biomarkers at most. However, a larger amount of information can be collected from single sample through multiplexing. For accurate detection and prognosis of glioma, multiplexing is necessary as multiple biomarkers with low predictive co-efficient can be combined to achieve better precision, resulting in personalized medical treatment and overall better management of disease. Microfluidic biosensors hold great promise in terms of high throughput multiplexed analysis. It integrates the sensitive detection of biomarkers via electrochemical or electronic biosensing platforms with microfluidic separation and mixing techniques. Microfluidics-based lab-on-chip devices open new direction in designing novel approaches for multiplexed, scaled-down automated biosensors for monitoring of glioma. These platforms can also be explored to study how different biomarker effect the prognosis of cancer at different stages, thereby improving our understanding of cancer related processes. Overall, POC based liquid biopsy platforms require multiplexed, high throughput biomarker analysis, which have not been achieved with a single biosensor platform, but can be implemented by integrating microfluidic technologies with it.

2.3.3. Implantable Devices

Implantable devices are a moon-shot target for current biosensor technology due to plethora of limitations ranging from continuous monitoring to biofouling. Taking the simpler problem first, continuous monitoring of biomarkers hasn't been explored much in the literature. A biosensing device dies after certain number of use due to saturation of available receptor probes on the surface, thus requiring surface regeneration or cleaning via external methods like flushing. Some receptor-analyte bonds like antibody-antigen are so strong that they cannot be separated in some cases even with flushing. However, an implantable biosensor is required to have a longer lifetime, thus having the ability to auto-clean its surface is essential. Recent study by Fercher *et. al.*[195] showed that this can be achieved in antibody-protein interaction by changing the antibody protein sequence at specific binding sites. This allows the antibody to have a weakened interaction with the target protein, thereby allowing reversible reaction between them. The key is to increase the reverse rate constant without effecting the forward rate much. Such approaches are easier to implement in nucleic acid sequences due to their sequence simplicity and can be used to design specific receptors for implantable biosensors. This could lead to a great first step towards implantable biosensors which can revolutionise the current medical system.

2.3.4. Challenges related to complex biofluids

Biosensing of specific biomarkers in real biofluids are often advantageous in terms of point-of-care analysis. Depending on the complexity of biofluid, biosensors are required to achieve higher levels of sensitivity in order to detect specific biomolecules. For example, detection of biomolecules is relatively easier from saliva than it is from urine, since saliva contains much less biological “noise” to interfere with the desired signal[196]. Therefore, as the complexity of a biofluid matrix increases, the necessity of performing pre-processing steps also increases in order to reduce the presence of non-specific biomolecules in the sample. Systematic biomarkers for glioma (or any other form of cancer) are shown to be present in all levels of biological fluids starting from blood and cerebrospinal fluid to lymph to secondary biofluids such as urine, sweat and saliva. However, the levels and diversity of such biomarkers decreases as they reach from a complex biofluid like blood to relatively simpler biofluids like sweat or saliva.

Biological “noise” originates from the non-specific binding of interfering biomolecules on the surface of the biosensor. Depending on the transduction principle, signal may originate from these biomolecules as well and get amplified, interfering with the actual signal from specific binding. Current biosensing technology relies on functionalization of sensor surface with receptor molecules which are highly specific to the biomarker of interest. However, a full coverage of the biosensor surface with receptor molecules is unlikely to be achieved, leaving spaces for non-specific bindings. Therefore, anti-fouling of the surface is generally done to suppress non-specific binding of interfering molecules. Some examples of anti-fouling treatment include bovine serum albumin (BSA)[197] and casein, which are known to block non-specific protein binding. Other than that polyethylene glycol[198–200] and zwitterions[201] can also be used as anti-fouling coating. Such coatings have shown improved sensitive performance and lower limit of detection when tested under complex biofluids such as plasma or serum. The width of an effective anti-fouling layer with respect to SERS is required to be around 10-20 nm. These typically pushes the receptors away from the hotspot region, thereby reducing the overall enhancement factor of the sensor. Currently, there is no universal method for anti-fouling a biosensing surface, with specific treatment methods working well for specific transduction type.

2.4. Summary

This literature review covers the recent advances made for label-free detection various glioma biomarkers and to the best of our knowledge, it is the first review targeting glioma biosensors. Given the relative rarity of glioma in comparison to other forms of cancer like lung cancer and breast cancer, the reported number of literatures related to glioma biomarker detection were also less. However, given the poor prognosis and survival rate, glioma biosensors should be of given greater importance. In this review, we reported key literatures from different peer-reviewed journals that made significant development in glioma detection. We explored different biosensing schemes ranging from optical, electrochemical and electronics and analysed their pros and cons in perspective of future research direction. We also did a brief literature survey analysing the plethora of biomarkers reported to be associated with glioma and summarized a few important of them based on their frequency in available papers. Overall, current biosensors have demonstrated significantly high sensitivity and specificity with ability to detect biomolecules at ultra-low concentration, however certain other characteristics such as stability, multiplexing, specificity under real biofluids are still some of the few problems that need to be worked on before they can be applied on clinical fields. We concluded our review with a short perspective of future research specific to different application fields. It is expected that this review will assist researchers to have a better understanding of the current state-of-the-art biosensing platforms and motivate them to develop novel approaches for biosensing glioma biomarkers for better diagnosis, prognosis and therapeutics.

Chapter 3

Modeling and Simulation of nanoparticle-based SERS biosensing platforms

3.1. Introduction

Raman scattering is a useful phenomenon which has found plethora of applications in various chemical and biological analysis[202]. Since Raman spectroscopy relies on signature Raman peaks originating from vibrational energies of different chemical bonds, one can specifically detect and analyse different functional groups present in an organic molecule. Raman spectroscopy can also provide quantitative information about the sample molecule[203], and thus can be very useful for biosensing applications.

Surface enhanced Raman scattering or SERS provides amplification of these Raman signals via metallic nanostructured surface modification. The technique relies on electromagnetic field enhancement via localised surface plasmons. The electric field enhancement allows the spontaneous Raman spectroscopy to detect even weak signature peaks, thereby facilitating highly sensitive and specific biosensing. Different studies have been done in with respect to SERS biosensing implementing noble metal nanostructures such as gold and silver. Different types of nanostructures have been implemented in literatures ranging from simple spherical nanoparticles[204–206] to nanorods[207, 208] or even complex nanostructures like nanobowtie[160, 209, 210] or nanoflower[211].

Amplification or enhancement factor of a SERS biochip modified with metallic nanostructures depend on various parameters such as nanostructure size and shape, interstructure nanogaps and incident wavelength[22–25]. All these factors influence the resonance of the localised surface plasmon, which provides the local electric field enhancement. Therefore, it is necessary to determine correct design parameters of a SERS biochip beforehand in order to maximize its sensitivity. In this present study, we discuss a simple model implementation of nanoparticle-based SERS biosensing platform in COMSOL Multiphysics[34]. A comprehensive simulation study is performed with both gold and silver material, taking into consideration different single, multiple nanospheres and periodic nanosphere system. Polarization dependency of enhancement factor has been studied in order to understand the effect of orientation in regularly structured SERS platforms. An interesting phenomenon of local hotspot switching is observed in multiple nanosphere systems trimer and tetramer, which hasn't been reported in literature yet. The implemented model could be very useful to optimize design parameters of a SERS biochip, and can be easily extended to various nanostructures, both simple and complex.

3.2. Near field simulations and optimization of nanoparticle systems

Finite element modeling of nanoparticles has been performed using COMSOL wave optics module[34]. The model is developed by creating a spherical geometry of nanometre radius as shown in Figure 3.1. In order to truncate the simulation physical domain, a perfectly matched layer (PML) is introduced and a scattering boundary condition is applied on the inner surface of the layer shell. The perfectly matched layer is commonly used in RF models as boundary condition which provides a reflectionless interface for the outgoing wave at all incident angles. A background wave is defined as a TM polarized wave with travelling in the positive x-direction with electric field polarized along the z-direction and unit amplitude ($E_{0z} = 1\ V/m$), as shown in Equation 3.1. Amplitudes in other directions are considered to be zero.

$$\vec{E} = E_{0z}\exp\left(-jK_0 x\right)\hat{z} \tag{3.1}$$

Here, K_0 is the wave number in free space. Simulations were performed over isolated nanospheres and multiple nanosphere systems in the wavelength domain. The numerical model in COMSOL Multiphysics wave optics module solves the Maxwell's equation with respect to scattered electric field E_{sca} as given in Equation 3.2.

$$\nabla \times \left[\frac{1}{\mu_r}\left(\nabla \times E_{sca}\right)\right] - K_0^2\left[\left(\varepsilon_r - \frac{j\sigma}{\omega\varepsilon_0}\right)\right]E_{sca} = 0 \tag{3.2}$$

Here, μ_r is the relative permeability and ε_r is the relative permittivity of the medium, σ is the conductivity of the material, ω is the angular frequency and ε_0 is the permittivity of free space. Materials were defined for each respective geometric domain. For the spherical domain around the nanosphere(s), the medium is defined as air with real refractive index (n) of 1 and imaginary refractive index (k) of 0. For the nanosphere medium, gold and silver were defined. Since the complex refractive index of noble metals varies with the incident radiation wavelength, a refractive index model is required to be defined. For our simulations, we used the Brendel-Bormann model of refractive indices for Au and Ag at different wavelengths as described in Rakić et. al. (1998)[212] and predefined in the material library of COMSOL Multiphysics.

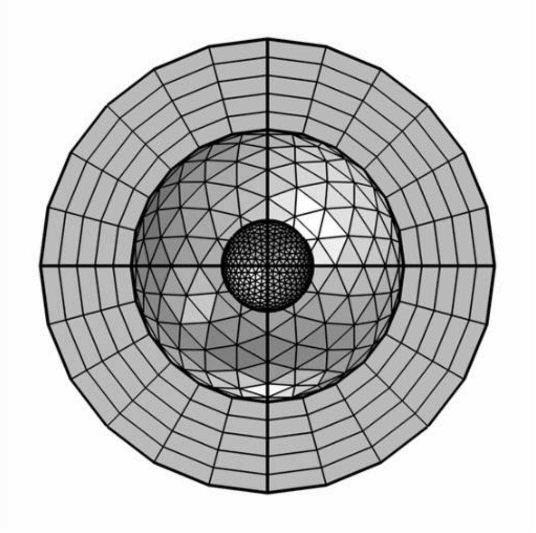

Figure 3.1: *Geometry and mesh of single nanosphere with physical domain and perfectly matched layer.*

The enhancement factor of a nanoparticle-based SERS system varies according to the size of the nanoparticles and the gap between them. For maximum electric field enhancement, the localised plasmons are required to resonate with the incident wavelength and the resonating frequency of a nanoparticle depends on its size. Again, the gap length between two nanoparticles influences the extend of dipole coupling, thereby effecting the enhancement factor of the SERS hotspot. Smaller gap lengths with larger nanoparticles around them is expected to have higher SERS enhancement factor. However, larger nanoparticles decrease the number of SERS hotspot per unit area of the biosensor surface. Larger nanoparticle may not necessarily resonate with the incident wavelength as well. Thus, optimization with respect to nanoparticle size and gap length is required to maximize the enhancement factor of a SERS biosensing system.

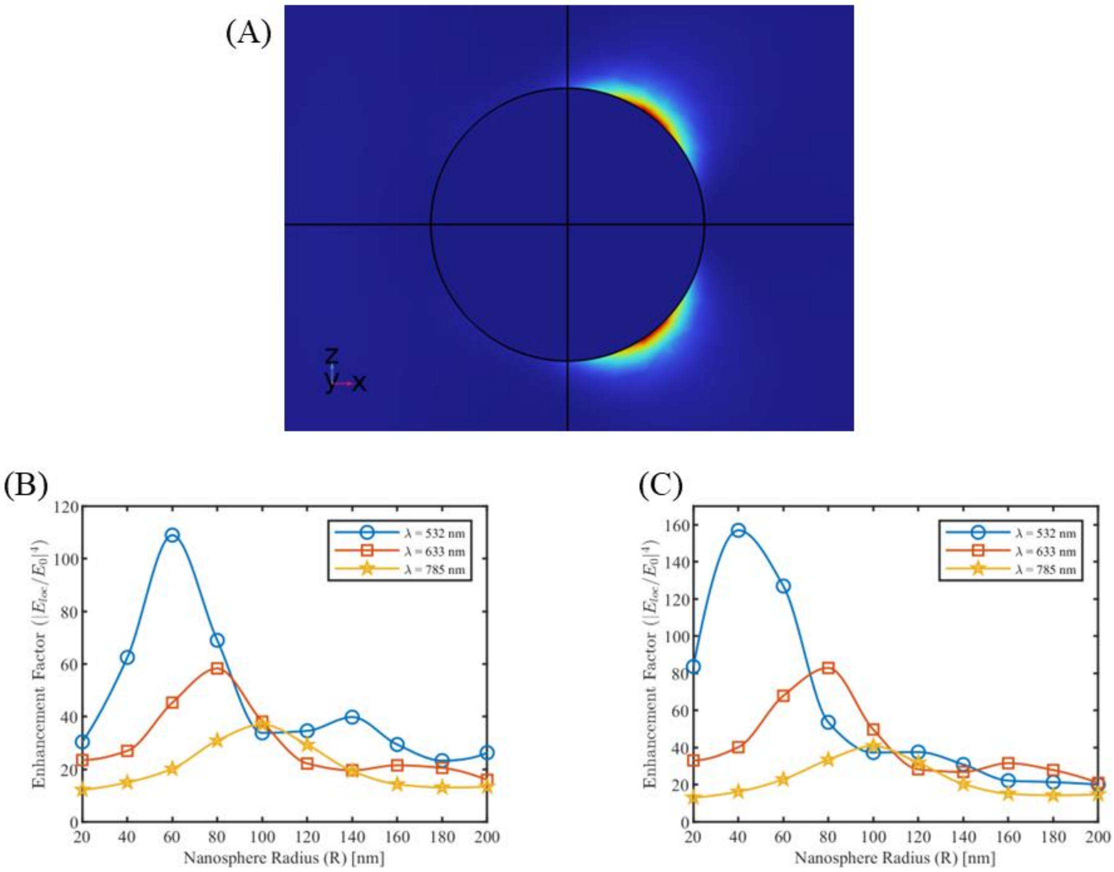

Figure 3.2: *(a) Enhancement factor of a single nanosphere. Enhancement factor plots at different Raman wavelengths for single nanosphere of (b) silver and (c) gold.*

Simulations were carried out for a single silver and gold nanosphere of different size, bounded with the perfectly matched layer in the physical domain. Raman wavelengths of 532 nm, 633 nm and 785 nm were selected for our simulations. The enhancement factor is defined as the fourth power of normalised maximum local electric field. Since we defined a background wave of unity amplitude, the fourth power of local electric field will suffice for the enhancement factor calculations. This definition of enhancement factor is also known as single molecule enhancement factor[157]. For silver nanosphere, a maximum enhancement factor of 109 is calculated for a radius of 60 nm at 532 nm wavelength. As shown in Figure 3.2(b), the enhancement factor peaks at different values of radius for different wavelengths, demonstrating the resonance effect of surface plasmons. Also, the value of peak enhancement factor decreases for increasing Raman wavelengths, suggesting that 532 nm might be the best wavelength to be applied for isolated silver nanoparticle. Similar results were obtained for single gold nanosphere simulation at different Raman wavelengths as shown in Figure 3.2(c).

Single nanosphere does not generate much enhancement factor (range ~10^2) to have practical applications. Simulations were extended to multiple nanosphere systems, to include the effect of dipole coupling. The geometry of the nanosphere dimer is defined such that the common axis aligns with the polarization (z-direction) of the background E-field (Figure 3.3(a)). Simulations over nanosphere dimers for different radius and gap lengths demonstrated the effect of SERS hotspot with enhancement factors in the range of $10^6 - 10^9$. Selected simulation results for silver and gold nanosphere dimer for wavelengths 633 nm and 785 nm respectively are shown in Figure 3.3(b, c), and rest of the simulation results are presented in Figures S2-S3 of Supplementary Information. As indicated in Figure 3.3(b, c), the effective dipole coupling decreases with increase in gap length, which decreases the enhancement factor. A maximum enhancement factor of $\sim 10^9$ occurred in case of silver nanodimers for a gap length of 1 nm over a radius range of 40-120 nm. Similarly for gold nanodimers, the maximum enhancement factor reached $\sim 10^9$ for gap length of 1nm over a radius range of 60-140 nm.

Orientation of the nanodimers with the polarization of the background radiation has significant effect on the enhancement factor. Maximum enhancement factor is observed when the nanodimers are aligned with the direction of polarization (z-axis in this case). When the dimers are rotated in the y-z plane (Figure 3.4(a, b)), the enhancement factor of the hotspot decreases exponentially, with complete loss of the hotspot observed at perpendicular alignment (Figure 3.4(b)). For single nanosphere, we observed that the area of maximum localized electric field occurs in the plane of electric field polarisation, and when two such areas come to close proximity, as in case of nanodimers, the effective dipolar coupling of surface plasmons results in very high enhancement of local electric field. With rotation of the dimer system, the effective plasmon coupling decreases, with no coupling at perpendicular alignment. As per hybridization theory[213], a high dipolar electric field is generated when polarization charges of opposite type on the nanosphere surface comes close to each other in case of perfect alignment, and no such field is generated for perpendicular alignment as shown in Figure 3.5. Such phenomenon of polarization dependent SERS is important point for SERS biosensing surfaces with regular array of nanostructures, as alignment of polarization with the array direction required to achieve maximum enhancement.

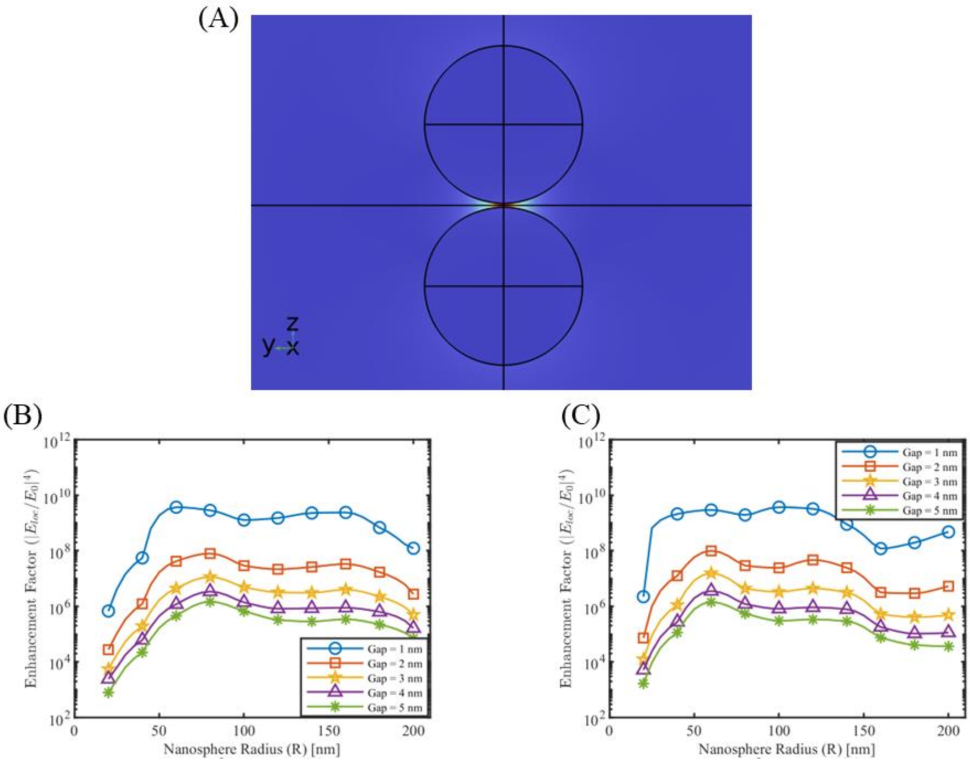

Figure 3.3: *(a) Electric field of a nanodimer system. Enhancement factor plots of nanodimer system (b) gold at λ = 785 nm and (c) silver at λ = 633 nm.*

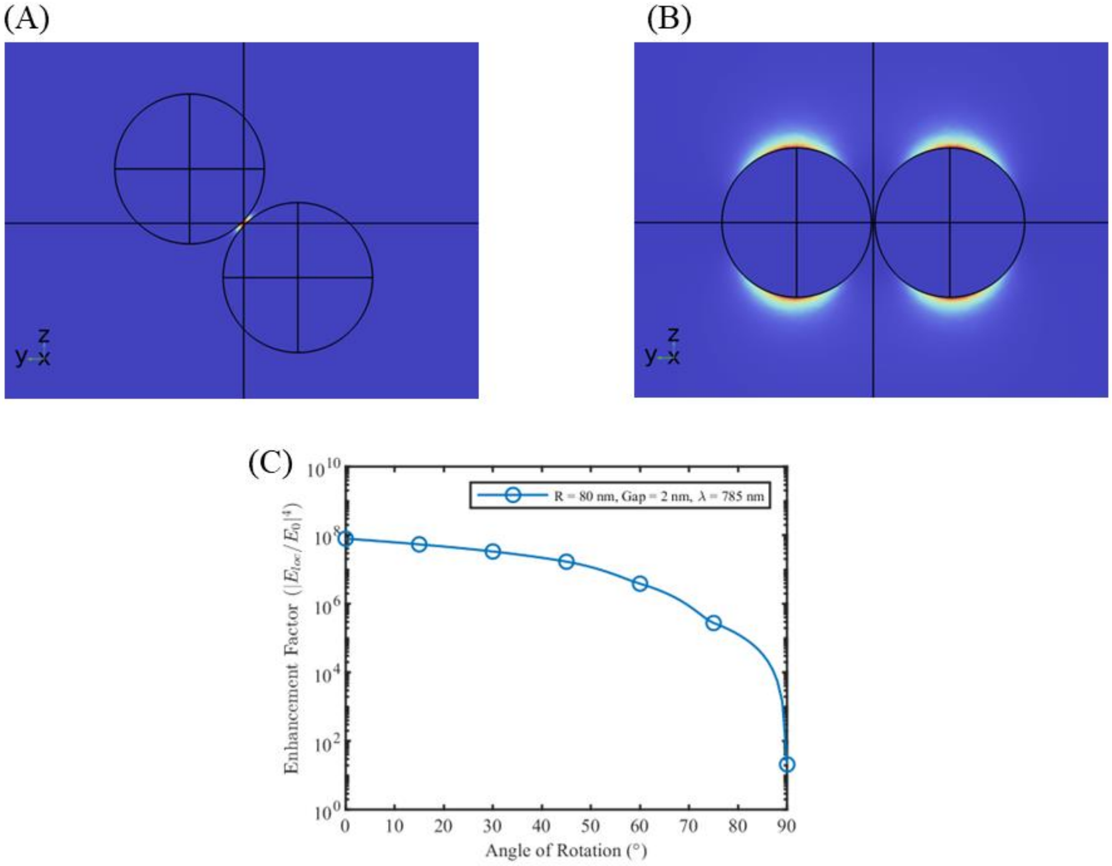

Figure 3.4: Enhancement factor of nanodimer system at orientation (a) 45° and (b) 90° with respect to direction of incident polarization. (c) Enhancement factor variation with orientation for gold nanodimers of radius 80 nm, gap 2 nm and λ = 785 nm.

Multiple nanosphere systems with three (trimers) and four (tetramers) nanospheres were simulated similarly taking care of different orientation possible with respect to the direction of background wave polarization. For nanotrimers, three nanospheres were placed on the three vertices of an equilateral triangle, maintaining same gap length between them. As shown in Figure 3.6, two possible orientations are possible in this case. Figure 3.6(a) shows the orientation where there is a partial plasmonic coupling between nanosphere 1-2 and nanosphere 1-3, but no coupling between nanosphere 2-3. We call this orientation as △. Figure 3.6(b) can be obtained by simply rotating the orientation △ anti-clockwise in the z-y plane by 30°. In this case, there is a full plasmonic coupling between nanosphere 1-2 and negligible coupling with nanosphere 3. We call this orientation as ▷. Enhancement factor plots for silver and gold nanotrimers at 633 nm and 785 nm at orientation △ are shown in Figure 3.6(c, d) with rest of the simulation results depicted in Figures S4-S7 of Supplementary Information. Nanosphere tetramers were modelled by placing four nanospheres on the vertices of a rhombus. This geometry allows the formation of maximum five possible hotspot locations. In case of nanotetramers, three possible orientations are possible as shown in Figure 3.7 and accordingly two to five hotspot regions can activate at a time. Enhancement factor plots for selected cases are shown in Figure 3.8 with rest of the simulation result included in Figures S8 – S11 of Supplementary Information. Similar to nanodimers, a maximum enhancement factor in the range of $10^5 - 10^9$, despite adding more nanospheres in the system. All this due to dipolar misalignment with the direction of polarization at particular orientation which does not allow full plasmonic coupling of all the nanospheres. Nonetheless, a nanotrimers and nanotetramer system generate multiple hotspots which should contribute to better sensitivity of the overall sensor system.

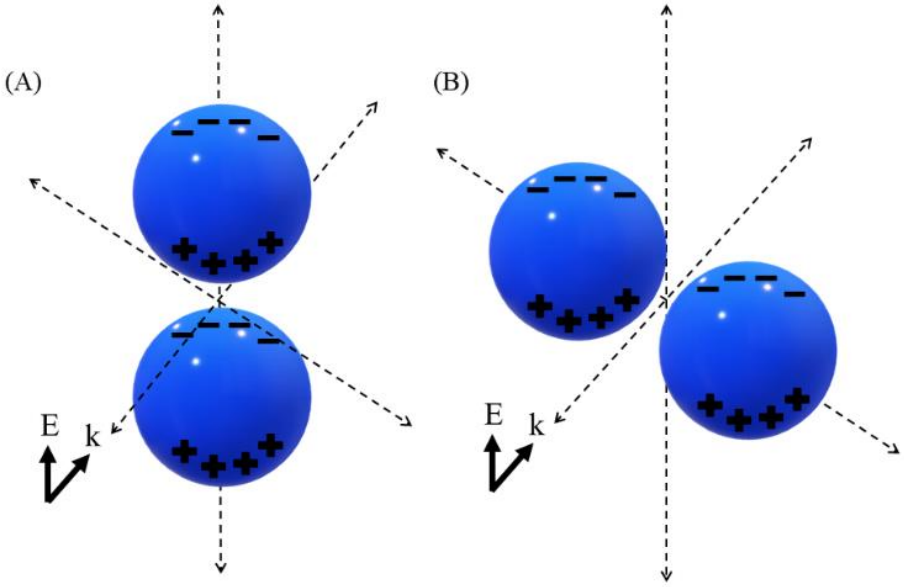

Figure 3.5: *Polarization charge of nanodimer system at different orientation: (a) perfectly aligned with the direction of polarization and (b) perpendicular alignment with the direction of polarization.*

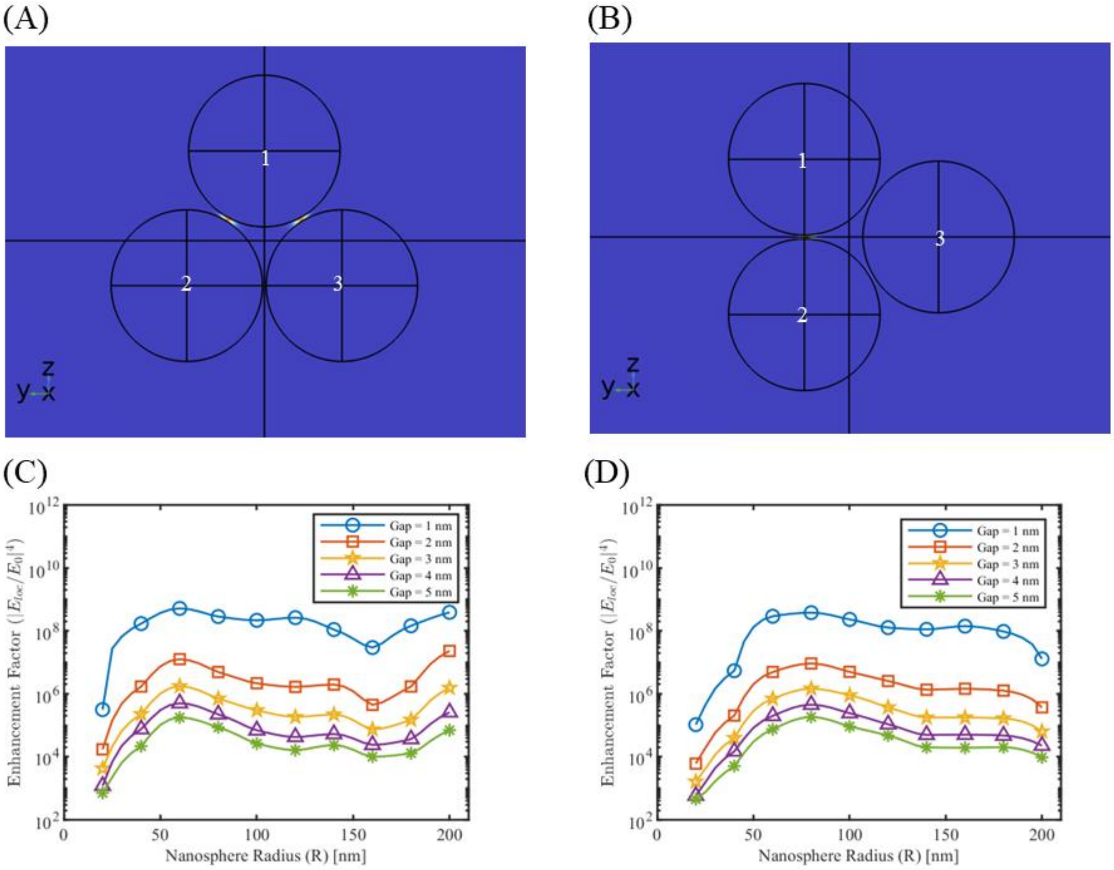

Figure 3.6: *Enhancement factor of nanotrimer system for orientation (a) △ and (b) ▷. Here polarization is in the positive z-direction. Enhancement factor plots for nanotrimer system orientation △ for (c) silver at λ = 633 nm and (d) gold at λ = 785 nm.*

Switching between multiple hotspots were observed in case of nanotetramers orientation ◁▷, specifically either of hotspot 1,2,3,4 or hotspot 5 (Figure 3.9) gets activated for particular combinations of nanosphere size, gap length and wavelength. In order to understand the hotspot switching, simulations were performed with silver medium, probing into individual hotspot enhancement factor. The enhancement factor for hotspot 1 and hotspot 5 is probed for all combinations of nanosphere radius, gap lengths and wavelengths. Figure 3.10(a) shows

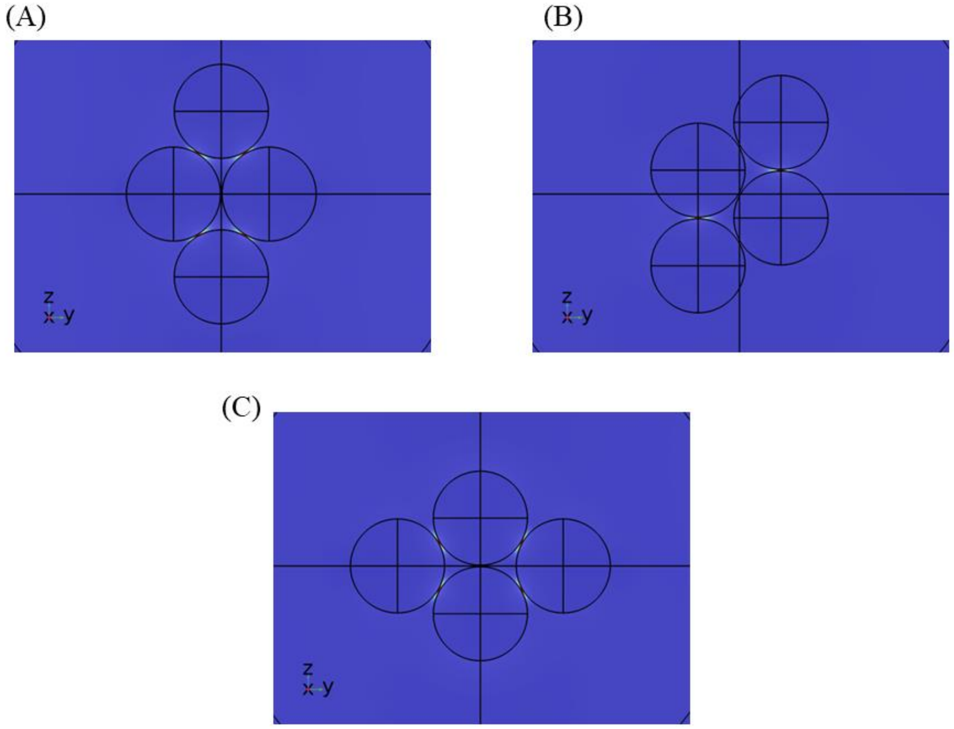

Figure 3.7: *Electric field of nanotetramer systems at different orientations (a) ◊ (b) | | and (c) ◁▷. The direction of polarization is positive z.*

that hotspot 5, or the hotspot between two nanospheres perfectly aligned with the polarization direction, has a tendency to switch off for a particular radius value. As for 532 nm wavelength this switch off happens for a radius of 60 nm or 80 nm depending on gap length. Enhancement factor for hotspot 1 on the other hand remain fairly constant for these radius values. Similar results were obtained for 633 nm and 785 nm wavelengths, where the radius window of switch off shifted to larger radius value (Figures S14, S15). This switch off could be a result of multiple resonance pattern between the nanosphere system, and a better explanation require understanding the plasmonic hybridization between multiple nanosphere in this system. Similar switch off patters were observed for nanotrimers system orientation ▷ as well (Figures S12, S13), however the extend of enhancement factor reduction is much less than that of nanotetramers, suggesting that the nanospheres on the sides influences the switching off. We also performed an orientation sweep study on both nanotrimers and nanotetramers system to realise that the hotspot switching makes the enhancement factor of the systems fairly polarization independent, as shown in Figure 3.10(c, d).

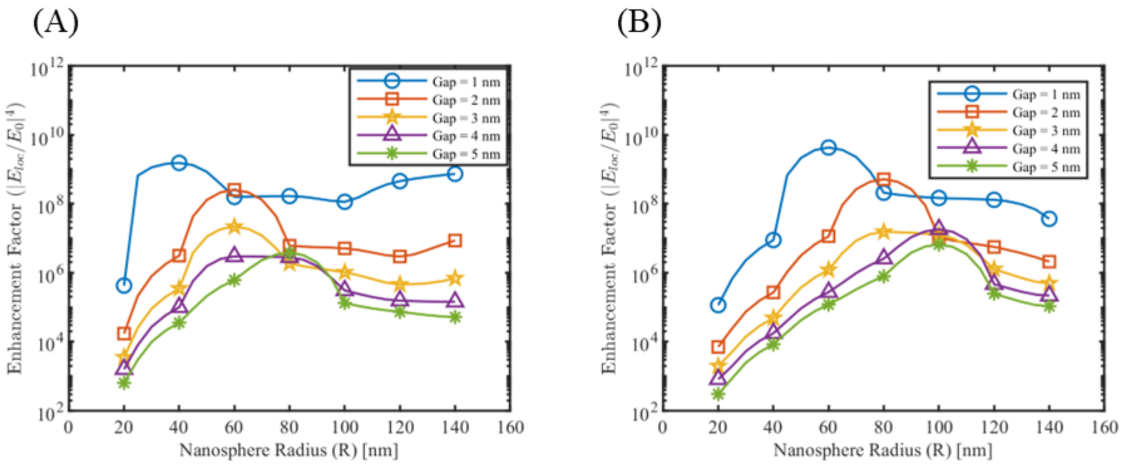

Figure 3.8: *Enhancement factor plots for nanotetramer system orientation ◁▷ for (c) silver at λ = 633 nm and (d) gold at λ = 785 nm.*

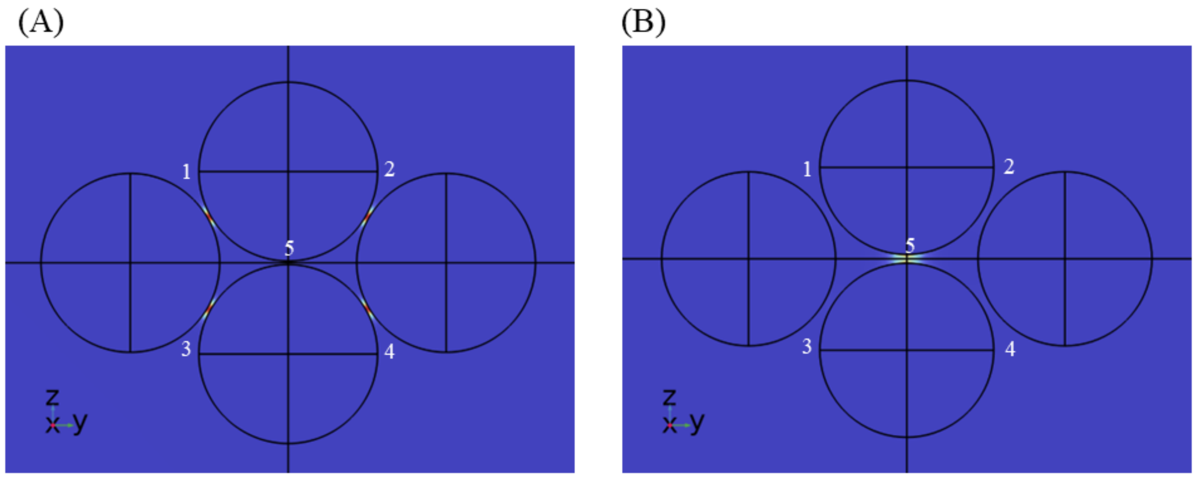

Figure 3.9: *Nanotetramer system at orientation ◁▷ showing the phenomenon of hotspot switching. (a) Hotspot 1-4 are on, hotspot 5 is off for silver nanotetramer radius 100nm, gap of 4nm and λ = 633 nm. (b) Hotspot 1-4 are off, hotspot 5 is on for silver nanotetramer radius 40 nm, gap of 4 nm and λ = 633 nm.*

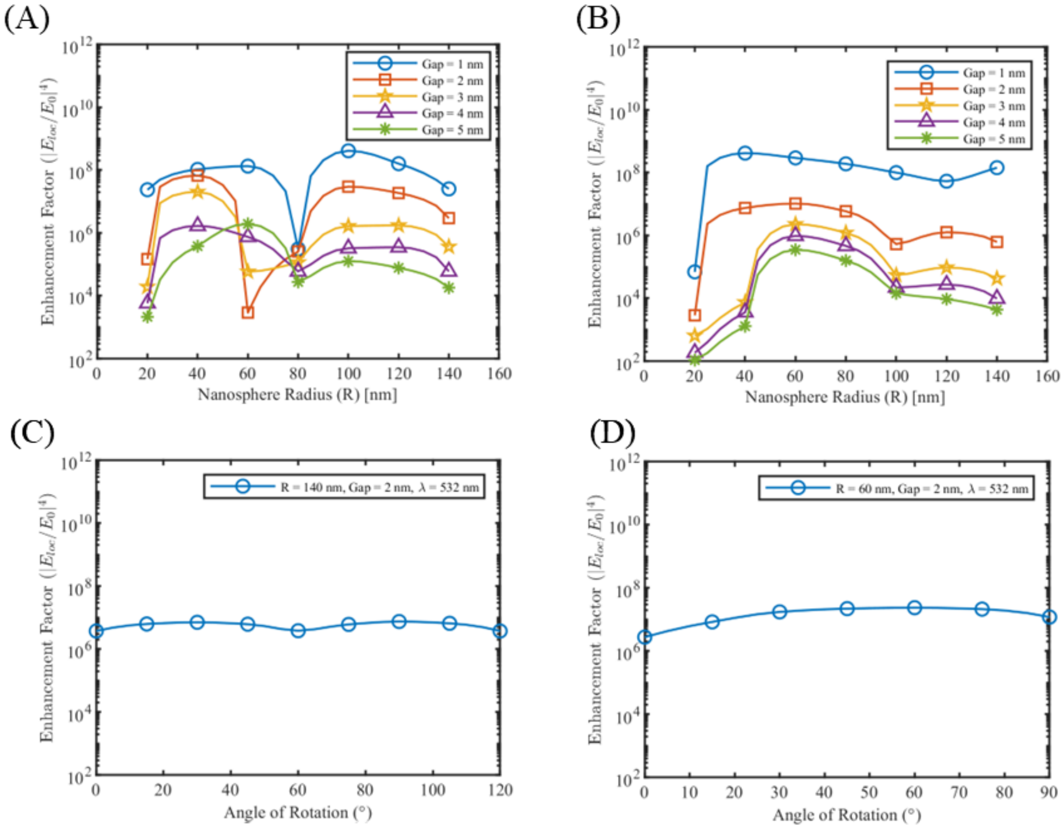

Figure 3.10: *Enhancement factor plot of (a) hotspot 5 and (b) hotspot 1 for silver nanotetramer at λ = 532 nm. Variation of enhancement factor with orientation of silver (c) nanotrimer of radius 140 nm, gap 2 nm at λ = 532 nm and (d) nanotetramer of radius 60 nm, gap 2 nm at λ = 532 nm.*

3.3. Near field simulations and optimization of periodic nanoparticle array

Finite element modeling of an array of nanospheres on a selected substrate provides a much comprehensive understanding of the biosensing system. A finite array of nanospheres can be computationally demanding which limits the number of nanoparticles that can be simulated. Periodic boundary conditions in COMSOL allows one to simulate periodic structures by computing only over one unit cell. The periodic unit cell of an array of nanospheres is shown in Figure 3.11(b), which effectively reduces the computation to one nanosphere only. In the model, we described the upper medium as water with real refractive index (n) of 1.33 and imaginary refractive index (k) of 0. The lower substrate is defined as Silicon with predefined refractive index model according to Green et. al. (2008)[214].

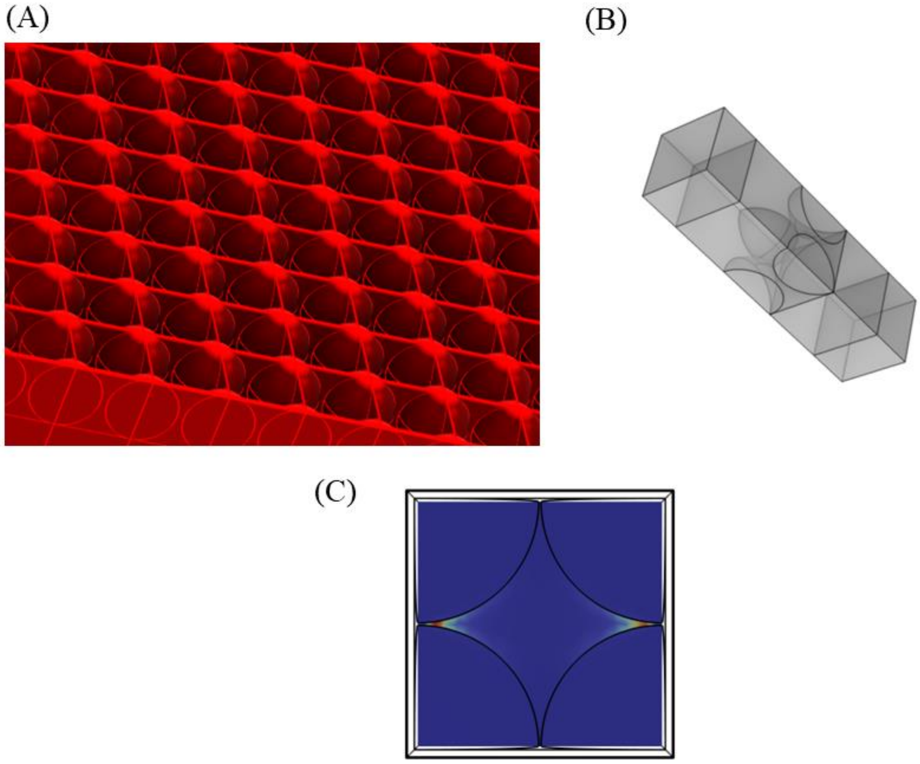

Figure 3.11: *(a) A three-dimensional view of a periodic array of nanospheres. (b) Unit cell of the periodic nanosphere array. (c) Enhancement factor of the unit cell showing an effective domain of one nanosphere only.*

In order to ensure proper compilation of the model, one need to ensure that the free triangular mesh on opposite faces with periodic boundary conditions applied are exactly same. Mesh of one face is copied to the opposite one to ensure proper application of the periodic boundary condition. PML layers were defined on both the ends of the model to ensure proper truncation of physical domain. Periodic boundary conditions with floquet periodicity are applied on each opposite walls of the physical domain. Instead of background wave, port boundary conditions are required to be defined in this case. Input port with an intensity of $0.001\,mW/\mu m^2$ is defined, emitting a linearly polarized wave travelling in x-direction and polarization in z-direction. An average enhancement factor is evaluated from the simulations which is defined in Equation 3.3[26].

$$EF_{av} = \frac{1}{A_0} \iint |\frac{E_{loc}}{E_0}|^4 \, dA \tag{3.3}$$

Here, A_0 is the area of the unit cell of silicon substrate, undecorated with nanoparticles. Enhancement factor plots for silver nanospheres at 532 nm and 633 nm wavelengths and gold nanospheres at 785 nm wavelength are shown in Figure 3.12(a-c), with rest of the simulations included in Figures S17, S18 of Supplementary Information.

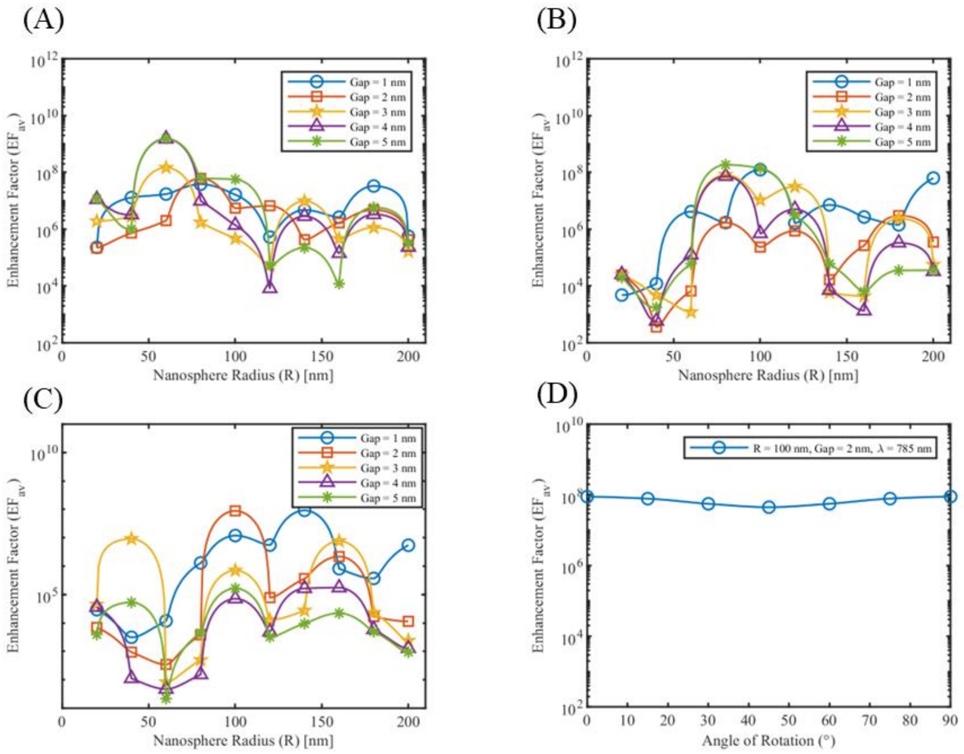

Figure 3.12: *Average enhancement factor plot of periodic silver nanospheres at (a) λ = 532 nm, (b) λ = 633 nm and for periodic gold nanospheres at (c) λ = 785 nm. Variation of average enhancement factor with orientation of a periodic gold nanosphere array of radius 100 nm, gap 2 nm at λ = 785 nm.*

As shown in Figure 3.11(c), only two of four hotspots are activated, which are aligned with the direction of polarization. The enhancement factor by definition provides the average enhancement of the dipolar coupling between two metallic nanospheres, and the hotspot between metal and semiconductor junction. This results in a key difference between the enhancement factor plots of free nanosphere models in Section 3.2 and enhancement factor plots in Figure 3.12, which is regularity. Including the metal-semiconductor hotspot results in enhancement factor peaks for different gap length at different radius values. The average enhancement factor provides a much comprehensive picture for SERS biosensing platform simulations. Polarization dependent enhancement factor for periodic nanoparticle structure is studied for gold nanospheres at 785nm. As the direction of polarization is rotated from 0° to 90° (i.e., from z-direction to y-direction), the enhancement factor of hotspots aligned along the z-direction decreases, while the enhancement factor of hotspots aligned along the y-direction increases. This keeps the average enhancement factor over the unit cell fairly constant as shown in Figure 3.12(d).

3.4. Limitations of the model

The above-described model with isolated noble metal nanospheres or periodic array of noble metal nanospheres solves the Maxwell's equation for scattering E-field, and can be applied for various applications including SERS biosensing. However, the current model does not include the charge transfer between two metallic nanospheres via quantum tunnelling and the charge transfer in the metal-semiconductor junction. Charge transfer via quantum tunnelling in the metal nanogaps can decrease the overall SERS enhancement factor[215], which cannot be tapped in with this current model. For this reason, the nanogaps between metal nanospheres in the simulations are limited to a minimum value of 1 nm only. Nanogaps less than 1 nm will have significant effect of quantum tunnelling, thereby increasing the error of our simulated results. A better model including the quantum tunnelling effects with the Maxwell's equations is a scope of our future research.

Chapter 4

Experiments on nanoparticle-based SERS surfaces

4.1. Introduction

In order to validate the simulation results obtained in Chapter 3, a simple SERS biosensing platform is fabricated by self-assembling gold nanoparticles on a silicon substrate. Methylene blue is used as the Raman probe molecule of choice for validation of enhancement factor obtained from the periodic nanoparticle array simulation. The experimental methods and materials required are described in Sections 4.2 – 4.4.

4.2. Materials

Sulphuric acid (H_2SO_4), hydrogen peroxide (H_2O_2), ACS grade acetone (CH_3COCH_3) and methylene blue powder were purchased from Fisher Chemicals. Ethanolamine ($HOCH_2CH_2NH_2$) was purchased from Alfa Aesar and dimethyl sulfoxide (DMSO) (CH_3SOCH_3) was purchased from Sigma Aldrich. A suspension of gold nanoparticles (100 nm diameter) OD 1 stabilised in 0.1 mM PBS was purchased from Aldrich Chemistry. 1X phosphate buffer saline (PBS) at pH 7.4 was purchased from Gibco by Life technologies. Silicon (100) wafers of 1 µm total thickness with a top oxide layer of 300 nm were purchased from Alpha Nanotech.

4.3. Fabrication Methods

Initially the silicon samples were cleaned in a 3:1 piranha solution of 98% concentrated sulphuric acid (30 mL) with 3% hydrogen peroxide (10 mL) for 15 mins to remove any organic substances on the surface. The cleaned samples were then ultrasonicated with acetone for 20 mins to remove any dust particles and impurities. The cleaned substrates were dried over a heating surface at 110°C. Substrates were further processed through an air plasma treatment (320 W, 8 ccm, 150 mT) for 10 mins for further cleaning and activation of surface dangling bonds for amine functionalisation in the next step.

Gold nanoparticles can be self-assembled over a Si surface via simple physisorption. However, the weakly physisorbed nanoparticles have a higher chance of getting washed out in future processing steps. Therefore, it is required to decorate the Si surface with a functional group that can form chemical bonds with Au. Ethanolamine is a good choice for self-assembly of gold and silver nanoparticles. The $-OH$ end of ethanolamine anchors with SiO_2 while the $-NH_2$ forms Au-N bonds with gold to hold the nanoparticles. While for silicon substrates, (3-Aminopropyl) triethoxysilane (APTES) functionalization is much popular due to stronger anchoring with the substrate (three bonds with silicon), ethanolamine provides much denser coverage (one bond with silicon)[216, 217]. An ethanolamine solution was prepared by mixing 3.3 mL of ethanolamine with 6.6 mL of DMSO and gently heated to 70°C. Clean samples of silicon were then immersed in the solution and kept under vacuum condition inside a desiccator for 12 hours. The amino functionalised silicon samples were then removed and air dried.

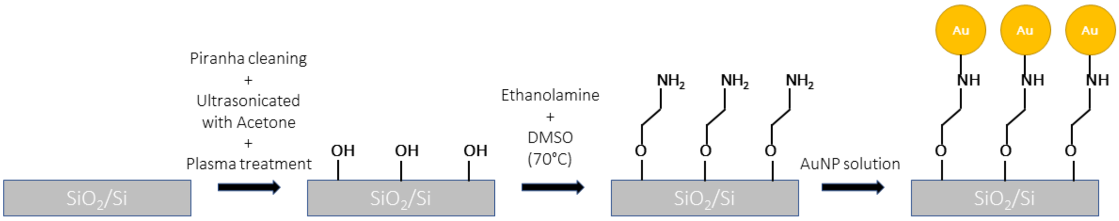

Figure 4.1: *Functionalization steps of gold nanoparticles on SiO_2 surface.*

In the final step, the amino functionalised Si substrates were immersed in a gold nanoparticle solution for self-assembly process at room temperature. Precisely, 5 mL of gold nanoparticle solution is mixed with 5 mL of 1x PBS solution and 40 mL of DI water. The substrates were kept immersed for different amount of time (6 hours, 11 hours, 18 hours and 24 hours) to control the gap length between nanoparticles. After the desirable time, each substrate was removed, washed in DI water and air dried.

4.4. Raman Spectroscopy with probe molecules

Enhancement factor of the self-assembled gold nanoparticles over Si substrate is measured by performing Raman spectroscopy over the surface with a desired Raman tag. For our experiments, methylene blue (MB) is chosen as Raman tag. Two solutions of MB are prepared of concentrations 1 mM and 1 µM respectively. Around 10 µL of 1 µM MB is drop casted on the Si substrates self-assembled with gold nanoparticles for different durations and 1 mM MB is drop casted over a clean silicon surface (no gold nanoparticles) for control experiment. The droplets were allowed to dry under room temperature forming the coffee ring on the surface and Raman spectroscopy was done on the boundary of the resulting coffee ring.

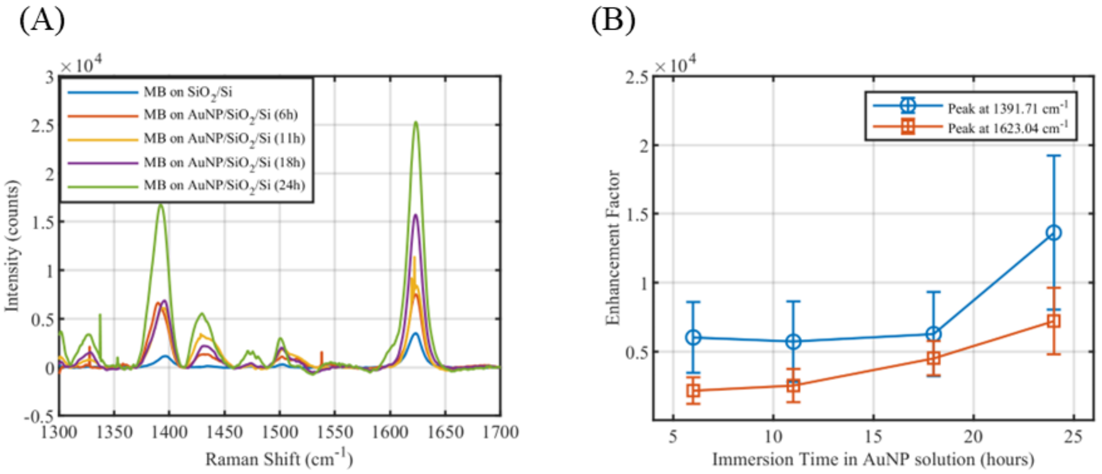

Figure 4.1: *(a) Baseline corrected Raman spectrum of 1 mM methylene blue on bare SiO_2 surface and 1 µM methylene blue on SiO_2 surface self-assembled with gold nanoparticles at different immersion times. (b) Enhancement factor measured for two signature peaks of methylene blue at different immersion times in gold nanoparticle solution.*

Enhancement factor can be calculated according to Equation 4.1[157].

$$EF_{exp} = \frac{I_{SERS}/C_{SERS}}{I_{Raman}/C_{Raman}} \tag{4.1}$$

Here, I_{SERS} is the characteristic peak intensity of the tag molecule obtained from the modified SERS surface at a concentration of C_{SERS}, and I_{Raman} is the intensity of the same characteristic peak of the same tag molecule obtained from an unmodified surface at a concentration of C_{Raman}.

Since for an unmodified SiO_2 surface, the Raman peak intensity of 1 µM MB could be quite less, we drop casted 1 mM MB to determine I_{Raman}. Raman spectroscopy is performed using Horiba Jobin Yvon HR800 LabRAM Raman Spectrometer over each surface at 633 nm wavelength. An acquisition time of 120 secs with an accumulation of 2, grid size of 1800 gr/mm and 10% intensity filter settings are applied for our Raman experiments. Initially the Raman spectrum is auto-calibrated to $520.74\ cm^{-1}$ with a SiO_2 surface. Baseline of each obtained Raman spectrums were corrected by subtracting a B-Spline interpolated baseline curve over 12 points in Origin[218]. The baseline corrected Raman spectrums of 1 mM MB over SiO_2 surface and 1 µM MB over self-assembled AuNP over SiO_2 surface are shown in Figure 4.1(a). Between $1300\ cm^{-1}$ and $1700\ cm^{-1}$, two characteristic peaks of methylene blue are obtained at $1391.71\ cm^{-1}$ and $1623.04\ cm^{-1}$, correspond to assigned band $v(C-C)\ ring$ and $\alpha(C-H)$ respectively[219, 220]. The enhancement factor plot is shown in Figure 4.1(b). As expected, with higher immersion time, more gold nanoparticles were self-assembled over the surface, thereby decreasing the intermetallic nanogaps between them. Accordingly, the enhancement factor increased with higher immersion time. From our simulated results of periodic gold nanospheres on silicon substrate at 633 nm wavelength (Figure S18(b)), we obtained an enhancement factor in the range of $10^4 - 10^5$ for nanoparticles of radius 50 nm. From our experiments with 50 nm gold nanoparticles, we obtained an enhancement factor of 1.3×10^4 with an immersion time of 24 hours, within the range of the simulated enhancement factor.

4.5. Conclusion

To conclude, we performed verification experiment in order to understand the practical limitation of our nanoparticle-based SERS biosensor model as described in Chapter 3. A SERS platform is fabricated by self-assembling gold nanoparticles over a SiO_2/Si substrate. Standard method of wafer surface cleaning and amine functionalisation is done, followed by immersion in a gold nanoparticle solution for self-assembly. The gap length is controlled by varying the immersion time. Raman spectroscopy experiments were performed on these fabricated SERS platforms with methylene blue as probe molecule. A highest enhancement factor of $\sim 10^4$ is observed for a 24 hours immersion time, closely corelating with the simulation results.

Chapter 5

Conclusions and Future Work

To conclude this thesis, gliomas are highly malignant tumour with high mortality rate and require proper management with early detection and frequent monitoring, both can be facilitated with biosensing technologies. Overall, current biosensors have demonstrated significantly high sensitivity and specificity with ability to detect biomolecules at ultra-low concentration, however certain other characteristics such as stability, multiplexing, specificity under real biofluids are still some of the few problems that need to be worked on before they can be applied on clinical fields.

A simple strategy of modeling multiple nanoparticle SERS systems and periodic nanoparticle SERS platform is presented in this current work involving COMSOL RF module. The presented nanoparticle models could be very useful in understanding the local plasmon resonance, plasmonic dipolar coupling and thus surface induced local electric field amplification in SERS biosensing systems. Since the local surface plasmons highly depends on the incident wavelength, nanoparticle size and interparticle gap, this model can also be implemented for optimization of a SERS biochip design.

A comprehensive simulation study over the model is presented to understand some underlying phenomenon such as polarization dependent enhancement and local hotspot switching. In case of nanodimers, strong polarization dependent enhancement was observed, with enhancement factor reduces drastically at perpendicular alignment with the direction of polarization. The dependence of polarization can be explained with polarization charge concept in hybridization theory. In case of certain orientation of nanotrimer and nanotetramer, a new type of switching between multiple hotspots was observed which hasn’t been reported in literature yet. Here the middle hotspot of the multiple nanosphere systems abruptly switches off for a particular condition of incident wavelength, nanoparticle radius and interparticle gap.

Our simulation results revealed that number of nanoparticles on the sides influences the extend of this hotspot switch off dip. While our study revealed this phenomenon, a better understanding of this hotspot switching is required with a plasmonic hybridization study of this multiple nanosphere systems, which is a future scope of research.

Simulations were extended to periodic nanoparticle systems in order to get a much comprehensive picture of practical SERS biosensing systems. While our model could be very useful for practical design applications, where the goal is typically to maximize the enhancement factor, it has limitations regarding the minimum interparticle gap that can be simulated. Simulations for gap less than 1 nm require coupled solution of Maxwell's electromagnetic equations with electronic density of states of the metallic nanoparticles in order to tap in the quantum tunnelling effect. While such future study may not have practical interest due to reduced enhancement factor, it may reveal interesting fundamental phenomenon at angstrom level gap lengths.

Lastly, verification experiments were performed by self-assembling gold nanoparticles over a silicon substrate using standard protocols. Raman spectroscopy was performed over these SERS chips with methylene blue as Raman tags, which revealed a practical SERS enhancement factor up to 10^4, corelating with the results obtained from simulations.

References

[1] Q. T. Ostrom *et al.*, ‘CBTRUS Statistical Report: Primary Brain and Other Central Nervous System Tumors Diagnosed in the United States in 2012-2016’, *Neuro-Oncology*, vol. 21. 2019. doi: 10.1093/neuonc/noz150.

[2] ‘Cancer statistics at a glance’, Sep. 01, 2022. https://cancer.ca/en/research/cancer-statistics/cancer-statistics-at-a-glance (accessed Aug. 31, 2022).

[3] F. Hanif, K. Muzaffar, K. Perveen, S. M. Malhi, and S. U. Simjee, ‘Glioblastoma multiforme: A review of its epidemiology and pathogenesis through clinical presentation and treatment’, *Asian Pacific Journal of Cancer Prevention*, vol. 18, no. 1. 2017. doi: 10.22034/APJCP.2017.18.1.3.

[4] ‘Survival statistics for brain and spinal cord tumours’, Sep. 01, 2022. https://cancer.ca/en/cancer-information/cancer-types/brain-and-spinal-cord/prognosis-and-survival/survival-statistics (accessed Aug. 31, 2022).

[5] J. Müller Bark, A. Kulasinghe, B. Chua, B. W. Day, and C. Punyadeera, ‘Circulating biomarkers in patients with glioblastoma’, *British Journal of Cancer*, vol. 122, no. 3. 2020. doi: 10.1038/s41416-019-0603-6.

[6] G. M. Shankar, L. Balaj, S. L. Stott, B. Nahed, and B. S. Carter, ‘Liquid biopsy for brain tumors’, *Expert Review of Molecular Diagnostics*, vol. 17, no. 10. 2017. doi: 10.1080/14737159.2017.1374854.

[7] C. Nieder, A. L. Grosu, S. Astner, and M. Molls, ‘Treatment of unresectable glioblastoma multiforme’, *Anticancer Res*, vol. 25, no. 6 C, 2005.

[8] P. D. Delgado-López, E. Riñones-Mena, and E. M. Corrales-García, ‘Treatment-related changes in glioblastoma: a review on the controversies in response assessment criteria and the concepts of true progression, pseudoprogression, pseudoresponse and radionecrosis’, *Clinical and Translational Oncology*, vol. 20, no. 8. 2018. doi: 10.1007/s12094-017-1816-x.

[9] A. Khanmohammadi *et al.*, ‘Electrochemical biosensors for the detection of lung cancer biomarkers: A review’, *Talanta*, vol. 206. 2020. doi: 10.1016/j.talanta.2019.120251.

[10] Z. Altintas and I. Tothill, ‘Biomarkers and biosensors for the early diagnosis of lung cancer’, *Sensors and Actuators, B: Chemical*, vol. 188. 2013. doi: 10.1016/j.snb.2013.07.078.

[11] S. K. Arya and S. Bhansali, ‘Lung cancer and its early detection using biomarker-based biosensors’, *Chemical Reviews*, vol. 111, no. 11. 2011. doi: 10.1021/cr100420s.

[12] A. Roointan *et al.*, ‘Early detection of lung cancer biomarkers through biosensor technology: A review’, *Journal of Pharmaceutical and Biomedical Analysis*, vol. 164. 2019. doi: 10.1016/j.jpba.2018.10.017.

[13] G. Yang, Z. Xiao, C. Tang, Y. Deng, H. Huang, and Z. He, ‘Recent advances in biosensor for detection of lung cancer biomarkers’, *Biosensors and Bioelectronics*, vol. 141. 2019. doi: 10.1016/j.bios.2019.111416.

[14] S. Getachew *et al.*, ‘Perceived barriers to early diagnosis of breast Cancer in south and southwestern Ethiopia: a qualitative study’, *BMC Womens Health*, vol. 20, no. 1, 2020, doi: 10.1186/s12905-020-00909-7.

[15] M. Hasanzadeh, N. Shadjou, and M. de la Guardia, ‘Early stage screening of breast cancer using electrochemical biomarker detection’, *TrAC - Trends in Analytical Chemistry*, vol. 91. 2017. doi: 10.1016/j.trac.2017.04.006.

[16] P. Ranjan *et al.*, ‘Biosensor-based diagnostic approaches for various cellular biomarkers of breast cancer: A comprehensive review’, *Analytical Biochemistry*, vol. 610. 2020. doi: 10.1016/j.ab.2020.113996.

[17] S. Mittal, H. Kaur, N. Gautam, and A. K. Mantha, ‘Biosensors for breast cancer diagnosis: A review of bioreceptors, biotransducers and signal amplification strategies’, *Biosens Bioelectron*, vol. 88, 2017, doi: 10.1016/j.bios.2016.08.028.

[18] F. Ghorbani, H. Abbaszadeh, J. E. N. Dolatabadi, L. Aghebati-Maleki, and M. Yousefi, ‘Application of various optical and electrochemical aptasensors for detection of human prostate specific antigen: A review’, *Biosensors and Bioelectronics*, vol. 142. 2019. doi: 10.1016/j.bios.2019.111484.

[19] K. M. Chan, J. M. Gleadle, M. O’Callaghan, K. Vasilev, and M. MacGregor, ‘Prostate cancer detection: a systematic review of urinary biosensors’, *Prostate Cancer and Prostatic Diseases*, vol. 25, no. 1. 2022. doi: 10.1038/s41391-021-00480-8.

[20] D. A. Healy, C. J. Hayes, P. Leonard, L. McKenna, and R. O’Kennedy, ‘Biosensor developments: application to prostate-specific antigen detection’, *Trends in Biotechnology*, vol. 25, no. 3. 2007. doi: 10.1016/j.tibtech.2007.01.004.

[21] S. Singh, A. A. S. Gill, M. Nlooto, and R. Karpoormath, ‘Prostate cancer biomarkers detection using nanoparticles based electrochemical biosensors’, *Biosensors and Bioelectronics*, vol. 137. 2019. doi: 10.1016/j.bios.2019.03.065.

[22] K. Karn-Orachai, ‘Gap-Dependent Surface-Enhanced Raman Scattering (SERS) Enhancement Model of SERS Substrate-Probe Combination Using a Polyelectrolyte Nanodroplet as a Distance Controller’, *Langmuir*, vol. 37, no. 36, 2021, doi: 10.1021/acs.langmuir.1c01556.

[23] F. Benz *et al.*, ‘SERS of Individual Nanoparticles on a Mirror: Size Does Matter, but so Does Shape’, *Journal of Physical Chemistry Letters*, vol. 7, no. 12, 2016, doi: 10.1021/acs.jpclett.6b00986.

[24] K. Sugawa *et al.*, ‘Particle size dependence of the surface-enhanced Raman scattering properties of densely arranged two-dimensional assemblies of Au(core)-Ag(shell) nanospheres’, *Physical Chemistry Chemical Physics*, vol. 17, no. 33, 2014, doi: 10.1039/c4cp05058d.

[25] R. Pilot and M. Massari, ‘Silver nanoparticle aggregates: Wavelength dependence of their SERS properties in the first transparency window of biological tissues’, *Chemical Physics Impact*, vol. 2, 2021, doi: 10.1016/j.chphi.2021.100014.

[26] I. Knorr, K. Christou, and J. Meinertz, ‘Prediction and Optimization of Surface-Enhanced Raman Scattering Geometries using COMSOL Multiphysics’, *Procedings of the COMSOL Conference*, vol. 14, no. 2002, 2008.

[27] R. K. Saini, A. K. Sharma, A. Agarwal, and R. Prajesh, ‘Near field FEM simulations of plasmonic gold nanoparticle based SERS substrate with experimental validation’, *Mater Chem Phys*, vol. 287, 2022, doi: 10.1016/j.matchemphys.2022.126288.

[28] J. L. Yang, R. P. Li, J. H. Han, and M. J. Huang, ‘FDTD simulation study of size/gap and substrate-dependent SERS activity study of Au@SiO2 nanoparticles’, *Chinese Physics B*, vol. 25, no. 8, 2016, doi: 10.1088/1674-1056/25/8/083301.

[29] T. Wang *et al.*, ‘The Effect of Dielectric Constants on Noble Metal/Semiconductor SERS Enhancement: FDTD Simulation and Experiment Validation of Ag/Ge and Ag/Si Substrates’, *Sci Rep*, vol. 4, 2014, doi: 10.1038/srep04052.

[30] D. M. Solís, J. M. Taboada, F. Obelleiro, L. M. Liz-Marzán, and F. J. García De Abajo, ‘Optimization of Nanoparticle-Based SERS Substrates through Large-Scale Realistic Simulations’, *ACS Photonics*, vol. 4, no. 2, 2017, doi: 10.1021/acsphotonics.6b00786.

[31] Q. Sun, Q. Y. Zhang, N. Zhou, L. Y. Zhang, Q. Hu, and C. Y. Ma, ‘FDTD simulation of Ag-decorated ZnO nanorods for optimization of 3D SERS substrates’, *Appl Surf Sci*, vol. 565, 2021, doi: 10.1016/j.apsusc.2021.150524.

[32] H. Yockell-Lelièvre, F. Lussier, and J. F. Masson, ‘Influence of the Particle Shape and Density of Self-Assembled Gold Nanoparticle Sensors on LSPR and SERS’, *Journal of Physical Chemistry C*, vol. 119, no. 51, 2015, doi: 10.1021/acs.jpcc.5b09570.

[33] B. xin Yan, Y. ying Zhu, Y. Wei, and H. Pei, ‘Study on surface enhanced Raman scattering of Au and Au@Al2O3 spherical dimers based on 3D finite element method’, *Sci Rep*, vol. 11, no. 1, 2021, doi: 10.1038/s41598-021-87997-z.

[34] 'COMSOL Multiphysics® Software'. https://www.comsol.com/wave-optics-module (accessed Mar. 05, 2023).

[35] A. J. Atkinson *et al.*, 'Biomarkers and surrogate endpoints: Preferred definitions and conceptual framework', *Clinical Pharmacology and Therapeutics*, vol. 69, no. 3. 2001. doi: 10.1067/mcp.2001.113989.

[36] F.-N. B. W. Group, 'BEST (Biomarkers, EndpointS, and other Tools) resource. 2016', *US FDA: Silver Spring, MD*, 2016.

[37] W. J. Allard *et al.*, 'Tumor cells circulate in the peripheral blood of all major carcinomas but not in healthy subjects or patients with nonmalignant diseases', *Clinical Cancer Research*, vol. 10, no. 20, 2004, doi: 10.1158/1078-0432.CCR-04-0378.

[38] P. Kuhn and K. Bethel, 'A fluid biopsy as investigating technology for the fluid phase of solid tumors', *Physical Biology*, vol. 9, no. 1. 2012. doi: 10.1088/1478-3975/9/1/010301.

[39] E. Heitzer, I. S. Haque, C. E. S. Roberts, and M. R. Speicher, 'Current and future perspectives of liquid biopsies in genomics-driven oncology', *Nature Reviews Genetics*, vol. 20, no. 2. 2019. doi: 10.1038/s41576-018-0071-5.

[40] G. Siravegna, S. Marsoni, S. Siena, and A. Bardelli, 'Integrating liquid biopsies into the management of cancer', *Nature Reviews Clinical Oncology*, vol. 14, no. 9. 2017. doi: 10.1038/nrclinonc.2017.14.

[41] A. M. Miller *et al.*, 'Tracking tumour evolution in glioma through liquid biopsies of cerebrospinal fluid', *Nature*, vol. 565, no. 7741, 2019, doi: 10.1038/s41586-019-0882-3.

[42] H. Wolburg, S. Noell, P. Fallier-Becker, A. F. MacK, and K. Wolburg-Buchholz, 'The disturbed blood-brain barrier in human glioblastoma', *Molecular Aspects of Medicine*, vol. 33, no. 5–6. 2012. doi: 10.1016/j.mam.2012.02.003.

[43] Z. Chen and D. Hambardzumyan, 'Immune microenvironment in glioblastoma subtypes', *Frontiers in Immunology*, vol. 9, no. MAY. 2018. doi: 10.3389/fimmu.2018.01004.

[44] C. Zhao, H. Wang, C. Xiong, and Y. Liu, 'Hypoxic glioblastoma release exosomal VEGF-A induce the permeability of blood-brain barrier', *Biochem Biophys Res Commun*, vol. 502, no. 3, 2018, doi: 10.1016/j.bbrc.2018.05.140.

[45] D. P. Bartel, 'MicroRNAs: Genomics, Biogenesis, Mechanism, and Function', *Cell*, vol. 116, no. 2. 2004. doi: 10.1016/S0092-8674(04)00045-5.

[46] K. Kamińska *et al.*, 'Prognostic and Predictive Epigenetic Biomarkers in Oncology', *Molecular Diagnosis and Therapy*, vol. 23, no. 1. 2019. doi: 10.1007/s40291-018-0371-7.

[47] A. Baraniskin *et al.*, ‘Identification of microRNAs in the cerebrospinal fluid as biomarker for the diagnosis of glioma’, *Neuro Oncol*, vol. 14, no. 1, 2012, doi: 10.1093/neuonc/nor169.

[48] J. Wang, F. Che, and J. Zhang, ‘Cell-free microRNAs as non-invasive biomarkers in glioma: a diagnostic meta-analysis’, *International Journal of Biological Markers*, vol. 34, no. 3, 2019, doi: 10.1177/1724600819840033.

[49] M. ParvizHamidi *et al.*, ‘Circulating miR-26a and miR-21 as biomarkers for glioblastoma multiform’, *Biotechnol Appl Biochem*, vol. 66, no. 2, 2019, doi: 10.1002/bab.1707.

[50] Y. Song, M. He, J. Zhang, and J. Xu, ‘High expression of microRNA 221 is a poor predictor for glioma’, *Medicine*, vol. 99, no. 49, 2020, doi: 10.1097/MD.0000000000023163.

[51] Y. Song, J. Zhang, M. He, and J. Xu, ‘Prognostic Role of MicroRNA 222 in Patients with Glioma: A Meta-analysis’, *BioMed Research International*, vol. 2020. 2020. doi: 10.1155/2020/4689689.

[52] Y. Zhang *et al.*, ‘Prognostic Significance of MicroRNAs in Glioma: A Systematic Review and Meta-Analysis’, *Biomed Res Int*, vol. 2019, 2019, doi: 10.1155/2019/4015969.

[53] G. Jiang *et al.*, ‘Prognostic value of miR-21 in gliomas: comprehensive study based on meta-analysis and TCGA dataset validation’, *Sci Rep*, vol. 10, no. 1, 2020, doi: 10.1038/s41598-020-61155-3.

[54] L. Shi, J. Chen, J. Yang, T. Pan, S. Zhang, and Z. Wang, ‘MiR-21 protected human glioblastoma U87MG cells from chemotherapeutic drug temozolomide induced apoptosis by decreasing Bax/Bcl-2 ratio and caspase-3 activity’, *Brain Res*, vol. 1352, 2010, doi: 10.1016/j.brainres.2010.07.009.

[55] H. S. Gwak *et al.*, ‘Silencing of MicroRNA-21 Confers Radio-Sensitivity through Inhibition of the PI3K/AKT Pathway and Enhancing Autophagy in Malignant Glioma Cell Lines’, *PLoS One*, vol. 7, no. 10, 2012, doi: 10.1371/journal.pone.0047449.

[56] G. Gabriely *et al.*, ‘Human glioma growth is controlled by microRNA-10b’, *Cancer Res*, vol. 71, no. 10, 2011, doi: 10.1158/0008-5472.CAN-10-3568.

[57] W. Zhang *et al.*, ‘MiR-181d: Predictive glioblastoma biomarker that downregulates MGMT expression’, *Neuro Oncol*, vol. 14, no. 6, 2012, doi: 10.1093/neuonc/nos089.

[58] M. Westphal and K. Lamszus, ‘Circulating biomarkers for gliomas’, *Nature Reviews Neurology*, vol. 11, no. 10. 2015. doi: 10.1038/nrneurol.2015.171.

[59] C. Kahlert and R. Kalluri, ‘Exosomes in tumor microenvironment influence cancer progression and metastasis’, *Journal of Molecular Medicine*, vol. 91, no. 4. 2013. doi: 10.1007/s00109-013-1020-6.

[60] R. Xu, A. Rai, M. Chen, W. Suwakulsiri, D. W. Greening, and R. J. Simpson, 'Extracellular vesicles in cancer — implications for future improvements in cancer care', *Nature Reviews Clinical Oncology*, vol. 15, no. 10. 2018. doi: 10.1038/s41571-018-0036-9.

[61] C. Quezada *et al.*, 'Role of extracellular vesicles in glioma progression', *Molecular Aspects of Medicine*, vol. 60. 2018. doi: 10.1016/j.mam.2017.12.003.

[62] D. Osti *et al.*, 'Clinical significance of extracellular vesicles in plasma from glioblastoma patients', *Clinical Cancer Research*, vol. 25, no. 1, 2019, doi: 10.1158/1078-0432.CCR-18-1941.

[63] J. C. Akers *et al.*, 'miR-21 in the Extracellular Vesicles (EVs) of Cerebrospinal Fluid (CSF): A Platform for Glioblastoma Biomarker Development', *PLoS One*, vol. 8, no. 10, 2013, doi: 10.1371/journal.pone.0078115.

[64] J. M. Figueroa *et al.*, 'Detection of wild-Type EGFR amplification and EGFRvIII mutation in CSF-derived extracellular vesicles of glioblastoma patients', *Neuro Oncol*, vol. 19, no. 11, 2017, doi: 10.1093/neuonc/nox085.

[65] J. Skog *et al.*, 'Glioblastoma microvesicles transport RNA and proteins that promote tumour growth and provide diagnostic biomarkers', *Nat Cell Biol*, vol. 10, no. 12, 2008, doi: 10.1038/ncb1800.

[66] H. Shao *et al.*, 'Protein typing of circulating microvesicles allows real-time monitoring of glioblastoma therapy', *Nat Med*, vol. 18, no. 12, 2012, doi: 10.1038/nm.2994.

[67] W. W. Chen *et al.*, 'Beaming and droplet digital pcr analysis of mutant idh1 mrna in glioma patient serum and cerebrospinal fluid extracellular vesicles', *Mol Ther Nucleic Acids*, vol. 2, 2013, doi: 10.1038/mtna.2013.28.

[68] B. D. Choi *et al.*, 'EGFRvIII-targeted vaccination therapy of malignant glioma', in *Brain Pathology*, 2009. doi: 10.1111/j.1750-3639.2009.00318.x.

[69] S. K. Guo, M. F. Shen, H. W. Yao, and Y. S. Liu, 'Enhanced expression of TGFBI promotes the proliferation and migration of glioma cells', *Cellular Physiology and Biochemistry*, vol. 49, no. 3, 2018, doi: 10.1159/000493293.

[70] D. Choi, L. Montermini, D. K. Kim, B. Meehan, F. P. Roth, and J. Rak, 'The impact of oncogenic egfrviii on the proteome of extracellular vesicles released from glioblastoma cells', *Molecular and Cellular Proteomics*, vol. 17, no. 10, 2018, doi: 10.1074/mcp.RA118.000644.

[71] S. Misra *et al.*, 'Hyaluronan-CD44 interactions as potential targets for cancer therapy', *FEBS Journal*, vol. 278, no. 9. 2011. doi: 10.1111/j.1742-4658.2011.08071.x.

[72] T. Yoshida, Y. Matsuda, Z. Naito, and T. Ishiwata, ‘CD44 in human glioma correlates with histopathological grade and cell migration’, *Pathol Int*, vol. 62, no. 7, 2012, doi: 10.1111/j.1440-1827.2012.02823.x.

[73] Y. Akiyama *et al.*, ‘Hyaluronate receptors mediating glioma cell migration and proliferation’, *J Neurooncol*, vol. 53, no. 2, 2001, doi: 10.1023/A:1012297132047.

[74] M. Herrmann, P. Vos, M. T. Wunderlich, C. H. M. M. de Bruijn, and K. J. B. Lamers, ‘Release of glial tissue-specific proteins after acute stroke: A comparative analysis of serum concentrations of protein S-100B and glial fibrillary acidic protein’, *Stroke*, vol. 31, no. 11, 2000, doi: 10.1161/01.STR.31.11.2670.

[75] P. E. Vos *et al.*, ‘GFAP and S100B are biomarkers of traumatic brain injury: An observational cohort study’, *Neurology*, vol. 75, no. 20, 2010, doi: 10.1212/WNL.0b013e3181fd62d2.

[76] J. G. Pérez-Larraya *et al.*, ‘Diagnostic and prognostic value of preoperative combined GFAP, IGFBP-2, and YKL-40 plasma levels in patients with glioblastoma’, *Cancer*, vol. 120, no. 24, 2014, doi: 10.1002/cncr.28949.

[77] J. Tichy *et al.*, ‘Prospective evaluation of serum glial fibrillary acidic protein (GFAP) as a diagnostic marker for glioblastoma’, *J Neurooncol*, vol. 126, no. 2, 2015, doi: 10.1007/s11060-015-1978-8.

[78] C. S. Jung *et al.*, ‘Serum GFAP is a diagnostic marker for glioblastoma multiforme’, *Brain*, vol. 130, no. 12, 2007, doi: 10.1093/brain/awm263.

[79] A. Kiviniemi *et al.*, ‘Serum levels of GFAP and EGFR in primary and recurrent high-grade gliomas: correlation to tumor volume, molecular markers, and progression-free survival’, *J Neurooncol*, vol. 124, no. 2, 2015, doi: 10.1007/s11060-015-1829-7.

[80] N. A. Schultz and J. S. Johansen, ‘YKL-40-a protein in the field of translational medicine: A role as a biomarker in cancer patients?’, *Cancers*, vol. 2, no. 3. 2010. doi: 10.3390/cancers2031453.

[81] G. Qin *et al.*, ‘Prognostic Value of YKL-40 in Patients with Glioblastoma: a Systematic Review and Meta-analysis’, *Mol Neurobiol*, vol. 54, no. 5, 2017, doi: 10.1007/s12035-016-9878-2.

[82] D. Bernardi *et al.*, ‘Serum YKL-40 following resection for cerebral glioblastoma’, *J Neurooncol*, vol. 107, no. 2, 2012, doi: 10.1007/s11060-011-0762-7.

[83] F. Shen *et al.*, ‘Proteomic analysis of cerebrospinal fluid: Toward the identification of biomarkers for gliomas’, *Neurosurgical Review*, vol. 37, no. 3. 2014. doi: 10.1007/s10143-014-0539-5.

[84] F. W. Khwaja *et al.*, ‘Proteomic identification of biomarkers in the cerebrospinal fluid (CSF) of astrocytoma patients’, *J Proteome Res*, vol. 6, no. 2, 2007, doi: 10.1021/pr060240z.

[85] P. Sampath, C. E. Weaver, A. Sungarian, S. Cortez, L. Alderson, and E. G. Stopa, ‘Cerebrospinal fluid (vascular endothelial growth factor) and serologic (recoverin) tumor markers for malignant glioma’, *Cancer Control*, vol. 11, no. 3. 2004. doi: 10.1177/107327480401100305.

[86] M. Verma and U. Manne, ‘Genetic and epigenetic biomarkers in cancer diagnosis and identifying high risk populations’, *Critical Reviews in Oncology/Hematology*, vol. 60, no. 1. 2006. doi: 10.1016/j.critrevonc.2006.04.002.

[87] M. Kalinich and D. A. Haber, ‘Cancer detection: Seeking signals in blood’, *Science*, vol. 359, no. 6378. 2018. doi: 10.1126/science.aas9102.

[88] C. Bettegowda *et al.*, ‘Detection of circulating tumor DNA in early- and late-stage human malignancies’, *Sci Transl Med*, vol. 6, no. 224, 2014, doi: 10.1126/scitranslmed.3007094.

[89] I. Lavon, M. Refael, B. Zelikovitch, E. Shalom, and T. Siegal, ‘Serum DNA can define tumor-specific genetic and epigenetic markers in gliomas of various grades’, *Neuro Oncol*, vol. 12, no. 2, 2010, doi: 10.1093/neuonc/nop041.

[90] C. Balañá *et al.*, ‘Tumour and serum MGMT promoter methylation and protein expression in glioblastoma patients’, *Clinical and Translational Oncology*, vol. 13, no. 9, 2011, doi: 10.1007/s12094-011-0714-x.

[91] A. Majchrzak-Celińska *et al.*, ‘Detection of MGMT, RASSF1A, p15INK4B, and p14ARF promoter methylation in circulating tumor-derived DNA of central nervous system cancer patients’, *J Appl Genet*, vol. 54, no. 3, 2013, doi: 10.1007/s13353-013-0149-x.

[92] J. L. Ramirez *et al.*, ‘Serum DNA as a tool for cancer patient management.’, *Rocz Akad Med Bialymst*, vol. 48, 2003.

[93] K. D. Weaver, S. A. Grossman, and J. G. Herman, ‘Methylated tumor-specific DNA as a plasma biomarker in patients with glioma’, *Cancer Invest*, vol. 24, no. 1, 2006, doi: 10.1080/07357900500449546.

[94] L. de Mattos-Arruda *et al.*, ‘Cerebrospinal fluid-derived circulating tumour DNA better represents the genomic alterations of brain tumours than plasma’, *Nat Commun*, vol. 6, 2015, doi: 10.1038/ncomms9839.

[95] B. Boisselier *et al.*, ‘Detection of IDH1 mutation in the plasma of patients with glioma’, *Neurology*, vol. 79, no. 16, 2012, doi: 10.1212/WNL.0b013e31826e9b0a.

[96] S. Nobusawa, T. Watanabe, P. Kleihues, and H. Ohgaki, ‘IDH1 mutations as molecular signature and predictive factor of secondary glioblastomas’, *Clinical Cancer Research*, vol. 15, no. 19, 2009, doi: 10.1158/1078-0432.CCR-09-0715.

[97] J. Wang and C. Bettegowda, ‘Applications of DNA-Based Liquid Biopsy for Central Nervous System Neoplasms’, *Journal of Molecular Diagnostics*, vol. 19, no. 1. 2017. doi: 10.1016/j.jmoldx.2016.08.007.

[98] W. J. Chung *et al.*, ‘Inhibition of cystine uptake disrupts the growth of primary brain tumors’, *Journal of Neuroscience*, vol. 25, no. 31, 2005, doi: 10.1523/JNEUROSCI.5258-04.2005.

[99] E. H. Panosyan, H. J. Lin, J. Koster, and J. L. Lasky, ‘In search of druggable targets for GBM amino acid metabolism’, *BMC Cancer*, vol. 17, no. 1, 2017, doi: 10.1186/s12885-017-3148-1.

[100] L. Mörén, A. Tommy Bergenheim, S. Ghasimi, T. Brännström, M. Johansson, and H. Antti, ‘Metabolomic screening of tumor tissue and serum in glioma patients reveals diagnostic and prognostic information’, *Metabolites*, vol. 5, no. 3, 2015, doi: 10.3390/metabo5030502.

[101] J. de Groot and H. Sontheimer, ‘Glutamate and the biology of gliomas’, *Glia*, vol. 59, no. 8, 2011, doi: 10.1002/glia.21113.

[102] J. S. So, H. Kim, and K. S. Han, ‘Mechanisms of Invasion in Glioblastoma: Extracellular Matrix, Ca2+ Signaling, and Glutamate’, *Frontiers in Cellular Neuroscience*, vol. 15. 2021. doi: 10.3389/fncel.2021.663092.

[103] Q. Wang *et al.*, ‘Plasma specific miRNAs as predictive biomarkers for diagnosis and prognosis of glioma’, *Journal of Experimental and Clinical Cancer Research*, vol. 31, no. 1, 2012, doi: 10.1186/1756-9966-31-97.

[104] M. Visani *et al.*, ‘Expression of 19 microRNAs in glioblastoma and comparison with other brain neoplasia of grades I-III’, *Mol Oncol*, vol. 8, no. 2, 2014, doi: 10.1016/j.molonc.2013.12.010.

[105] X. Ye *et al.*, ‘Identification of microRNAs associated with glioma diagnosis and prognosis’, *Oncotarget*, vol. 8, no. 16, 2017, doi: 10.18632/oncotarget.14445.

[106] M. Piwecka *et al.*, ‘Comprehensive analysis of microRNA expression profile in malignant glioma tissues’, *Mol Oncol*, vol. 9, no. 7, 2015, doi: 10.1016/j.molonc.2015.03.007.

[107] A. Conti *et al.*, ‘miR-21 and 221 upregulation and miR-181b downregulation in human grade II-IV astrocytic tumors’, *J Neurooncol*, vol. 93, no. 3, 2009, doi: 10.1007/s11060-009-9797-4.

[108] A. Buruiană *et al.*, ‘The roles of miRNA in glioblastoma tumor cell communication: Diplomatic and aggressive negotiations’, *International Journal of Molecular Sciences*, vol. 21, no. 6. 2020. doi: 10.3390/ijms21061950.

[109] J. C. Akers *et al.*, ‘A cerebrospinal fluid microRNA signature as biomarker for glioblastoma’, *Oncotarget*, vol. 8, no. 40, 2017, doi: 10.18632/oncotarget.18332.

[110] C. Li *et al.*, ‘Prognostic role of microRNA-21 expression in gliomas: a meta-analysis’, *Journal of Neuro-Oncology*, vol. 130, no. 1. 2016. doi: 10.1007/s11060-016-2233-7.

[111] N. M. Teplyuk *et al.*, ‘MicroRNAs in cerebrospinal fluid identify glioblastoma and metastatic brain cancers and reflect disease activity’, *Neuro Oncol*, vol. 14, no. 6, 2012, doi: 10.1093/neuonc/nos074.

[112] P. Ivo D’Urso, O. Fernando D’Urso, C. Damiano Gianfreda, V. Mezzolla, C. Storelli, and S. Marsigliante, ‘miR-15b and miR-21 as Circulating Biomarkers for Diagnosis of Glioma’, *Curr Genomics*, vol. 16, no. 5, 2015, doi: 10.2174/1389202916666150707155610.

[113] K. Møllersen, M. Zortea, T. R. Schopf, H. Kirchesch, and F. Godtliebsen, ‘Comparison of computer systems and ranking criteria for automatic melanoma detection in dermoscopic images’, *PLoS One*, vol. 12, no. 12, 2017, doi: 10.1371/journal.pone.0190112.

[114] C. M. Garcia and S. A. Toms, ‘The Role of Circulating MicroRNA in Glioblastoma Liquid Biopsy’, *World Neurosurgery*, vol. 138. 2020. doi: 10.1016/j.wneu.2020.03.128.

[115] Y. Zhou *et al.*, ‘Prognostic role of microRNA-155 expression in gliomas: A meta-analysis’, *Clinical Neurology and Neurosurgery*, vol. 176. 2019. doi: 10.1016/j.clineuro.2018.12.005.

[116] G. Sun *et al.*, ‘Decreased expression of miR-15b in human gliomas is associated with poor prognosis’, *Cancer Biother Radiopharm*, vol. 30, no. 4, 2015, doi: 10.1089/cbr.2014.1757.

[117] C. Yang *et al.*, ‘Identification of seven serum microRNAs from a genome-wide serum microRNA expression profile as potential noninvasive biomarkers for malignant astrocytomas’, *Int J Cancer*, vol. 132, no. 1, 2013, doi: 10.1002/ijc.27657.

[118] X. Li, J. Zheng, L. Chen, H. Diao, and Y. Liu, ‘Predictive and Prognostic Roles of Abnormal Expression of Tissue miR-125b, miR-221, and miR-222 in Glioma’, *Mol Neurobiol*, vol. 53, no. 1, 2016, doi: 10.1007/s12035-014-9017-x.

[119] R. Zhang *et al.*, ‘Plasma miR-221/222 Family as Novel Descriptive and Prognostic Biomarkers for Glioma’, *Mol Neurobiol*, vol. 53, no. 3, 2016, doi: 10.1007/s12035-014-9079-9.

[120] H. G. Møller, A. P. Rasmussen, H. H. Andersen, K. B. Johnsen, M. Henriksen, and M. Duroux, ‘A systematic review of MicroRNA in glioblastoma multiforme: Micro-modulators in the

mesenchymal mode of migration and invasion', *Molecular Neurobiology*, vol. 47, no. 1. 2013. doi: 10.1007/s12035-012-8349-7.

[121] S. A. Ciafrè *et al.*, 'Extensive modulation of a set of microRNAs in primary glioblastoma', *Biochem Biophys Res Commun*, vol. 334, no. 4, 2005, doi: 10.1016/j.bbrc.2005.07.030.

[122] S. Srinivasan, I. R. P. Patric, and K. Somasundaram, 'A Ten-microRNA expression signature predicts survival in Glioblastoma', *PLoS One*, vol. 6, no. 3, 2011, doi: 10.1371/journal.pone.0017438.

[123] Z. Shi *et al.*, 'MiR-124 governs glioma growth and angiogenesis and enhances chemosensitivity by targeting R-Ras and N-Ras', *Neuro Oncol*, vol. 16, no. 10, 2014, doi: 10.1093/neuonc/nou084.

[124] X. T. Wei, D. Chen, T. Lv, G. Li, and S. T. Qu, 'Serum MicroRNA-125b as a Potential Biomarker for Glioma Diagnosis', *Mol Neurobiol*, vol. 53, no. 1, 2016, doi: 10.1007/s12035-014-8993-1.

[125] L. Dong, Y. Li, C. Han, X. Wang, L. She, and H. Zhang, 'miRNA microarray reveals specific expression in the peripheral blood of glioblastoma patients', *Int J Oncol*, vol. 45, no. 2, 2014, doi: 10.3892/ijo.2014.2459.

[126] H. Johnson, A. M. del Rosario, B. D. Bryson, M. A. Schroeder, J. N. Sarkaria, and F. M. White, 'Molecular characterization of EGFR and EGFRvIII signaling networks in human glioblastoma tumor xenografts', *Molecular and Cellular Proteomics*, vol. 11, no. 12, 2012, doi: 10.1074/mcp.M112.019984.

[127] M. M. Knüpfer, H. Poppenborg, M. Hotfilder, K. Kühnel, J. E. A. Wolff, and M. Domula, 'CD44 expression and hyaluronic acid binding of malignant glioma cells', *Clin Exp Metastasis*, vol. 17, no. 1, 1999.

[128] D. v. Brown *et al.*, 'Expression of CD133 and CD44 in glioblastoma stem cells correlates with cell proliferation, phenotype stability and intratumor heterogeneity', *PLoS One*, vol. 12, no. 2, 2017, doi: 10.1371/journal.pone.0172791.

[129] Q. Dong *et al.*, 'Elevated CD44 expression predicts poor prognosis in patients with low-grade glioma', *Oncol Lett*, vol. 18, no. 4, 2019, doi: 10.3892/ol.2019.10728.

[130] C. Hou *et al.*, 'Overexpression of CD44 is associated with a poor prognosis in grade II/III gliomas', *J Neurooncol*, vol. 145, no. 2, 2019, doi: 10.1007/s11060-019-03288-8.

[131] W. Zhang, H. Chen, S. Lv, and H. Yang, 'High CD133 Expression Is Associated with Worse Prognosis in Patients with Glioblastoma', *Mol Neurobiol*, vol. 53, no. 4, 2016, doi: 10.1007/s12035-015-9187-1.

[132] I. Bryukhovetskiy and V. Shevchenko, ‘Molecular mechanisms of the effect of TGF-β1 on U87 human glioblastoma cells’, *Oncol Lett*, vol. 12, no. 2, 2016, doi: 10.3892/ol.2016.4756.

[133] B. Kaminska, M. Kocyk, and M. Kijewska, ‘TGF beta signaling and its role in glioma pathogenesis’, *Adv Exp Med Biol*, vol. 986, 2013, doi: 10.1007/978-94-007-4719-7_9.

[134] A. P. Halestrap, ‘The monocarboxylate transporter family-Structure and functional characterization’, *IUBMB Life*, vol. 64, no. 1. 2012. doi: 10.1002/iub.573.

[135] C. B. Colen *et al.*, ‘Metabolic targeting of lactate efflux by malignant glioma inhibits invasiveness and induces necrosis: An in vivo study1’, *Neoplasia*, vol. 13, no. 7, 2011, doi: 10.1593/neo.11134.

[136] V. Miranda-Gonçalves *et al.*, ‘Hypoxia-mediated upregulation of MCT1 expression supports the glycolytic phenotype of glioblastomas’, *Oncotarget*, vol. 7, no. 29, 2016, doi: 10.18632/oncotarget.10114.

[137] A. Thakur *et al.*, ‘Label-free sensing of exosomal MCT1 and CD147 for tracking metabolic reprogramming and malignant progression in glioma’, *Sci Adv*, vol. 6, no. 26, 2020, doi: 10.1126/sciadv.aaz6119.

[138] N. W. Colangelo and E. I. Azzam, ‘Extracellular vesicles originating from glioblastoma cells increase metalloproteinase release by astrocytes: The role of CD147 (EMMPRIN) and ionizing radiation’, *Cell Communication and Signaling*, vol. 18, no. 1, 2020, doi: 10.1186/s12964-019-0494-4.

[139] S. W. Lai, H. J. Lin, Y. S. Liu, L. Y. Yang, and D. Y. Lu, ‘Monocarboxylate transporter 4 regulates glioblastoma motility and monocyte binding ability’, *Cancers (Basel)*, vol. 12, no. 2, 2020, doi: 10.3390/cancers12020380.

[140] A. Hormigo *et al.*, ‘YKL-40 and matrix metalloproteinase-9 as potential serum biomarkers for patients with high-grade gliomas’, *Clinical Cancer Research*, vol. 12, no. 19, 2006, doi: 10.1158/1078-0432.CCR-06-0181.

[141] H. Nagashima *et al.*, ‘Diagnostic value of glutamate with 2-hydroxyglutarate in magnetic resonance spectroscopy for IDH1 mutant glioma’, *Neuro Oncol*, vol. 18, no. 11, 2016, doi: 10.1093/neuonc/now090.

[142] E. Subramani *et al.*, ‘Glutamate is a noninvasive metabolic biomarker of IDH1-mutant glioma response to temozolomide treatment’, *Cancer Res*, vol. 80, no. 22, 2020, doi: 10.1158/0008-5472.CAN-20-1314.

[143] M. Radoul *et al.*, ‘Early noninvasive metabolic biomarkers of mutant idh inhibition in glioma’, *Metabolites*, vol. 11, no. 2, 2021, doi: 10.3390/metabo11020109.

[144] P. Damborský, J. Švitel, and J. Katrlík, ‘Optical biosensors’, *Essays Biochem*, vol. 60, no. 1, 2016, doi: 10.1042/EBC20150010.

[145] S. M. Yoo and S. Y. Lee, ‘Optical Biosensors for the Detection of Pathogenic Microorganisms’, *Trends in Biotechnology*, vol. 34, no. 1. 2016. doi: 10.1016/j.tibtech.2015.09.012.

[146] L. Xu, N. Shoaie, F. Jahanpeyma, J. Zhao, M. Azimzadeh, and K. T. Al−Jamal, ‘Optical, electrochemical and electrical (nano)biosensors for detection of exosomes: A comprehensive overview’, *Biosensors and Bioelectronics*, vol. 161. 2020. doi: 10.1016/j.bios.2020.112222.

[147] G. Qiu, A. Thakur, C. Xu, S. P. Ng, Y. Lee, and C. M. L. Wu, ‘Detection of Glioma-Derived Exosomes with the Biotinylated Antibody-Functionalized Titanium Nitride Plasmonic Biosensor’, *Adv Funct Mater*, vol. 29, no. 9, 2019, doi: 10.1002/adfm.201806761.

[148] A. Thakur *et al.*, ‘Direct detection of two different tumor-derived extracellular vesicles by SAM-AuNIs LSPR biosensor’, *Biosens Bioelectron*, vol. 94, 2017, doi: 10.1016/j.bios.2017.03.036.

[149] A. Thakur *et al.*, ‘In vivo liquid biopsy for glioblastoma malignancy by the AFM and LSPR based sensing of exosomal CD44 and CD133 in a mouse model’, *Biosens Bioelectron*, vol. 191, 2021, doi: 10.1016/j.bios.2021.113476.

[150] C. Xu *et al.*, ‘Determination of glioma cells’ malignancy and their response to TMZ via detecting exosomal BIGH3 by a TiO2-CTFE-AuNIs plasmonic biosensor’, *Chemical Engineering Journal*, vol. 415, 2021, doi: 10.1016/j.cej.2021.128948.

[151] L. Liu *et al.*, ‘Site specific biotinylated antibody functionalized Ag@AuNIs LSPR biosensor for the ultrasensitive detection of exosomal MCT4, a glioblastoma progression biomarker’, *Chemical Engineering Journal*, vol. 446, Oct. 2022, doi: 10.1016/j.cej.2022.137383.

[152] K. Hao *et al.*, ‘High-sensitive surface plasmon resonance microRNA biosensor based on streptavidin functionalized gold nanorods-assisted signal amplification’, *Anal Chim Acta*, vol. 954, 2017, doi: 10.1016/j.aca.2016.12.006.

[153] A. Kozomara, M. Birgaoanu, and S. Griffiths-Jones, ‘MiRBase: From microRNA sequences to function’, *Nucleic Acids Res*, vol. 47, no. D1, 2019, doi: 10.1093/nar/gky1141.

[154] A. Krell *et al.*, ‘MiR-16-5p is frequently down-regulated in astrocytic gliomas and modulates glioma cell proliferation, apoptosis and response to cytotoxic therapy’, *Neuropathol Appl Neurobiol*, vol. 45, no. 5, 2019, doi: 10.1111/nan.12532.

[155] T. Q. Yang *et al.*, ‘MicroRNA-16 inhibits glioma cell growth and invasion through suppression of BCL2 and the nuclear factor-κB1/MMP9 signaling pathway’, *Cancer Sci*, vol. 105, no. 3, 2014, doi: 10.1111/cas.12351.

[156] D. A. Long, *The Raman effect: a unified treatment of the theory of Raman scattering by molecules. 2002*, vol. 8. 2002.

[157] E. C. Le Ru and P. G. Etchegoin, *Principles of Surface-Enhanced Raman Spectroscopy*. 2009. doi: 10.1016/B978-0-444-52779-0.X0001-3.

[158] E. J. Blackie, E. C. le Ru, and P. G. Etchegoin, ‘Single-molecule surface-enhanced raman spectroscopy of nonresonant molecules’, *J Am Chem Soc*, vol. 131, no. 40, 2009, doi: 10.1021/ja905319w.

[159] J. R. Lombardi, R. L. Birke, T. Lu, and J. Xu, ‘Charge-transfer theory of surface enhanced Raman spectroscopy: Herzberg-Teller contributions’, *J Chem Phys*, vol. 84, no. 8, 1986, doi: 10.1063/1.450037.

[160] M. Jalali *et al.*, ‘Plasmonic nanobowtiefluidic device for sensitive detection of glioma extracellular vesicles by Raman spectrometry’, *Lab Chip*, vol. 21, no. 5, 2021, doi: 10.1039/d0lc00957a.

[161] D. Choi, L. Montermini, H. Jeong, S. Sharma, B. Meehan, and J. Rak, ‘Mapping Subpopulations of Cancer Cell-Derived Extracellular Vesicles and Particles by Nano-Flow Cytometry’, *ACS Nano*, vol. 13, no. 9, 2019, doi: 10.1021/acsnano.9b04480.

[162] W. H. Kim, J. U. Lee, S. Song, S. Kim, Y. J. Choi, and S. J. Sim, ‘A label-free, ultra-highly sensitive and multiplexed SERS nanoplasmonic biosensor for miRNA detection using a head-flocked gold nanopillar’, *Analyst*, vol. 144, no. 5, 2019, doi: 10.1039/c8an01745j.

[163] C. Novara *et al.*, ‘SERS-active metal-dielectric nanostructures integrated in microfluidic devices for label-free quantitative detection of miRNA’, *Faraday Discuss*, vol. 205, 2017, doi: 10.1039/c7fd00140a.

[164] A. Ali *et al.*, ‘Miniaturized Raman Instruments for SERS-Based Point-of-Care Testing on Respiratory Viruses’, *Biosensors (Basel)*, vol. 12, no. 8, Aug. 2022, doi: 10.3390/bios12080590.

[165] M. Lee, K. Lee, K. H. Kim, K. W. Oh, and J. Choo, ‘SERS-based immunoassay using a gold array-embedded gradient microfluidic chip’, *Lab Chip*, vol. 12, no. 19, 2012, doi: 10.1039/c2lc40353f.

[166] D. Choi, T. Kang, H. Cho, Y. Choi, and L. P. Lee, ‘Additional amplifications of SERS via an optofluidic CD-based platform’, *Lab Chip*, vol. 9, no. 2, 2009, doi: 10.1039/b812067f.

[167] K. R. Ackermann, T. Henkel, and J. Popp, ‘Quantitative online detection of low-concentrated drugs via a SERS microfluidic system’, *ChemPhysChem*, vol. 8, no. 18, 2007, doi: 10.1002/cphc.200700554.

[168] R. Gao *et al.*, ‘Highly sensitive trace analysis of paraquat using a surface-enhanced Raman scattering microdroplet sensor’, *Anal Chim Acta*, vol. 681, no. 1–2, 2010, doi: 10.1016/j.aca.2010.09.036.

[169] S. Damiati and B. Schuster, ‘Electrochemical biosensors based on S-layer proteins’, *Sensors (Switzerland)*, vol. 20, no. 6, 2020, doi: 10.3390/s20061721.

[170] S. M. Traynor *et al.*, ‘Review—Recent Advances in Electrochemical Detection of Prostate Specific Antigen (PSA) in Clinically-Relevant Samples’, *J Electrochem Soc*, vol. 167, no. 3, 2020, doi: 10.1149/1945-7111/ab69fd.

[171] A. B. Ganganboina, N. K. Dega, H. L. Tran, W. Darmonto, and R. A. Doong, ‘Application of sulfur-doped graphene quantum dots@gold-carbon nanosphere for electrical pulse-induced impedimetric detection of glioma cells’, *Biosens Bioelectron*, vol. 181, 2021, doi: 10.1016/j.bios.2021.113151.

[172] M. Hu *et al.*, ‘CoNi bimetallic metal–organic framework as an efficient biosensing platform for miRNA 126 detection’, *Appl Surf Sci*, vol. 542, 2021, doi: 10.1016/j.apsusc.2020.148586.

[173] C. Guo, Z. Li, F. Duan, Z. Zhang, F. Marchetti, and M. Du, ‘Semiconducting CuxNi3-x(hexahydroxytriphenylene)2framework for electrochemical aptasensing of C6 glioma cells and epidermal growth factor receptor’, *J Mater Chem B*, vol. 8, no. 43, 2020, doi: 10.1039/d0tb01910k.

[174] Z. Sun *et al.*, ‘An Electrochemical Biosensor Designed by Using Zr-Based Metal-Organic Frameworks for the Detection of Glioblastoma-Derived Exosomes with Practical Application’, *Anal Chem*, vol. 92, no. 5, 2020, doi: 10.1021/acs.analchem.9b05241.

[175] C. Wang *et al.*, ‘Electrochemical biosensing of circulating microRNA-21 in cerebrospinal fluid of medulloblastoma patients through target-induced redox signal amplification’, *Microchimica Acta*, vol. 189, no. 3, 2022, doi: 10.1007/s00604-022-05210-y.

[176] J. L. Scoggin *et al.*, ‘An enzyme-based electrochemical biosensor probe with sensitivity to detect astrocytic versus glioma uptake of glutamate in real time in vitro’, *Biosens Bioelectron*, vol. 126, 2019, doi: 10.1016/j.bios.2018.11.023.

[177] S. Poorahong *et al.*, ‘Development of amperometric α-ketoglutarate biosensor based on ruthenium-rhodium modified carbon fiber enzyme microelectrode’, *Biosens Bioelectron*, vol. 26, no. 8, 2011, doi: 10.1016/j.bios.2011.01.026.

[178] J. J. Xu, X. L. Luo, and H. Y. Chen, ‘Analytical aspects of FET-based biosensors’, *Frontiers in Bioscience*, vol. 10, no. 1. 2005. doi: 10.2741/1538.

[179] X. Luo and J. J. Davis, ‘Electrical biosensors and the label free detection of protein disease biomarkers’, *Chem Soc Rev*, vol. 42, no. 13, 2013, doi: 10.1039/c3cs60077g.

[180] E. Macchia *et al.*, ‘Single-molecule detection with a millimetre-sized transistor’, *Nat Commun*, vol. 9, no. 1, 2018, doi: 10.1038/s41467-018-05235-z.

[181] P. R. Nair and M. A. Alam, ‘Performance limits of nanobiosensors’, *Appl Phys Lett*, vol. 88, no. 23, 2006, doi: 10.1063/1.2211310.

[182] K. A. Malsagova *et al.*, ‘Micro-raman spectroscopy for monitoring of deposition quality of high-k stack protective layer onto nanowire FET chips for highly sensitive miRNA detection’, *Biosensors (Basel)*, vol. 8, no. 3, 2018, doi: 10.3390/bios8030072.

[183] D. Li *et al.*, ‘A supersensitive silicon nanowire array biosensor for quantitating tumor marker ctDNA’, *Biosens Bioelectron*, vol. 181, 2021, doi: 10.1016/j.bios.2021.113147.

[184] R. S. McNeill *et al.*, ‘PIK3CA missense mutations promote glioblastoma pathogenesis, but do not enhance targeted PI3K inhibition’, *PLoS One*, vol. 13, no. 7, 2018, doi: 10.1371/journal.pone.0200014.

[185] C. C. Wu, F. H. Ko, Y. S. Yang, D. L. Hsia, B. S. Lee, and T. S. Su, ‘Label-free biosensing of a gene mutation using a silicon nanowire field-effect transistor’, *Biosens Bioelectron*, vol. 25, no. 4, 2009, doi: 10.1016/j.bios.2009.08.031.

[186] E. Kebebew *et al.*, ‘The prevalence and prognostic value of BRAF mutation in thyroid cancer’, *Ann Surg*, vol. 246, no. 3, 2007, doi: 10.1097/SLA.0b013e318148563d.

[187] B. K. Kleinschmidt-Demasters, D. L. Aisner, D. K. Birks, and N. K. Foreman, ‘Epithelioid GBMs show a high percentage of BRAF V600E mutation’, *American Journal of Surgical Pathology*, vol. 37, no. 5, 2013, doi: 10.1097/PAS.0b013e31827f9c5e.

[188] J. Song *et al.*, ‘Extended Solution Gate OFET-Based Biosensor for Label-Free Glial Fibrillary Acidic Protein Detection with Polyethylene Glycol-Containing Bioreceptor Layer’, *Adv Funct Mater*, vol. 27, no. 20, 2017, doi: 10.1002/adfm.201606506.

[189] W. Yang, K. R. Ratinac, S. R. Ringer, P. Thordarson, J. J. Gooding, and F. Braet, ‘Carbon nanomaterials in biosensors: Should you use nanotubes or graphene’, *Angewandte Chemie - International Edition*, vol. 49, no. 12. 2010. doi: 10.1002/anie.200903463.

[190] F. Schedin *et al.*, ‘Detection of individual gas molecules adsorbed on graphene’, *Nat Mater*, vol. 6, no. 9, 2007, doi: 10.1038/nmat1967.

[191] L. Xu *et al.*, 'Detection of Glial Fibrillary Acidic Protein in Patient Plasma Using On-Chip Graphene Field-Effect Biosensors, in Comparison with ELISA and Single-Molecule Array', *ACS Sens*, vol. 7, no. 1, 2022, doi: 10.1021/acssensors.1c02232.

[192] D. K. Ban *et al.*, 'Direct DNA Methylation Profiling with an Electric Biosensor', *ACS Nano*, vol. 14, no. 6, 2020, doi: 10.1021/acsnano.9b10085.

[193] M. Selvaraj *et al.*, 'Label free detection of miRNA-21 with electrolyte gated organic field effect transistors (EGOFETs)', *Biosens Bioelectron*, vol. 182, 2021, doi: 10.1016/j.bios.2021.113144.

[194] Z. Li *et al.*, 'Evaluating glioma-associated microRNA by complementation on a biological nanosensor', *Biotechnol Appl Biochem*, Jun. 2022, doi: 10.1002/bab.2374.

[195] C. Fercher, M. L. Jones, S. M. Mahler, and S. R. Corrie, 'Recombinant Antibody Engineering Enables Reversible Binding for Continuous Protein Biosensing', *ACS Sens*, vol. 6, no. 3, 2021, doi: 10.1021/acssensors.0c01510.

[196] K. Sivashanmugan, Y. Zhao, and A. X. Wang, 'Tetrahydrocannabinol sensing in complex biofluid with portable raman spectrometer using diatomaceous SERS substrates', *Biosensors (Basel)*, vol. 9, no. 4, 2019, doi: 10.3390/bios9040125.

[197] J. Sabaté del Río, O. Y. F. Henry, P. Jolly, and D. E. Ingber, 'An antifouling coating that enables affinity-based electrochemical biosensing in complex biological fluids', *Nat Nanotechnol*, vol. 14, no. 12, 2019, doi: 10.1038/s41565-019-0566-z.

[198] J. T. Liu *et al.*, 'Surface plasmon resonance biosensor with high anti-fouling ability for the detection of cardiac marker troponin T', *Anal Chim Acta*, vol. 703, no. 1, 2011, doi: 10.1016/j.aca.2011.07.019.

[199] L. Chen, X. Liu, and C. Chen, 'Impedimetric biosensor modified with hydrophilic material of tannic acid/polyethylene glycol and dopamine-assisted deposition for detection of breast cancer-related BRCA1 gene', *Journal of Electroanalytical Chemistry*, vol. 791, 2017, doi: 10.1016/j.jelechem.2017.03.001.

[200] N. Ahmad *et al.*, 'Peptide cross-linked poly (Ethylene glycol) hydrogel films as biosensor coatings for the detection of collagenase', *Sensors (Switzerland)*, vol. 19, no. 7, 2019, doi: 10.3390/s19071677.

[201] A. M. C. Maan, A. H. Hofman, W. M. de Vos, and M. Kamperman, 'Recent Developments and Practical Feasibility of Polymer-Based Antifouling Coatings', *Advanced Functional Materials*, vol. 30, no. 32. 2020. doi: 10.1002/adfm.202000936.

[202] R. L. McCreery, *Raman Spectroscopy for Chemical Analysis*. 2005. doi: 10.1002/0471721646.

[203] P. A. Mosier-Boss, ‘Review of SERS substrates for chemical sensing’, *Nanomaterials*, vol. 7, no. 6. 2017. doi: 10.3390/nano7060142.

[204] W. Lee, S. Y. Lee, R. M. Briber, and O. Rabin, ‘Self-assembled SERS substrates with tunable surface plasmon resonances’, *Adv Funct Mater*, vol. 21, no. 18, 2011, doi: 10.1002/adfm.201101218.

[205] W. Li, P. H. C. Camargo, X. Lu, and Y. Xia, ‘Dimers of silver nanospheres: Facile synthesis and their use as hot spots for surface-enhanced raman scattering’, *Nano Lett*, vol. 9, no. 1, 2009, doi: 10.1021/nl803621x.

[206] V. Joseph, A. Matschulat, J. Polte, S. Rolf, F. Emmerling, and J. Kneipp, ‘SERS enhancement of gold nanospheres of defined size’, *Journal of Raman Spectroscopy*, vol. 42, no. 9, 2011, doi: 10.1002/jrs.2939.

[207] K. Ponlamuangdee, G. L. Hornyak, T. Bora, and S. Bamrungsap, ‘Graphene oxide/gold nanorod plasmonic paper-a simple and cost-effective SERS substrate for anticancer drug analysis’, *New Journal of Chemistry*, vol. 44, no. 33, 2020, doi: 10.1039/d0nj02448a.

[208] J. Dong *et al.*, ‘Nanoscale Vertical Arrays of Gold Nanorods by Self-Assembly: Physical Mechanism and Application’, *Nanoscale Res Lett*, vol. 14, 2019, doi: 10.1186/s11671-019-2946-6.

[209] J. Zhang, M. Irannejad, and B. Cui, ‘Bowtie Nanoantenna with Single-Digit Nanometer Gap for Surface-Enhanced Raman Scattering (SERS)’, *Plasmonics*, vol. 10, no. 4, 2015, doi: 10.1007/s11468-014-9870-5.

[210] N. A. Hatab, C. M. Rouleau, S. T. Retterer, G. Eres, P. B. Hatzinger, and B. Gu, ‘An integrated portable Raman sensor with nanofabricated gold bowtie array substrates for energetics detection’, *Analyst*, vol. 136, no. 8, 2011, doi: 10.1039/c0an00982b.

[211] F. Liebig, R. Henning, R. M. Sarhan, C. Prietzel, M. Bargheer, and J. Koetz, ‘A new route to gold nanoflowers’, *Nanotechnology*, vol. 29, no. 18, 2018, doi: 10.1088/1361-6528/aaaffd.

[212] A. D. Rakić, A. B. Djurišić, J. M. Elazar, and M. L. Majewski, ‘Optical properties of metallic films for vertical-cavity optoelectronic devices’, *Appl Opt*, vol. 37, no. 22, 1998, doi: 10.1364/ao.37.005271.

[213] F. Hao and P. Nordlander, ‘Plasmonic coupling between a metallic nanosphere and a thin metallic wire’, *Appl Phys Lett*, vol. 89, no. 10, 2006, doi: 10.1063/1.2345352.

[214] M. A. Green, ‘Self-consistent optical parameters of intrinsic silicon at 300 K including temperature coefficients’, *Solar Energy Materials and Solar Cells*, vol. 92, no. 11, 2008, doi: 10.1016/j.solmat.2008.06.009.

[215] L. Mao, Z. Li, B. Wu, and H. Xu, 'Effects of quantum tunneling in metal nanogap on surface-enhanced Raman scattering', *Appl Phys Lett*, vol. 94, no. 24, 2009, doi: 10.1063/1.3155157.

[216] Z. Gu *et al.*, 'Highly sensitive AlGaN/GaN HEMT biosensors using an ethanolamine modification strategy for bioassay applications', *RSC Adv*, vol. 9, no. 27, 2019, doi: 10.1039/c9ra02055a.

[217] A. Ebner, P. Hinterdorfer, and H. J. Gruber, 'Comparison of different aminofunctionalization strategies for attachment of single antibodies to AFM cantilevers', *Ultramicroscopy*, vol. 107, no. 10–11, 2007, doi: 10.1016/j.ultramic.2007.02.035.

[218] 'Origin: Data Analysis and Graphing Software'. https://www.originlab.com/index.aspx?go=Products/Origin#Data_Analysis_and_Statistics (accessed Mar. 15, 2023).

[219] G. N. Xiao and S. Q. Man, 'Surface-enhanced Raman scattering of methylene blue adsorbed on cap-shaped silver nanoparticles', *Chem Phys Lett*, vol. 447, no. 4–6, 2007, doi: 10.1016/j.cplett.2007.09.045.

[220] C. Ruan, W. Wang, and B. Gu, 'Single-molecule detection of thionine on aggregated gold nanoparticles by surface enhanced Raman scattering', *Journal of Raman Spectroscopy*, vol. 38, no. 5, 2007, doi: 10.1002/jrs.1691.

[221] S. Saha, M. Sachdev, and S. K. Mitra, 'Recent advances in label-free optical, electrochemical, and electronic biosensors for glioma biomarkers', *Biomicrofluidics*, vol. 17, no. 1, p. 011502, Jan. 2023, doi: 10.1063/5.0135525.

Supplementary Information

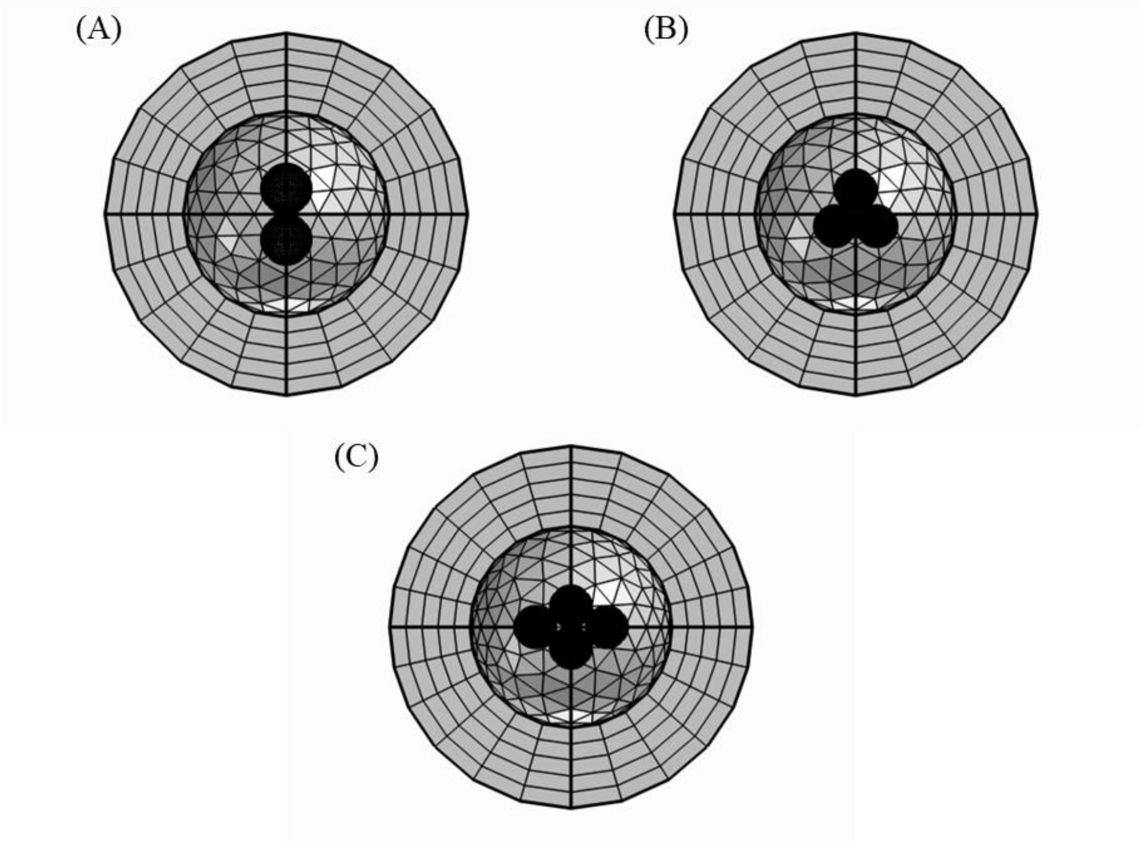

Figure S1: *Geometry and meshing of the multiple nanospheres system with the physical domain and perfectly matched layer (a) nanodimer (b) nanotrimers (c) nanotetramer.*

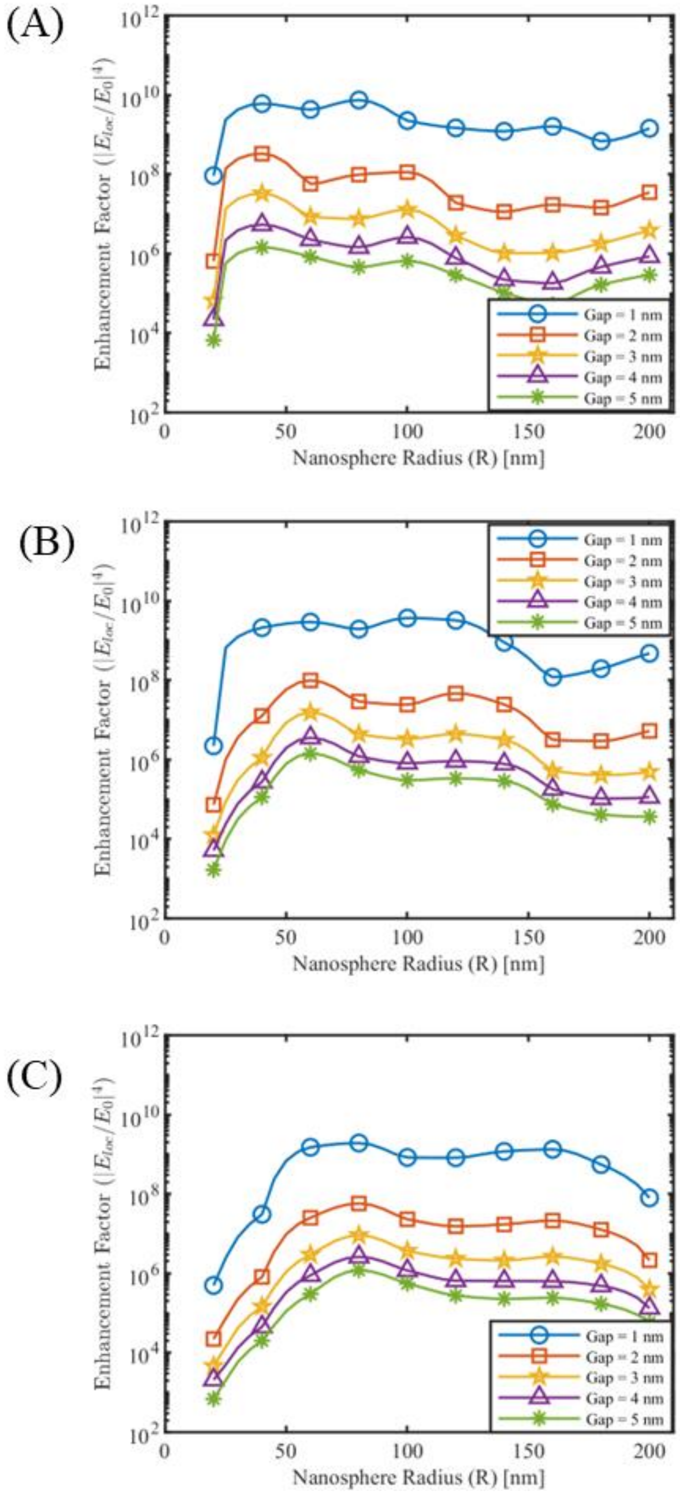

Figure S2: *Enhancement factor plots of silver nanodimer at wavelength (a) 532 nm (b) 633 nm and (c) 785 nm.*

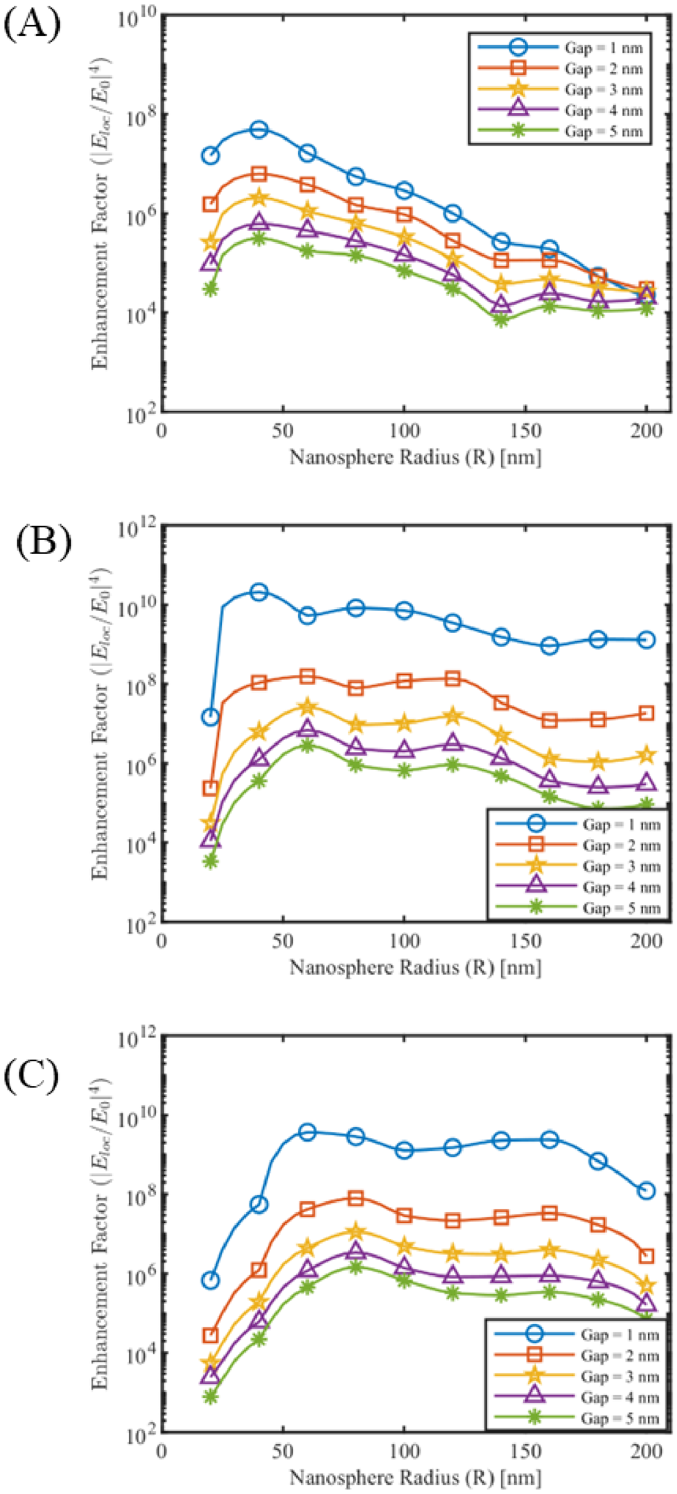

Figure S3: *Enhancement factor plots of gold nanodimer at wavelength (a) 532 nm (b) 633 nm and (c) 785 nm.*

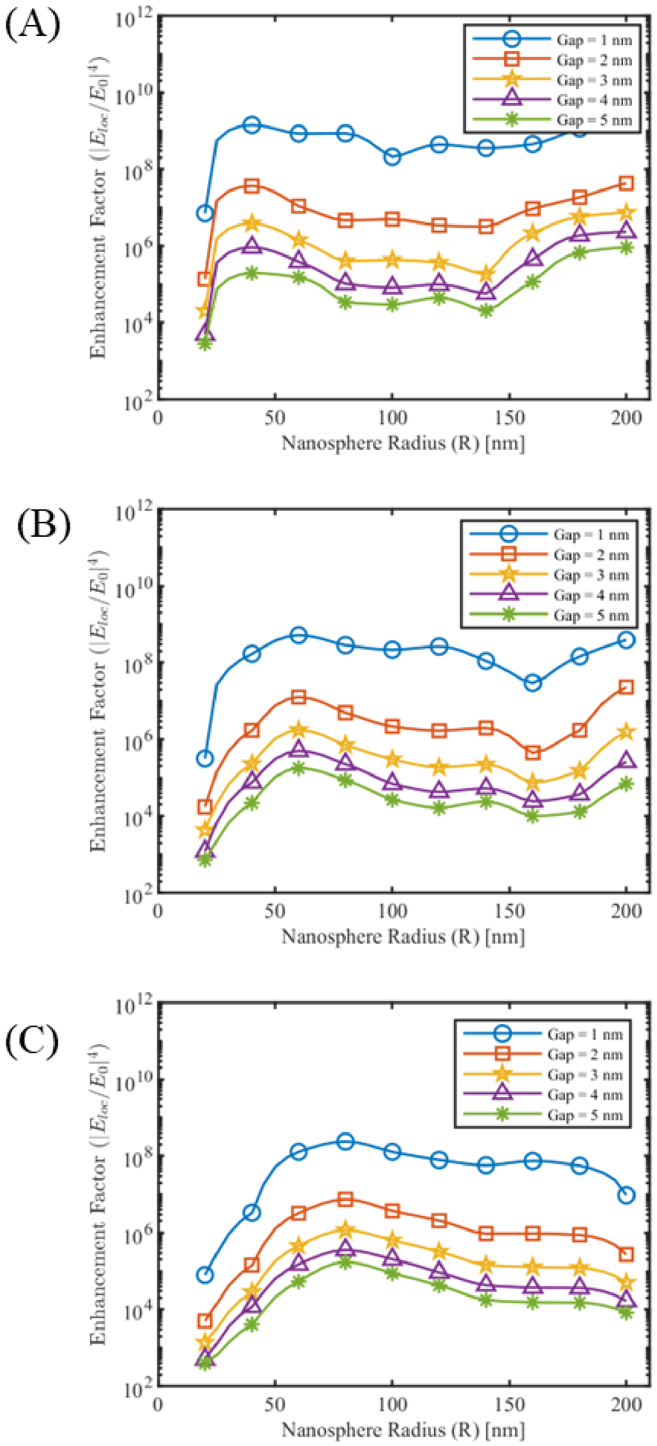

***Figure S4:** Enhancement factor plots of silver nanotrimer orientation △ at wavelength (a) 532 nm (b) 633 nm and (c) 785 nm.*

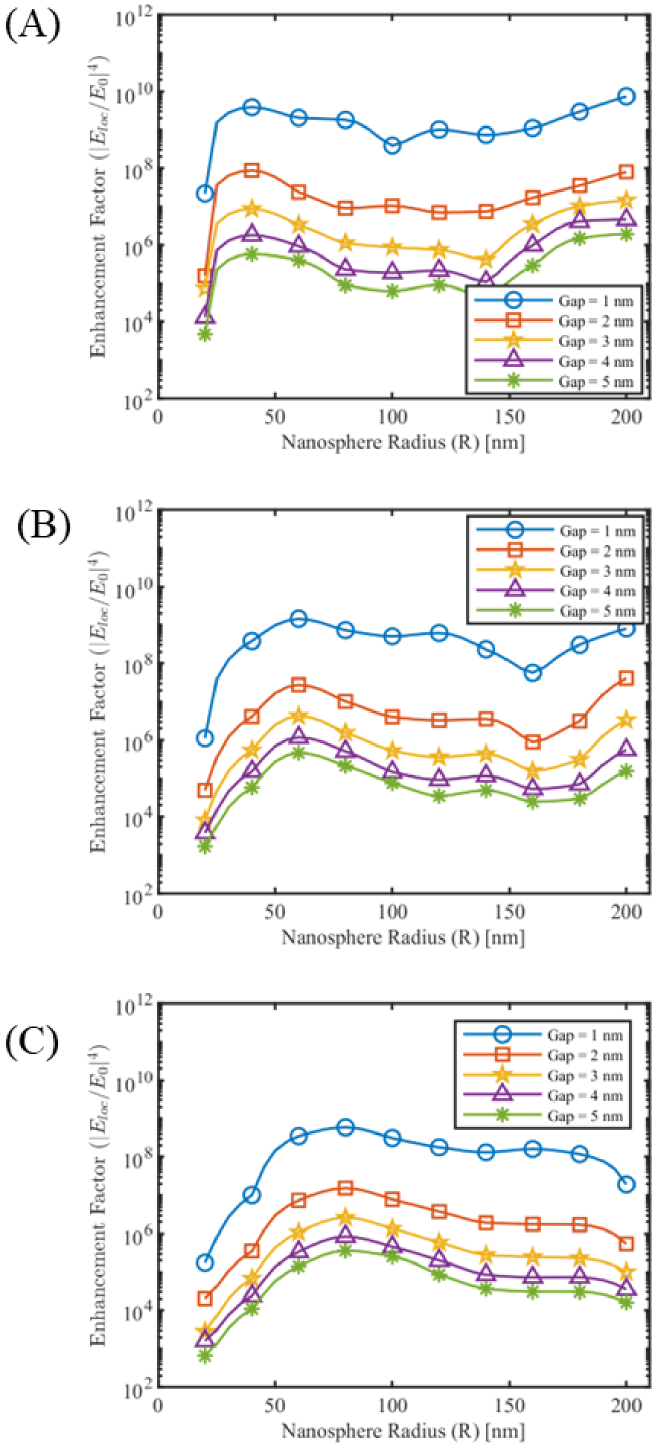

Figure S5: *Enhancement factor plots of silver nanotrimer orientation ▷ at wavelength (a) 532 nm (b) 633 nm and (c) 785 nm.*

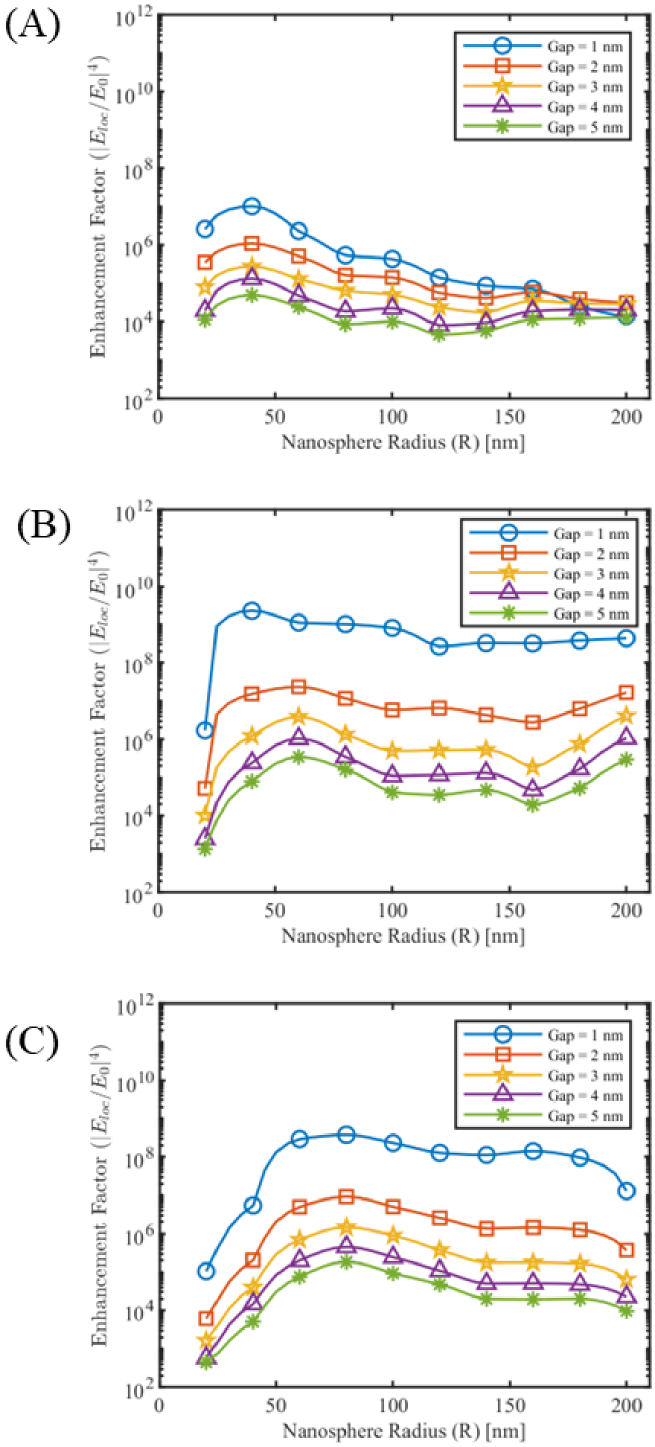

Figure S6: *Enhancement factor plots of gold nanotrimer orientation △ at wavelength (a) 532 nm (b) 633 nm and (c) 785 nm.*

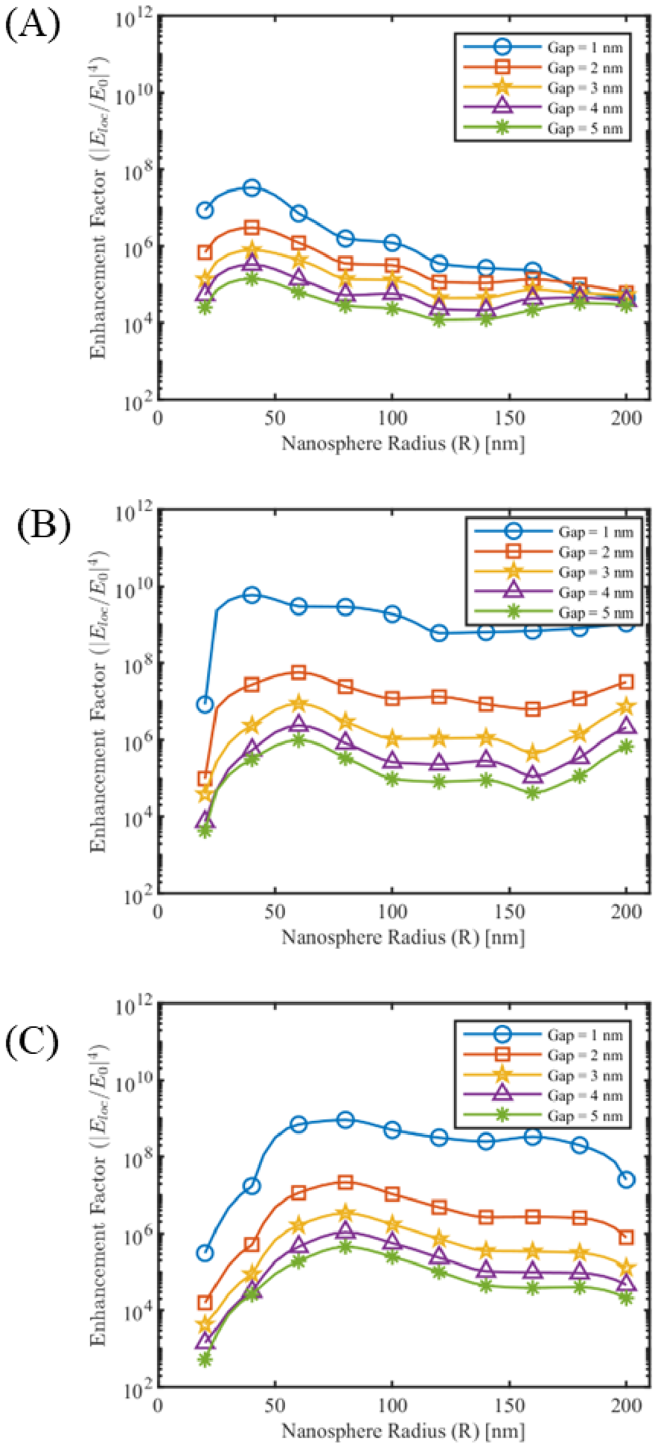

Figure S7: Enhancement factor plots of gold nanotrimer orientation ▷ at wavelength (a) 532 nm (b) 633 nm and (c) 785 nm.

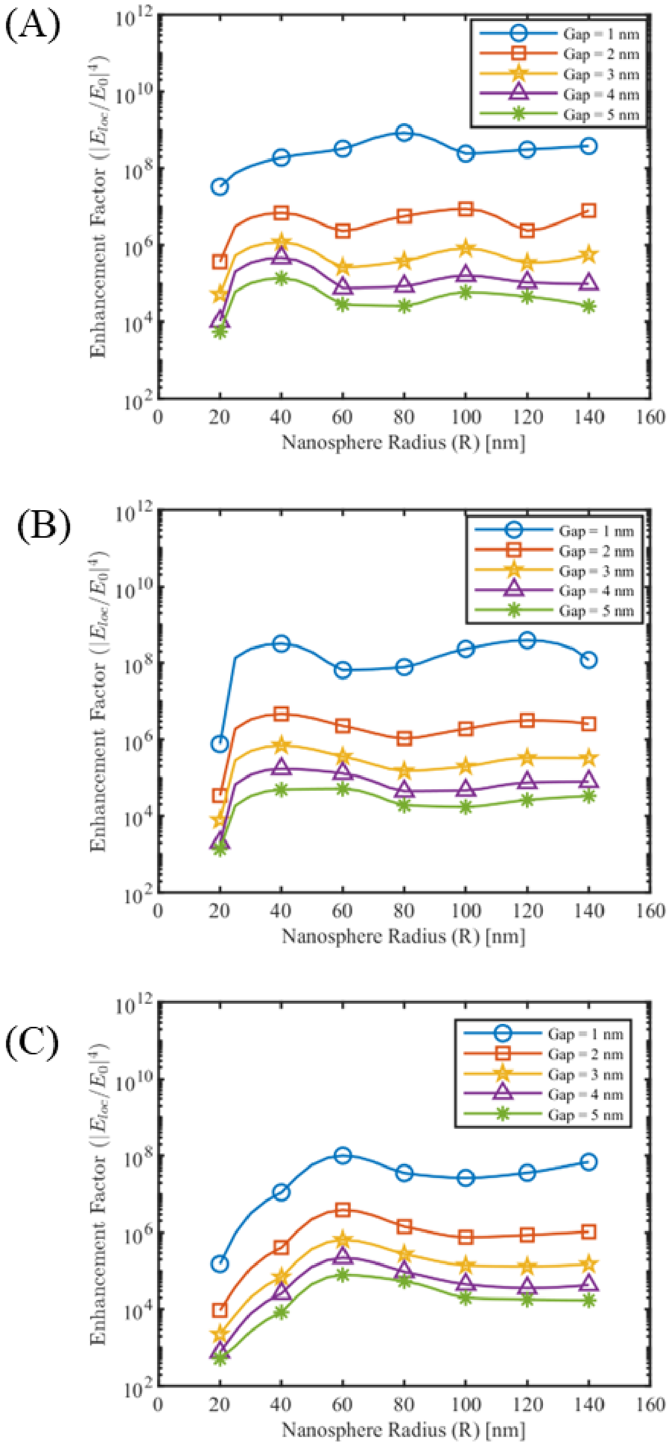

Figure S8: *Enhancement factor plots of silver nanotetramer orientation ◊ at wavelength (a) 532 nm (b) 633 nm and (c) 785 nm.*

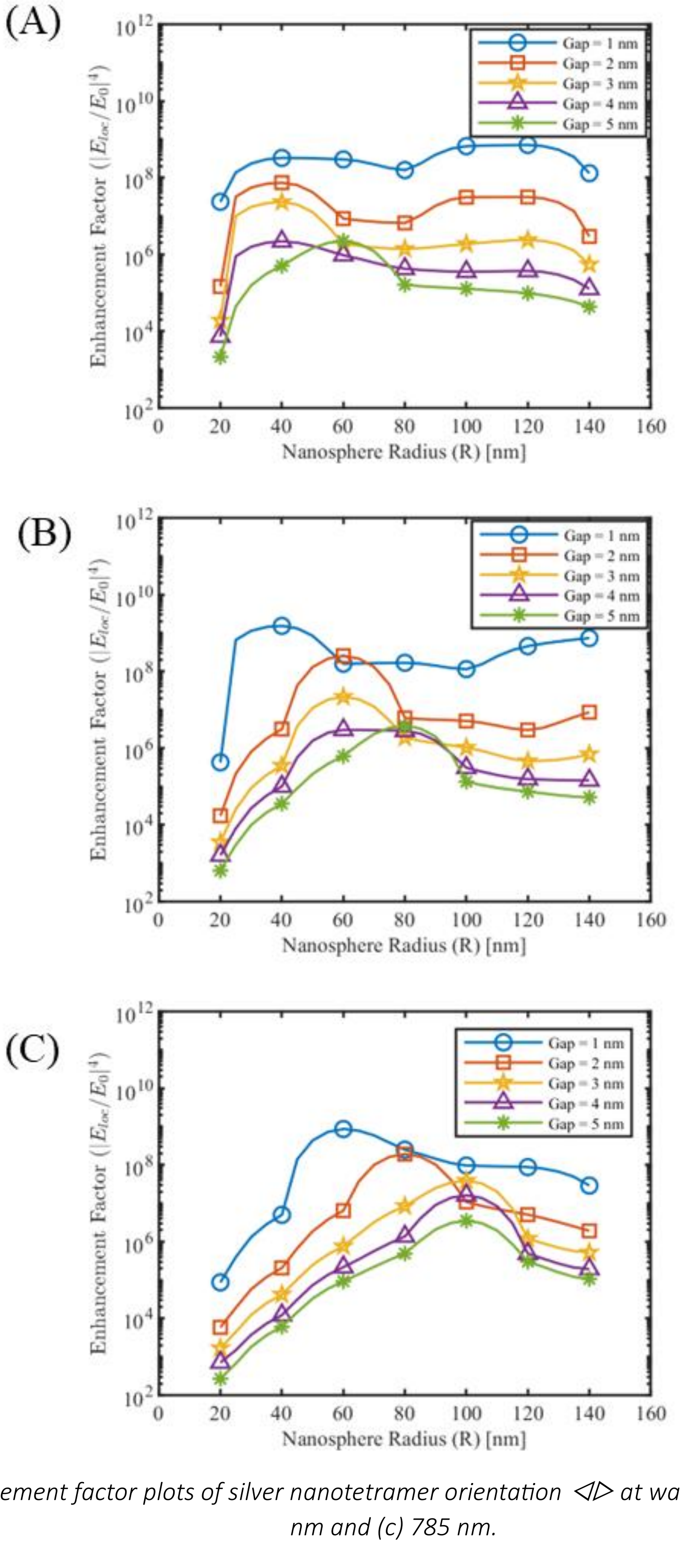

Figure S9: *Enhancement factor plots of silver nanotetramer orientation ◁▷ at wavelength (a) 532 nm (b) 633 nm and (c) 785 nm.*

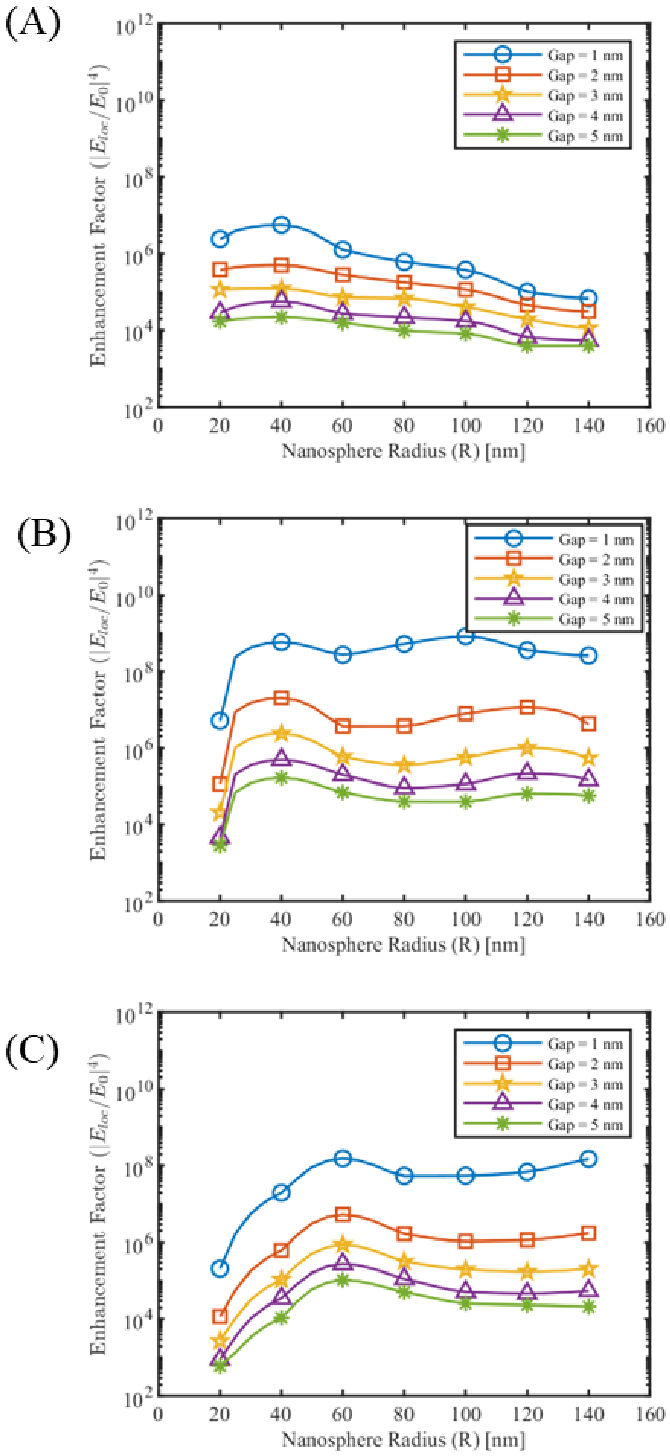

Figure S10: *Enhancement factor plots of gold nanotetramer orientation ◊ at wavelength (a) 532 nm (b) 633 nm and (c) 785 nm.*

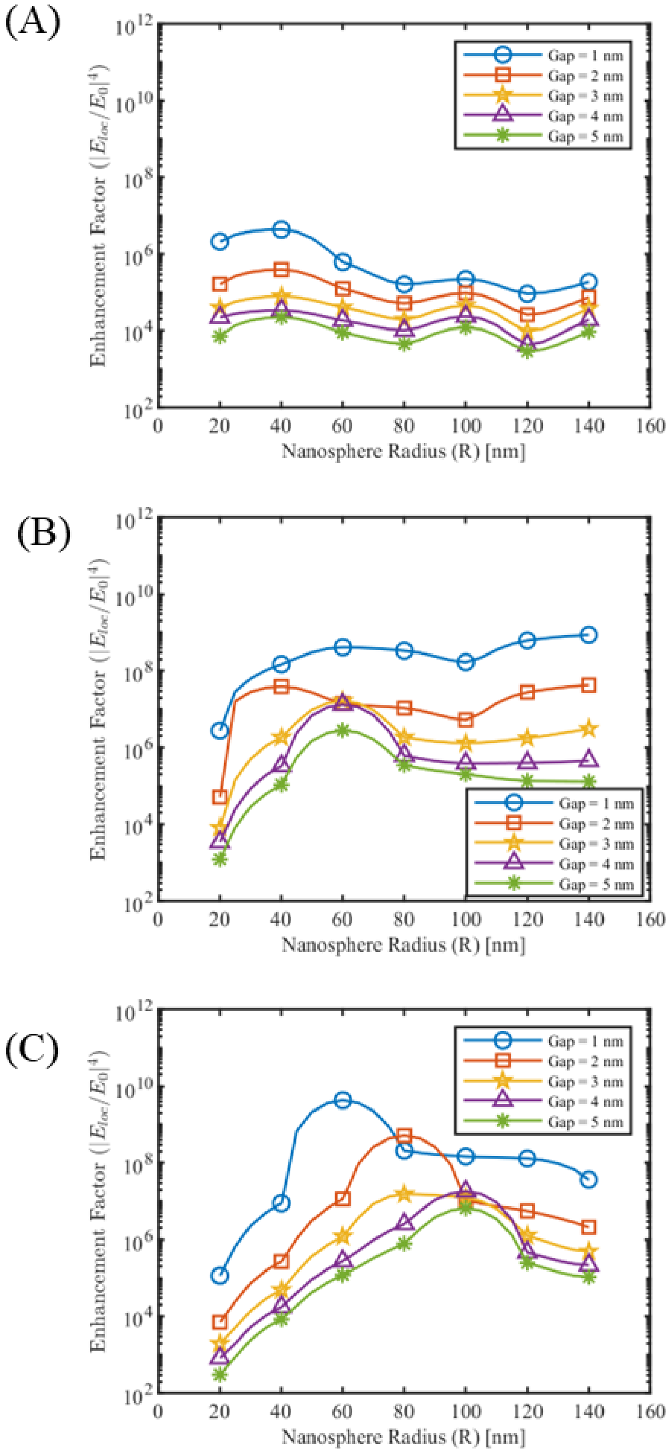

Figure S11: *Enhancement factor plots of gold nanotetramer orientation ◁▷ at wavelength (a) 532 nm (b) 633 nm and (c) 785 nm.*

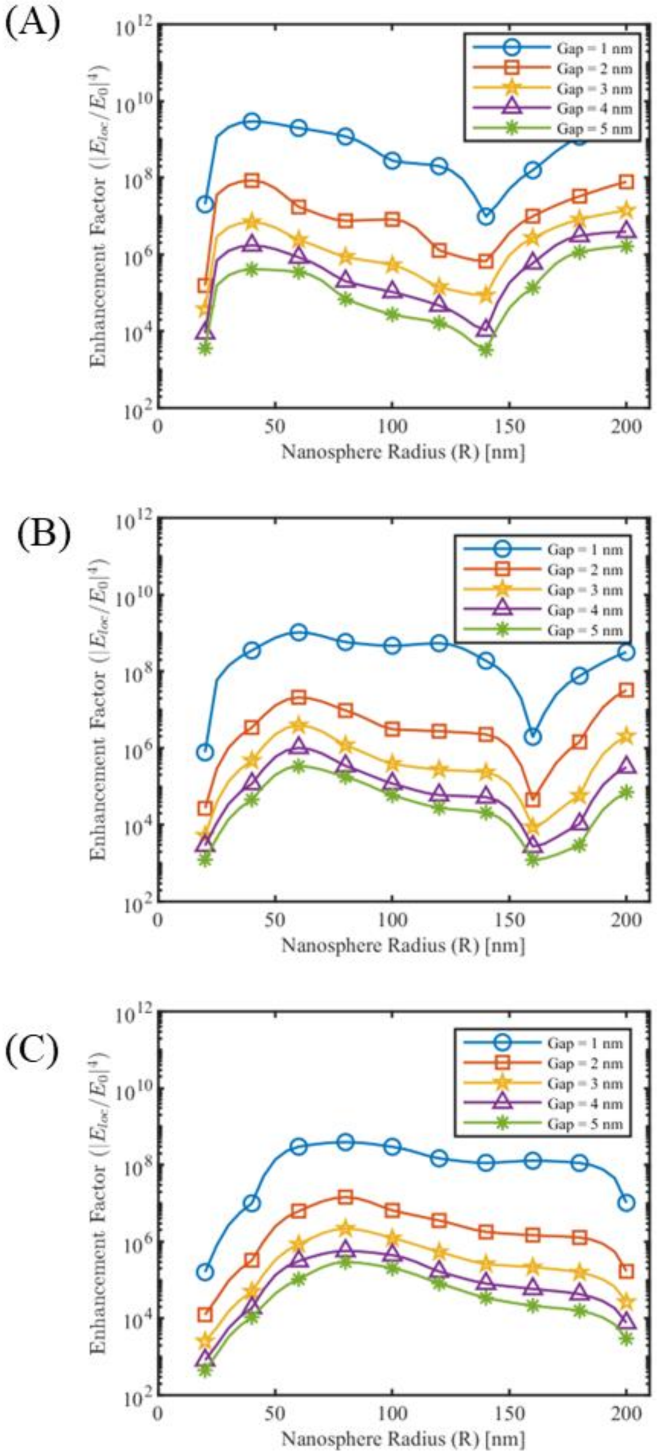

Figure S12: *Enhancement factor plots of hotspot between sphere 1 and 2 (middle hotspot) of silver nanotrimer orientation ▷ at wavelength (a) 532 nm (b) 633 nm and (c) 785 nm, demonstrating hotspot switching.*

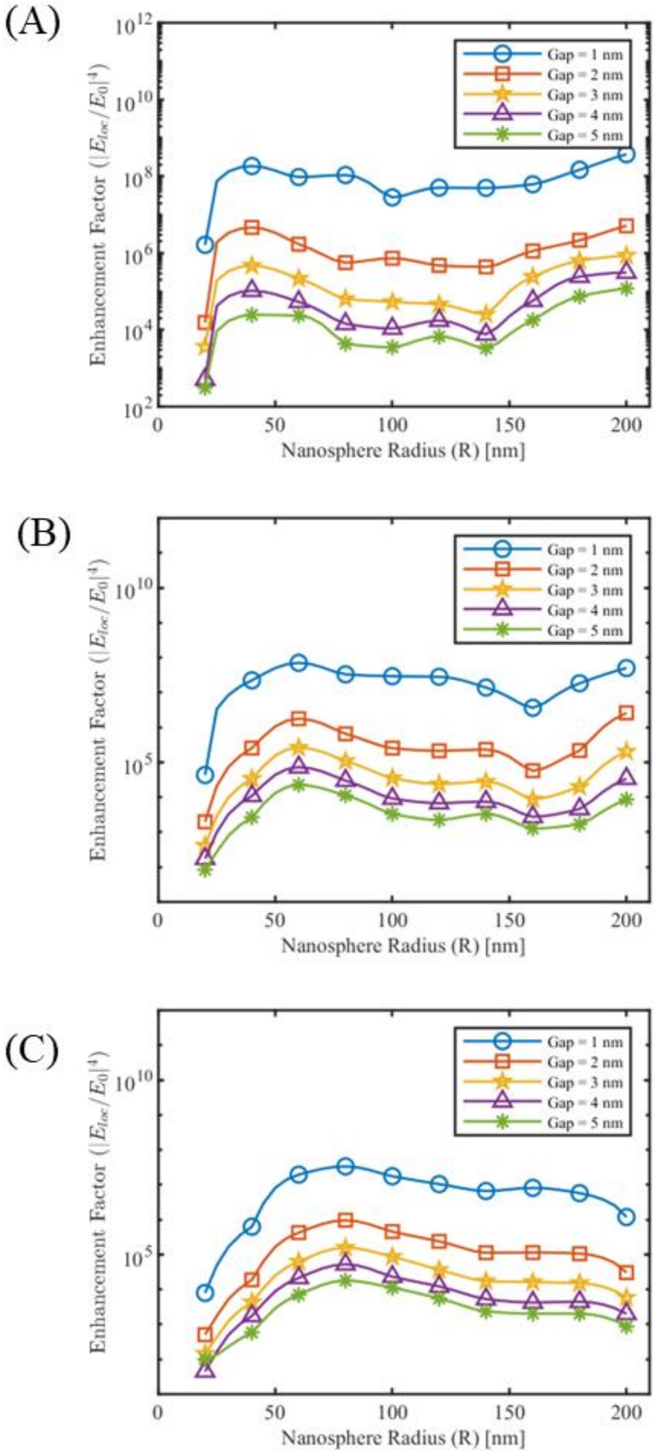

Figure S13: *Enhancement factor plots of hotspot between sphere 1 and 3 (side hotspot) of silver nanotrimer orientation ▷ at wavelength (a) 532 nm (b) 633 nm and (c) 785 nm, demonstrating hotspot switching.*

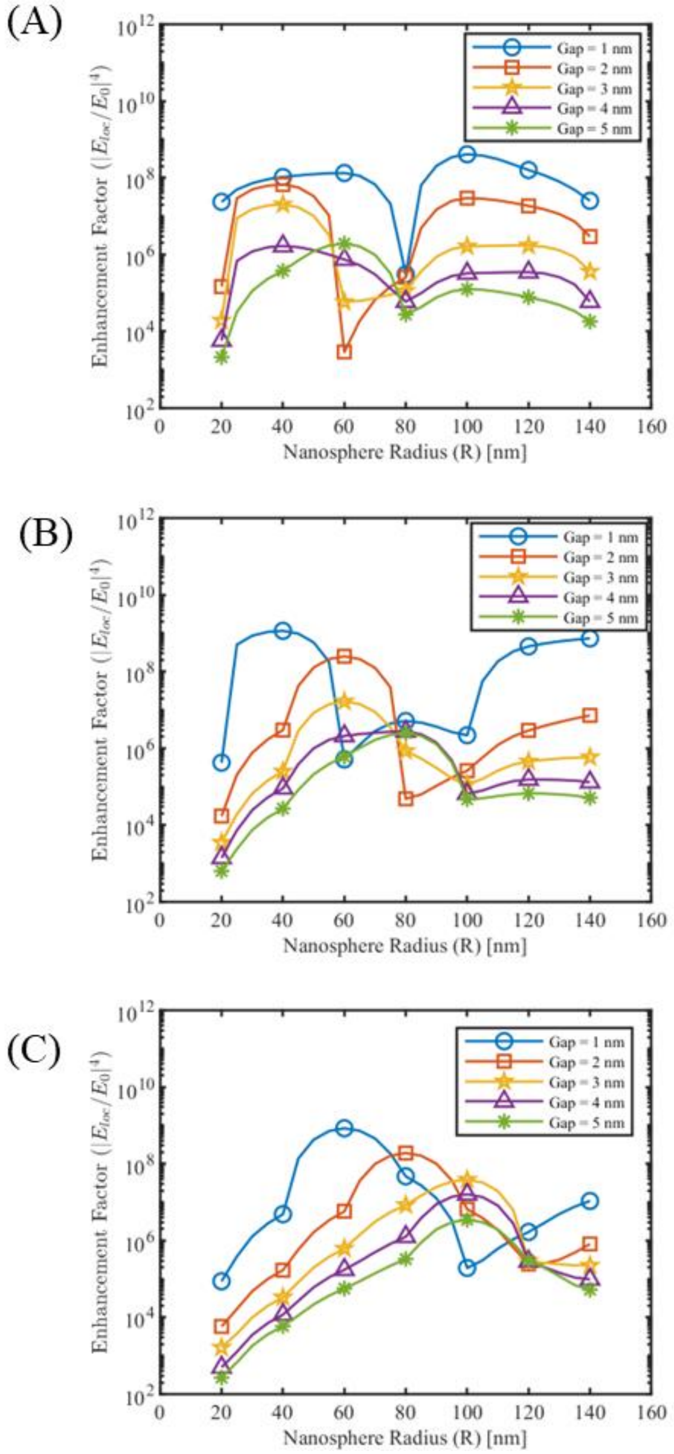

Figure S14: *Enhancement factor plots of hotspot 5 (middle hotspot) of silver nanotetramer orientation ◁▷ at wavelength (a) 532 nm (b) 633 nm and (c) 785 nm, demonstrating hotspot switching.*

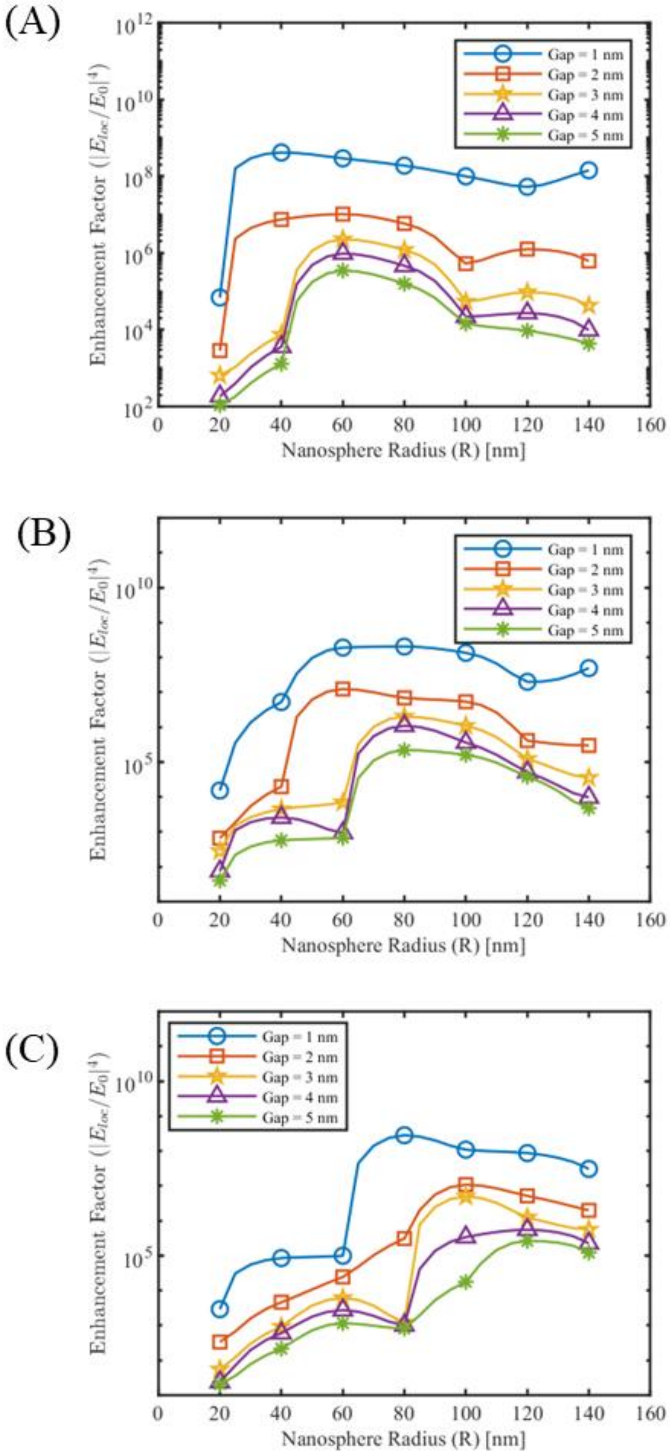

Figure S15: *Enhancement factor plots of hotspot 1 (side hotspot) of silver nanotetramer orientation ◁▷ at wavelength (a) 532 nm (b) 633 nm and (c) 785 nm, demonstrating hotspot switching.*

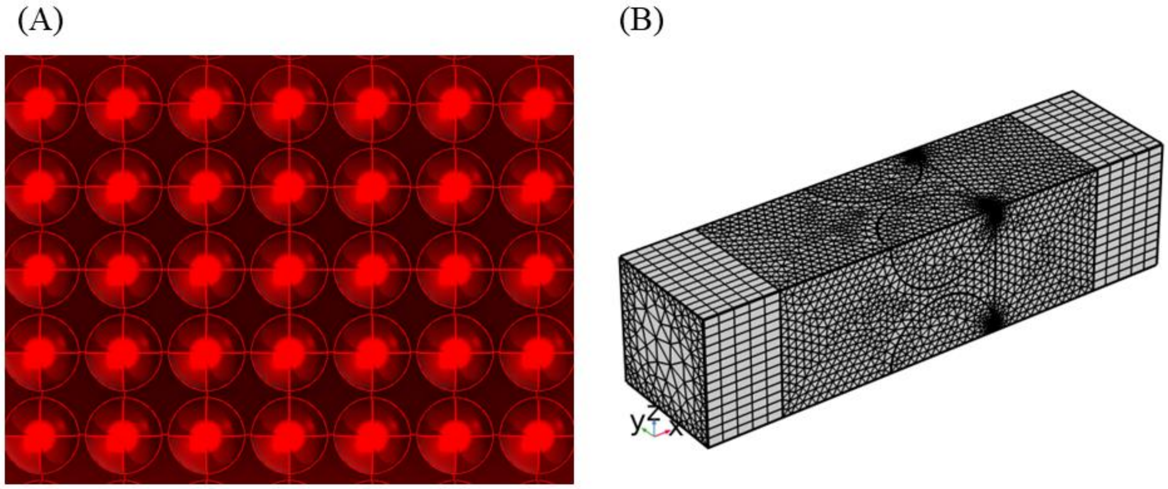

Figure S16: (a) Top view of the model of periodic array of silver nanospheres over a silicon substrate. (b) meshing of the unit cell of periodic array of nanospheres.

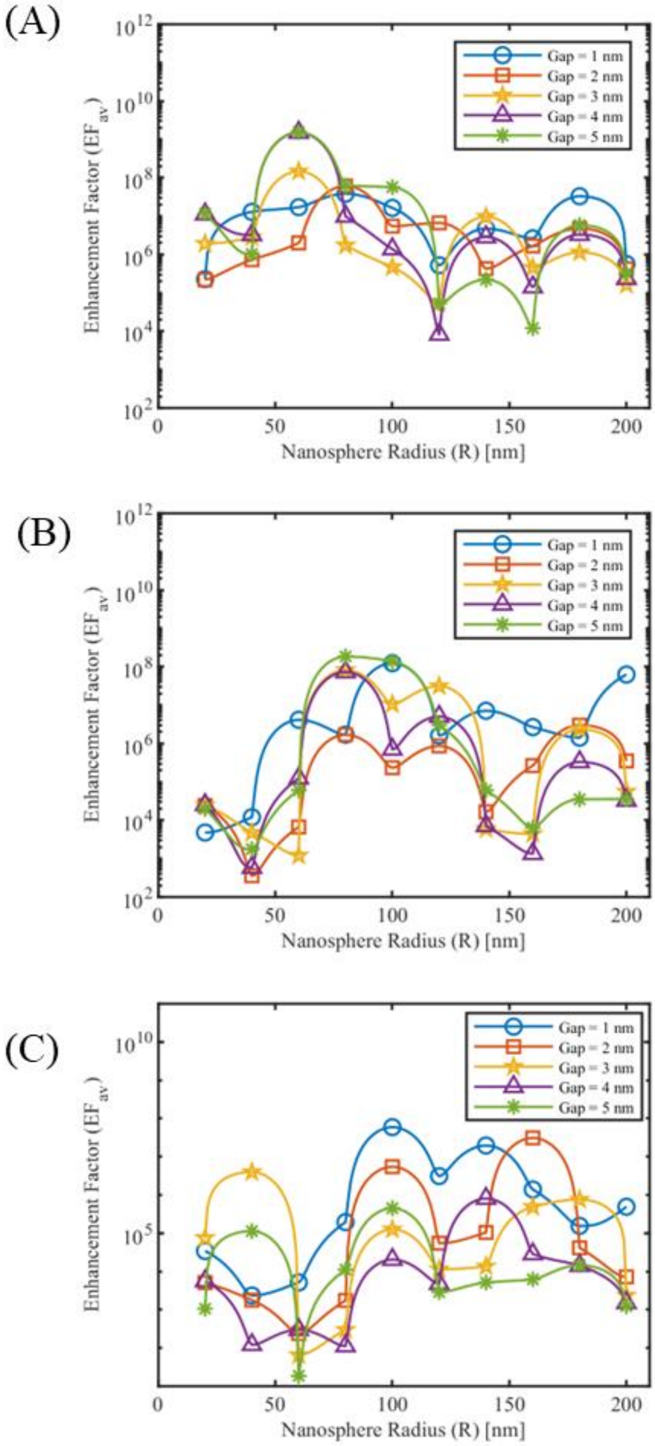

Figure S17: Average enhancement factor plots of periodic array of silver nanospheres at wavelength (a) 532 nm (b) 633 nm and (c) 785 nm.

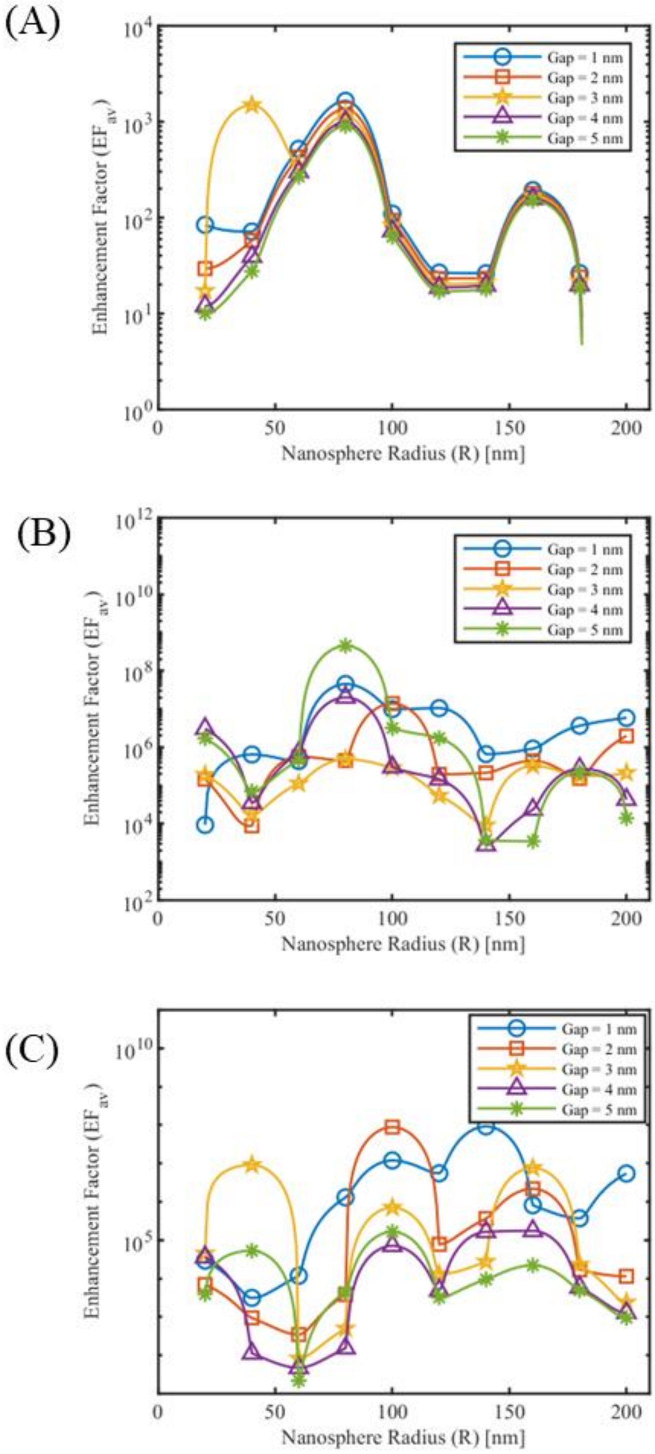

Figure S18: *Average enhancement factor plots of periodic array of gold nanospheres at wavelength (a) 532 nm (b) 633 nm and (c) 785 nm.*